ABSTRACT

Title of Dissertation: ACTUATION OF MULTIFUNCTIONAL HARD NANOPARTICLES FOR ACTIVELY CONTROLLED DRUG RELEASE

Ajmeeta Sangtani, Doctor of Philosophy, 2019

Dissertation directed by: Dr. James B. Delehanty
US Naval Research Laboratory

Professor Kimberly M. Stroka
Fischell Department of Bioengineering

Systemic drug delivery relies on repeated dosing of large concentrations of poorly targeted drug leading to off-target toxicity. Recently, nanoparticle (NP)-mediated drug delivery (NMDD) has been developed as an approach to overcome the limitations of traditional drug delivery. The unique size-dependent properties of NPs and their ability to augment the activity of attached/loaded cargos makes them attractive drug delivery vectors. NPs are classified into two categories (soft or hard depending on their material composition) and our understanding of how to load and control soft NP materials currently surpasses that of hard NPs. In this dissertation we seek to further our fundamental knowledge of hard NP-based drug delivery systems. In Aim 1 we utilize a quantum dot (QD)-cell uptake peptide complex as a central scaffold to append various responsive peptide-drug constructs in order to modulate the toxicity of one of the most widely used chemotherapeutics, doxorubicin. By doing a comparative study of four chemical linkages, we determine the role played by attachment chemistry in controlling drug release. In Aim 2, we utilize the knowledge gained from Aim 1 to develop a system capable of overcoming

multidrug resistance in cancer cells, which is known to severely limit the efficacy of chemotherapeutics. Our hard NP conjugate system is unique as it is one of the few systems reported in the literature to bypass multidrug resistance pumps without the need for exogenous drugs. Finally, in Aim 3 we append a peptide for membrane targeting and a photosensitizing drug capable of generating reactive oxygen species to the QD. This multifunctional system displays augmented therapeutic efficacy of the appended photosensitizer by delivering it to the membrane of cells and controlling its actuation using energy transfer. The work described here details basic concepts for the design of "smart" hard NP materials for internally and externally-triggered, active release of surface-appended drug cargos. Additionally, we hope to elucidate the important design considerations that must be taken into account when designing hard NP systems for controlled drug delivery.

ACTUATION OF MULTIFUNCTIONAL HARD NANOPARTICLES FOR ACTIVELY CONTROLLED DRUG RELEASE

Ajmeeta Sangtani

Dissertation submitted to the Faculty of the Graduate School of the
University of Maryland, College Park in partial fulfillment
of the requirements for the degree of
Doctorate of Philosophy
2019

Committee Members:
Dr. James B. Delehanty, Co-chair
Dr. Kimberly M. Stroka, Co-chair
Dr. Igor L. Medintz
Dr. Yu Chen
Dr. Ganesh Sriram, Dean's Representative

Dedication

For my parents, Lalit and Laetitia Sangtani

Acknowledgements

The work detailed in this dissertation would not have been possible without the encouragement, help, support, and teachings of my mentors, friends, and family.

I would first like to thank Dr. James Delehanty, my advisor, for everything he taught me about nanoparticles, for his advice and mentorship from beginning to end, and for helping turn me into a decent writer. Dr. Kimberly Stroka, my co-advisor, for keeping me on track to graduate and all her insightful advice. Dr. Igor Medintz, for all the advice and editorial comments. Drs. Kimhiro Susumu and Michael Stewart, for making all my quantum dots and teaching me how they work. Dr. Eunkeu Oh, for guidance on various subjects from characterization of nanoparticles to chemistry and coupling. The various post docs in my lab: Drs. Okhil Nag, Megan Muroski, Kelly Burns, and Lauren Field, for all their guidance and advice both in and out the lab. My officemates Drs. Divita Mathur, William Klein, and Sebastian Diaz and David H. My committee member, Dr. Yu Chen, and my Deans rep, Dr. Ganesh Sriram, for their help and advice.

I am grateful for the support of all my friends, both here in DC and those far away. A special thanks to my boyfriend Ben Bell, for being so supportive and for always keeping me motivated. To Sneha B., Linh T., and Chelsey K. for being there for me, even at a distance. To Sarah F., Ridhika K., Sarah L., Katy M., Ryan O, and Swetha R. for helping celebrate the wins and commiserate the losses. To my awesome housemates Maurice R., Eric W., and Sarah N. for their support this past year. And lastly, but certainly not least, a huge thank you to my family: Lalit, Laetitia, and Ajleeta Sangtani and Jaina and Dustin Baumgartner. And of course, Aditi, my sweet baby niece who always brings a smile to my face. I couldn’t have done it without their unwavering support and belief in me.

Table of Contents

Table of Figures

Table of Tables

List of Abbreviations

$^1O_2$	Singlet oxygen
ABC	ATP-binding cassette
AF647-Tf	AlexaFluor 647-transferrin
Ag	Silver
Aib	2-Aminoisobutyric acid
AMF	Alternating magnetic field
ANOVA	Univariate analysis of variance
ATCC	American Type Culture Collection
Au	Gold
AuNC	Gold nanocluster
$BaTiO_3$	Barium titanium oxide
BBB	Blood brain barrier
Bi_2S_3	Bismuth sulfide
BMSN	Mesoporous silica coated bismuth sulfide nanoparticles loaded with DOX
BS^3	Bis(sulfosuccinimidyl)suberate
BSA	Bovine serum albumin
CD	Carbon dots
CdSe	Cadmium selenide
Ce6	Chlorin e6
CL_4	Compact ligand 4
CM	Chains of magnetosomes
$CoFe_2O_4$	Cobalt iron oxide
CPP	Cell penetrating peptide
CPT	Camptothecin
CTB	Cathepsin-B
Cy5	Cyanine 5
DAPI	4′,6-diamidino-2-phenylindole
DHLA	Dihydrolipoic acid
DIC	Differential interference contrast
DIPEA	*N*,*N*-diisopropylethylamine
DLS	Dynamic light scattering
DMAP	4-(dimethylamino)pyridine
DMEM	Dulbecco's Modified Eagle's Medium
DMF	*N*,*N*-dimethlyformamide
DMSO	Dimethyl sulfoxide
DNA	Deoxyribonucleic acid

DNR	Daunorubicin
DOX	Doxorubicin
D-PBS	Dulbecco's phosphate buffered saline
DSP	3,3′-dithiodipropionic acid di(*N*-hydroxysuccinimide) ester
DTPA	Diethylene triamine pentaacetic acid
DTS	Dispersion technology software
EDC	1-Ethyl-3-(3-dimethylaminopropyl)-carbodiimide
EDTA	Ethylenediaminetetraacetic acid
EGFR	Epidermal growth factor receptor
EP4	Prostaglandin E4 receptor
EPR	Enhanced permeation and retention
EthD-1	Ethidium homodimer-1
FA	Folic Acid
FDA	Food and drug administration
FeO_3,FeO_4	Iron oxide
FITC	Fluorescein isothiocyanate
FLIM	Fluorescence lifetime imaging microscopy
FRET	Förster resonance energy transfer
GEM	Gemcitabine
GNOL	Gold nanoshell-coated oleanolic acid liposomes
GNR	Gold nanorods
GO	Graphene oxide
GQD	Graphene quantum dot
GSH	Glutathione
HA	Hyaluronic acid
HEPES	(4-(2-hydroxyethyl)-1-piperazinethanesulfonic acid)
IC_{50}	Half maximal inhibitory concentration
IFN-γ	Interferon gamma
IONP	Iron oxide nanoparticle
iPS	Induced pluripotent stem
LA	Lipoic acid
LCIS	Live cell imaging solution
LHRH	Luteinizing hormone-release hormone
MagMB	Magnetic microbubbles
MDR	Multidrug resistance
MEM	Eagle's Minimum Essential Medium
MENC	Magneto-electro Carriers
MION	Magnetic iron oxide nanocrystals
MNP	Magnetic nanoparticles
MPU	Multiblock polyurethane

MRgFUS	Magnetic resonance–guided focused ultrasound
MRI	Magnetic resonance imaging
MSN	Mesoporous silica nanoparticle
MTS	3-(4,5-dimethylthiazol-2-yl)-5-(3-carboxymethoxyphenyl)-2-(4-sulfophenyl)-2H-tetrazolium
NHS	*N*-hydroxysuccinimide
Ni-NTA	Nickel-nitrilotriacetic acid
NIR	Near-infrared
NMDD	Nanoparticle-mediated drug delivery
NP	Nanoparticle
O_{2^-}	Free radical
OMe	Methoxy
OMF	Oscillating magnetic field
PBS	Phosphate buffered saline
PCC	Pearson's correlation coefficient
PCL	Poly(E-caprolactone)
PDHP	Propionyl hydrazide
PDT	Photodynamic therapy
PEG	Polyethylene glycol
PEI	Polyethylenimine
PEO	Poly(ethylene oxide)
P-gp	P-glycoprotein
PHEA	PEG-b-poly-N-hydroxylethylacylamide
PL	Photoluminescence
PPO	Poly(propylene oxide)
PPy	Polypyrrole
PS	Photosensitizer
Pt	Platinum
PTT	Photothermal therapy
PTX	Paclitaxel
QD	Quantum dot
QY	Quantum yield
R_0	Förster Radius
RGD	Arginine-glycine-aspartate tripeptide
Rhod-PE	Lissamine Rhodamine B 1,2, dihexadecanoyl-sn-glycero-3-phosphoethanolamine
ROI	Region of interest
ROS	Reactive oxygen species
RPMI-1640	Roswell Park Memorial Institute medium
RT	Room temperature
$SiNc_4$	Silicon napthalocyanine bis (trihexylsilyloxide)

siRNA	Small interfering ribonucleic acid
SMCC	Succinimidyl 4-(N-maleimidomethyl)cyclohexane-1-carboxylate
SN-38	7-ethyl-10-hydroxycamptothecin
SPION	Superparamegnetic iron oxide nanoparticles
TaO	Tantalum oxide
TAT	Nuclear targeting peptide
TCEP	Tris(2-carboxyethyl)phosphine hydrochloride
TD	Transmitted light channel
TEM	Transmission electron microscopy
THF	Tetrahydrofuran
TiO_2	Titanium oxide
TNF	Tumor necrosis factor
TOP	Trioctylphosphine
TOPO	Trioctylphosphine oxide
TPGS	Tocopherol polyethylene glycol succinate
TRAIL	Tumor necrosis factor-related apoptosis inducing ligand
TRITC	Tetramethylrhodamine
UCNP	Upconversion nanoparticle
UPLC	Ultra performance liquid chromatography
ZnS	Zinc sulfide

Chapter 1: Introduction

Therapeutic drugs are materials that are aimed at preventing disease or aiding the restoration of health and drug delivery is the method of administering such a compound to achieve a therapeutic effect. Throughout history, there have been many schemes for drug delivery, dating back over 5000 years. As the fields of science and medicine have progressed, there have been significant improvements in such schemes, both in terms of improving the overall therapeutic efficacy as well as lowering the toxicity. Over the past few decades, nanoparticles (NPs) have emerged as a novel scaffold to overcome some of the historical limitations of earlier therapeutic methods. The goal of this dissertation is to develop a fundamental understanding of one such NP scaffold in order to control drug release and further improve the overall therapeutic efficacy of the appended drug cargo.

General Therapeutic Approaches

According to the earliest recorded texts from Indians, Chinese, Egyptians, Greeks, Romans, and Syrians, the treatment of disease using drug therapy has existed for over 5000 years.[17] Early examples of drug-based therapeutics comprise of extracts from natural sources such as herbs, plants, roots, vines, and fungi and were known as herbal medicine or phytotherapy.[17, 18] While some of these types of therapeutics, such as digitalis (foxglove) and Atropa belladonna (nightshade), are still used in clinics today, the high toxicity and low therapeutic efficacy of naturally-occurring therapeutics led to a transition to man-made drugs.[19, 20] In developing synthetic therapeutics, the overall goal has continually been to improve the therapeutic index by maximizing efficacy and minimizing toxicity. Additionally, the advancement of synthetic chemistry and an understanding of biochemical mechanisms of action and biological structure/function has led to the creation of novel

chemical structures.[18] For example, the first synthetic drug used in clinics, chloral hydrate (discovered in 1869) came about due to the observation of toxicity from alkaloid plants. [18] This led to the use of chemicals to synthesize drugs that could mimic the actions of such plants in a more controlled manner. The pharmaceutical industry can also be traced back to the manufacturing of textiles and synthetic dyes.[18] In the mid-1880s, Paul Ehrlich discovered the selective affinity of certain dyes for biological tissues, which led to the recognition of chemoreceptors that could be exploited for therapy and the eventual development of chemotherapy.[21] Similarly, advances in biochemistry aided in the synthesis of therapeutics through the discovery of enzymes and receptors that proved to be good targets for drugs.[22]

Despite significant progress in drug therapy, there are still several roadblocks in the development of therapeutics with maximum efficacy.[23] First, many highly active drugs have limited solubility, poor tissue uptake, and/or minimal clearance from the body which diminishes their bioavailability and efficacy.[23] Second, most conventional therapy schemes utilize systemic delivery which distributes the drug nonspecifically throughout the body, often limiting the accumulated dose at desired target sites.[23-25] Third, dosing regimens in traditional drug delivery typically use repeated doses of large concentrations of non-targeted or poorly targeted drug, which increases costs and reduces uptake, leading to poor clinical outcomes due to reduced patient compliance and efficacy.[25] Lastly, diseased tissues have developed mechanisms to defeat traditional drug delivery approaches. In many cancers, for example, multidrug resistance (either through active pumping of the drug out of the cell or direct drug neutralization) has become a considerable challenge.[23] Taken

together, these limitations of traditional drug therapies necessitate the need for new strategies to improve the overall therapeutic index of drugs.

Advent of Nanoparticle-Mediated Drug Delivery

In recent years, nanoparticle (NP)-mediated drug delivery (NMDD) has garnered significant interest and excitement as an approach to addressing the challenges involved in conventional drug therapies.[23] Nanotechnology focuses on the design, synthesis, characterization, and implementation of nanoscale-sized materials and seeks to take advantage of the unique attributes of these materials for use in a variety of applications, including medicine and drug therapy.[26] NPs, which are 1-100 nm in at least one dimension, come in various designs and configurations. Often they are comprised of a particle core, a protective layer for biocompatibility, and a linker molecular layer for attachment to/interfacing with biological moieties (such as drugs, targeting agents, imaging agents). These composite hybrid materials have shown great promise in the improvement of drug delivery system design.[26]

NPs possess many advantages that make them ideal for use as the basis of improved drug delivery systems. Chief among the unique attributes are NPs' small size—as they must be less than 100 nm in at least one dimension, they fall between molecules and cellular organelles, meaning they are significantly smaller than mammalian cells.[23] Their small size enables extended bloodstream circulation, improved cell and tissue penetration, elicitation of minimal immunogenicity and toxicity, and efficient clearance from the body through the renal system.[23, 26-28] Additionally, they are small enough to avoid aggregation in microcapillaries and to escape capture by macrophages lodged in the reticuloendothelial system. The size of NPs is often tunable which is important as particle size and distribution

can determine characteristics such as biological fate, stability, toxicity, targeting ability and can influence drug loading and release from the NP.[23, 24, 27] Their small size also imbues NPs with a large surface area to volume ratio meaning a large drug carrying capacity within a single particle, thereby reducing the quantity of scaffold materials needed for sufficient therapeutic efficacy per administration.[23] Further, the drug cargo can be loaded in the core and/or carried on the surface of NPs, depending on the structure and physicochemical composition.[23]

Another key feature of NPs is their multifunctionality— the capability to carry out several disparate functions such as cellular targeting and uptake, intracellular localization, sensing, imaging, and drug delivery - all on a single NP platform. The use of NPs as a drug delivery system has the ability to overcome two key limitations of traditional drug therapies: 1) they can target drugs to specific cellular organelles and/or specific subsets of cells and 2) they can controllably release appended/loaded cargo. Targeted delivery, which can be passive or active, can ultimately decrease the required drug dose and can improve overall therapeutic efficacy. Passive targeting relies on the disease microenvironment or pathophysiology to achieve accumulation of the therapeutic within the target population of cells.[26, 29] For example, the leaky vasculature of tumors due to neovascularization from rapidly dividing cancer cells results in an imbalance of angiogenic regulators making tumor vessels highly disorganized and dilated with large pores and gap junctions and a compromised lymphatic drainage system. This leads to the enhanced permeation and retention (EPR) effect, whereby NPs preferentially leak into and are retained within tumor tissue, which can also be used for tumor targeting.[23, 24, 29]Additionally, due to the high metabolic rate of cancer cells and the use of glycolysis to obtain extra energy, tumors are

known to have an acidic microenvironment which can be used for targeting.[23, 24, 29, 30] Active targeting, on the other hand, involves the use of targeting moieties that are specific to cancer cells. NMDD systems accomplish actively-targeted delivery through NP functionalization (i.e. through conjugation of or coating with ligands on the NP that bind to target cells or organelles). Active targeting can also refer to targeting of NP systems to specific subcellular organelles for improved therapeutic efficacy. For example, the plasma membrane can be a target of photodynamic therapeutics as it is susceptible to lipid peroxidation and the nucleus of cells is a target for many chemotherapeutics in order to hinder the DNA replication process.

The multifunctionality of NPs can also be used to control drug release through actuation of the nano-matrix. In use of NPs as drug delivery systems, the drug of interest can be adsorbed, attached, and/or encapsulated into or onto the NP scaffold.[27] Much like targeting, the actuation of NPs can follow two forms: passive or active.[23] Passive actuation involves desorption (from the NP surface) or efflux (from the NP core) of a non-covalently associated cargo, offering limited spatiotemporal control over drug release. Active actuation, on the other hand, offers a high amount of spatiotemporal control and follows either of two mechanisms: internal or external. In externally-triggered actuation, cargo release is controlled through induction of an external stimulus such as light, a magnetic field or ultrasound. Internally-triggered actuation, on the other hand, relies on innate cellular or physiological processes such as change in pH, redox potential, and/or enzymatic activity, to control cargo deployment.[23]

NPs can also be rendered biocompatible and non-immunogenic via coating with various surface ligands, thus significantly reducing or eliminating drug carrier side

effects.[26] Using a hydrophilic/polymeric surface on NPs can provide "stealth" resulting in escape of macrophage capture thus improving bioavailability and circulation time, and reducing nonspecific bindings.[23] They can also be synthesized in such a way so they can sustain release of drugs over time for systemic delivery and/or overcome multidrug resistance, by bypassing membrane-resident multidrug-resistant pumps.[23, 24, 27]

NMDD Systems

For NMDD to succeed, there are four parameters that need to be addressed: 1) the loading of the drug into or onto the NP, 2) the targeting of the NP to specific tissues, cells, and/or cellular organelles and 3) the controlled release of the drug cargo from the NP and 4) elimination from the body or detoxification to avoid buildup and resulting side effects. Additionally, it is crucial to develop a colloidally stable NP that is assembled with fidelity and that causes minimal toxicity. Thus the critical issue in NP development is the ability to make and control complex NP architectures that can "do more" all within a single NP scaffold.

The nature of the NP (hard versus soft), including both its surface and core determines both the type of cargo that can be loaded and when it needs to be incorporated into the NP. Hard NPs, which have a solid non-flexible core, are characterized by having only their external surface available for appending cargos, usually through passive adsorption via electrostatic interactions or covalent attachment through pendant handles on the NP surface. The attached cargo can be either hydrophilic or amphiphilic and is usually appended after NP synthesis. Examples here include gold (Au) and silver (Ag) NPs, oxides such as iron and graphene, and quantum dots (QDs) to name a few. Soft NPs, on the other hand, have a flexible structure and more variety in their cargo carrying capacity due to a

central core that is available for cargo-loading as well as an external surface that is amenable to cargo attachment. Examples here include micelles, liposomes, polymersomes, and protein NPs. Cargo in soft NPs can be loaded during or after NP synthesis. [23]

Currently, soft NPs are much better understood and implemented as compared to hard NPs.[23, 31, 32] This is exemplified by the fact that DOXIL, a liposomal (soft NP) formulation of the widely used cancer therapeutic doxorubicin (DOX), is one of the few FDA approved NP formulations. While DOXIL has been shown to extend circulation time of the loaded therapeutic and improve clearance, it utilizes passive actuation for sustained release of cargo deployment. Although there are some hard NP formulations currently in clinical trials, all FDA approved NP-formulations utilize soft NP scaffolds due to the inherent properties of soft NPs. Chief among these is the ability to synthesize soft NPs using biodegradable materials, thus improving the overall biocompatibility of the NP system and their capacity for self-assembly, meaning a facile synthesis process. Additionally, soft NPs have more flexibility in their cargo carrying capacity due to the hydrophilic core and hydrophobic bilayer, thus making them attractive candidates for drug delivery. As the core of the soft NPs is available for loading the cargo, they can also carry large drug payloads. While soft NPs have many attributes, they tend to be larger than hard NPs, making them ideal for taking advantage of the EPR effect of leaky vasculature, but limits their ability to penetrate into more dense tissues, and they lack inherent optical properties, such as luminescence.[33-35] The goal of the work presented here is to use a model hard NP scaffold to develop a fundamental understanding of controlled drug release from the surface of hard NPs. We seek to further our understanding of how to utilize both internal stimuli (such as esterases, pH, and reducing agents) and external stimuli (such as laser

irradiation) to modulate drug toxicity, overcome MDR, and improve the overall efficacy of the therapeutics. Additionally, the lessons learned from developing these systems can also be applied to other hard NP systems, to eventually develop a NP system with a more complex architecture that can do more.[23]

Semiconductor QDs: A Prototypical Hard NP

First synthesized in colloidal solutions by Louis E. Brus in 1986, quantum dots (QDs) are a type of hard NP that have garnered a great deal of interest for use as drug delivery scaffolds in biological systems (cells, tissues, etc.) over the last two decades due to their inherent optoelectronic properties that are directly tied to the small size (2-10 nm hard diameter) of the as-synthesized materials.[36] QDs are bright luminescent semiconductor nanocrystals that possess a number of advantageous attributes for studying many of the basic concepts required for the successful implementation of hard NPs in NMDD. Since their discovery, many efforts have been made to explore the basic properties of QDs, both for commercial and therapeutic processes.[37, 38]

One of the key features of QDs is their exceptional luminescence, which stems from their large extinction coefficient (efficient light absorption) and high quantum yield (high ratio of photons emitted compared to photons absorbed).[37, 39] They emit high-intensity light in a narrow spectral range and have a large "effective" Stokes shift, making it easy to separate the fluorescence signal of the QDs from the light source thus reducing the contribution of auto-fluorescence. Additionally, as they are resistant to photobleaching and highly stable, they are an ideal scaffold for use in real-time, long-term imaging using fluorescence microscopy.

As mentioned previously, a benefit of using NPs is the ability to fine-tune their size, which often leads to changes in other properties such as aqueous stability and fluorescence.[36, 40, 41] In the case of QDs, the size of the core can be used to fine-tune the emission maximum where smaller QD cores result in light emitted at shorter wavelengths (blue shift) and larger QDs emit light at longer wavelengths (red shift). The fluorescence emission spectral range of QDs is also determined by their elemental composition and their size. QDs tend to be alloyed with multiple semiconductors as the resulting nanostructure displays mixed or intermediate optoelectronic properties. CdS and CdSe QDs, for example, emit light over the visible spectrum, whereas CdTe QDs exhibit near-infrared emission. Thus the tenability of QDs make them an attractive candidate as a nano-matrix for use as a drug delivery scaffold.

Another key feature of QDs is the ability to append various biomolecules and other cargo using several mechanisms, such as direct covalent conjugation to the ligands on the QD or through histidine-mediated assembly.[42, 43] In order to be made dispersible in aqueous solutions as stable colloids and thus biocompatible for use in biological systems, the organic capping layer of the as-synthesized QDs are often replaced with a hydrophilic layer. Covalent linkages can then be used to conjugate biomolecules to the surface of QDs through use of coupling reagents such as EDC/NHS for conjugating carboxylic acids with primary amines and SMCC for conjugating thiols and primary amines.[44] [45] While this process forms a stable bond and allows for conjugation of a wide variety of molecules, it can be complex often requiring multiple conjugation and/or purification steps. Histidine-mediated metal-affinity, on the other hand, is a facile self-assembly process that allows for high control over peptide-to-QD ratio due to the fact that histidines have high affinity for

immobilized metals, such as the Zn on the QD surface. Polyhistidine sequences can be added to the end of any peptide sequence, thus making it easy to conjugate a variety of biomolecules in this manner.[46-48] This metal affinity interaction is often used in protein purification through binding of histidines to nickel in a purification column, and is unique to QD-biomolecule conjugation in NMDD.

Due to their large extinction coefficient and high quantum yield, QDs also serve as excellent Förster resonance energy transfer (FRET) donors.[49] FRET is a photophysical process where excitation of a donor results in energy transfer to an acceptor molecule causing emission of the acceptor.[49] The process is characterized by a decrease in donor emission and an increase in acceptor emission when compared to emission of the molecules alone. FRET is dependent on several factors: 1) the spectral overlap between the donor emission and acceptor absorbance, 2) the distance between the donor and acceptor, 3) the number of acceptors per donor, and 4) the quantum yield of the donor. The theoretical FRET efficiency between two molecules can be calculated using the equation:

$$FRET_E = \frac{n{R_0}^6}{r_{DA} + n{R_0}^6}$$

Where r_{DA} is the donor-acceptor separation, R_0 is the donor-acceptor separation at 50% transfer efficiency and n is the number of acceptors per donor.[50, 51] To calculate the experimental FRET efficiency, the following equation is used:

$$FRET_E = 1 - \frac{F_{DA}}{F_D}$$

Where F_{DA} is the fluorescence of the donor-acceptor complex and F_D is the fluorescence of the donor alone.[52] While QDs can serve as both FRET donors and acceptors, for the purposes in this dissertation, we only utilize them as donors.

One important concern regarding the use of QDs as a scaffold for NMDD is their biocompatibility. The core of QDs are generally made with heavy metals such as Cd and Pb which have been shown to cause toxic side effects when interfaced with cells.[42] However, passivation with a shell and capping with biocompatible ligands, such as PEG, has been shown to significantly improve the biocompatibility of QDs. A 2016 meta-analysis on the cytotoxicity of QDs containing Cd by researchers in our group, in addition to studies done by several other groups have shown that toxicity of QDs is highly dependent on QD size, surface chemistry, and exposure time.[53-56] Additionally, most studies using QDs *in vitro* report no significant changes in morphology, cell viability or development when used within the nM to μM range.[42] QDs can also be synthesized with non-Cd containing cores using materials such as InP and CuInS, which are significantly less toxic, but also have lower quantum yields.[57, 58] Thus, while there are still some concerns regarding the toxicity of these NPs, their many advantages still make them a powerful research tool that can be utilized to develop a fundamental understanding of controlled release from hard NP systems.

Specific Aims

This dissertation focuses on the development of a fundamental knowledge of actively controlled drug release from the surface of hard NPs in order to address some of the critical issues currently facing NMDD. We employ QDs as our model hard NP and we develop three representative multifunctional NMDD systems to develop a better understanding of controlled drug release.

Specific Aim 1: Intracellularly-actuated quantum dot-peptide-doxorubicin nanobioconjugates for controlled drug delivery via the endocytic pathway

As mentioned above, NMDD has emerged as a novel method to overcome the limitations of traditional systemic delivery of therapeutics, including the controlled release of NP-associated drug cargos. Currently, our most advanced understanding of how to control NP-associated cargos is in the context of soft NPs, where there is little to no control over drug release. The goal of specific aim 1 is to employ a QD as a prototypical hard NP platform coupled with intracellularly-triggered actuation to achieve spatiotemporal control of drug release and modulation of drug efficacy. To accomplish this, two species of peptide are appended to the QD: 1) a cell penetrating peptide which facilitates uptake of the bioconjugate into the endocytic pathway and 2) a display peptide conjugated to the chemotherapeutic doxorubicin (DOX) via three different linkages (ester, disulfide, and hydrazone) that are responsive to enzymatic cleavage, reducing conditions, and low pH, respectively. These linkages were chosen due to their cleavage in conditions found within the cellular environment (i.e. the acidity of endosomes and the reducing environment of the cytosol). After delivery of the linkages, we expect to see significant differences both in terms of nuclear localization over time and cytotoxicity. Overall, this project will demonstrate the utility of hard NP-peptide bioconjugates as multifunctional scaffolds for simultaneous control over cell drug uptake and toxicity and the vital role played by the nature of the chemical linkage that appends the drug to the NP carrier.

Specific Aim 2: Nanoparticle-peptide-drug bioconjugates for unassisted defeat of multidrug resistance in a model cancer cell line

Multidrug resistance (MDR) is a significant challenge in the treatment of many types of cancers as membrane-associated transporters actively pump drugs out of the cell, limiting therapeutic efficacy. While nanoparticle (NP)-based therapeutics have emerged as a mechanism for overcoming MDR, they often rely on the delivery of multiple anticancer drugs, nucleic acid hybrids, or MDR pump inhibitors. The effectiveness of these strategies, however, can be limited by their off-target toxicity or the need for genetic transfection. In this aim, we describe a NP-peptide-drug bioconjugate that achieves significant cell killing in MDR-positive cancer cells without the need for additional drugs. We do so by using the QD-cell uptake peptide-ester-DOX bioconjugate from Aim 1 to facilitate endocytic internalization and controllably release drug cargo near the nucleus in order to overcome MDR. This approach relies on spatiotemporal control over drug release, where endosomes traffic drug away from membrane-resident pumps and release it closer to the nucleus. We expect to see a high uptake of the NP-drug complex and nuclear localization of the drug in MDR-positive cells. Additionally, we expect to see high toxicity for the bioconjugate compared to free drug, in order to confirm the utility of this system in overcoming MDR in cancer cells.

Specific Aim 3: Proof-of-concept of an extracellularly-actuated nanoparticle-peptide-drug-photosensitizer bioconjugate for targeted membrane delivery and improved photodynamic therapy

Photodynamic therapy (PDT) involves light activation at a specific wavelength of a photosensitizing agent which results in photochemical and photobiologic processes that

cause irreversible damage to tissues through generation of reactive oxygen species (ROS) and lipid peroxidation, causing cell death. As photosensitizers (PS) tend to be highly hydrophobic, they often require delivery systems which can improve both solubility, as well as targeting to specific locations within the cells, such as the plasma membrane, where lipid peroxidation is most effective. In this aim, we describe a NP-peptide-PS bioconjugate that can 1) facilitate targeted delivery of the PS to the cellular membrane through attachment of a membrane tethering peptide, 2) achieve PDT through activation of an attached PS (chlorin e6, Ce6), 3) indirectly excite the PS in a FRET configuration and 4) improve the aqueous solubility of the PS. By appending both Ce6 and the membrane targeting peptide to the surface of the QD, we can improve the solubility of the drug, target it specifically to the membrane, and control activation. After delivery of this complex to cells, we expect to see high colocalization of the NP bioconjugate with the plasma membrane. Additionally, we expect to see higher lipid peroxidation, uptake of a membrane impermeable dye, and toxicity for the PS in the complex compared to free drug.

Chapter 2: Mechanisms of Actively Triggered Drug Delivery from Hard Nanoparticle Carriers: A Review[*59]

Introduction

NMDD systems have garnered significant interest as an approach to address several considerable challenges in traditional systemic drug delivery, which include the need for repetitive dosing regimens, nonspecific drug targeting, and off-target toxicity. NPs are an attractive delivery platform to help overcome these limitations as they provide the potential for specific targeting and controlled release at the desired site, resulting in improved therapeutic efficacy. NPs can be characterized as hard or soft, based on their physicochemical composition and the manner in which cargo is loaded into/onto the NP. Soft NPs are typically liposomal or micellar formulations and have both the core and surface available for cargo loading resulting in extended release. Although these formulations comprise the majority of NPs that are currently approved by the Food and Drug Administration (FDA) for drug delivery, they often rely on passive uptake, which has limited targeting capability. Conversely, hard NPs are comprised of a solid core (e.g., gold, graphene oxides, and iron oxides), and due to their inherent optical properties, they provide a method to track drug delivery in real time. Their small size enables elimination from the body through renal clearance, and their amenability for surface functionalization enables biocompatibility as well as active or passive targeted delivery of therapeutic cargo.

[*] Reprinted with permission from Sangtani, A., Muroski, M. E., and Delehanty, J. B. (2019) Mechanisms of actively triggered drug delivery from hard nanoparticle carriers, in *Targeted nanosystems for therapeutic applications: New concepts, dynamic properties, efficiency, and toxicity* (Sakurai, K., and Ilies, M. A., Eds.) pp 157-185, American Chemical Society. Copyright 2019 American Chemical Society.

Currently, there are several hard NPs approved for clinical trials, including silica gold NPs for plasmonic photothermal treatment of atherosclerosis (NANOM, NCT01270139) and iron oxide NPs for the treatment of prostate cancer (Nanotherm®).

The goal of this chapter is to provide an overview of current systems of actively actuated drug release that utilize hard NP carriers. Active actuation offers significant control over cargo release from the surface of the NP as it can be controlled by internal and/or external triggers. Conversely, passive actuation relies on the diffusion of noncovalently associated cargo and often has limited control over drug release. We divide our coverage of the active actuation modality based on whether it is mediated internally within the cellular environment or externally (Figure 1). Internal actuation of NPs is dependent on innate biologic states or processes such as pH, redox state, and/or enzymatic activity to provide control over drug release. In pH-sensitive and redox-dependent release, the low pH found in endosomes, or the reducing environment of the cytosol, as well as the tumor microenvironment can facilitate drug release. Furthermore, enzymes overexpressed in or on cancer cells or those found within specific subcellular compartments are also able to trigger drug release. External actuation, on the other hand, provides spatiotemporal control using an external force, such as a magnetic field, photothermal therapy (PTT), irradiation, and/or ultrasound. For example, using an external magnet, drug delivery can be guided and/or triggered at the site of interest. PTT and focused ultrasound utilize near-infrared (NIR) light or ultrasonic waves, respectively, to locally increase the tissue temperature, resulting in cell killing or the induction of drug release from the NP surface. Finally, NPs have the ability to sensitize a specific area of treatment to radiation effects.

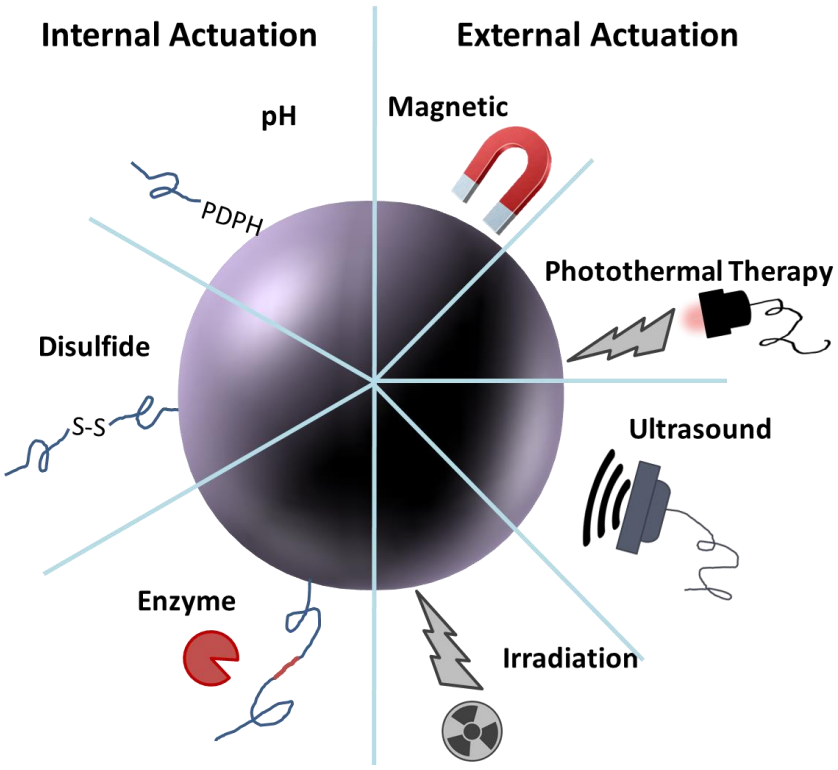

Figure 1: **Mechanisms of internal and external actuation of hard NPs.** Schematic representing methods of internal and external actuation of hard NPs. Internal methods rely on the innate cellular environment to control release whereas external methods utilize external stimuli.

Herein, we detail multiple examples of hard NP systems that employ these internal and external techniques to improve delivery mechanisms and overall efficacy of therapeutics.

Internally-Triggered Drug Release

Low pH

The use of a low pH environment to trigger intracellular drug release is an attractive delivery modality. It has emerged largely from the cancer field, where the tumor microenvironment has a lower pH (~6) compared to normal tissue (~7.4) due to increased lactate production and a shift to glycolytic metabolism in cancer cells.[60] Additionally, in mammalian cells, the endocytic pathway is known to acidify in a time- and spatial-dependent manner. Endocytosed materials taken up by early endosomes are maintained at near neutral pH (7.4) but are progressively exposed to the acidic environment of vesicles

as early endosomal compartments fuse with late endosomes/ lysosomes, where the pH ranges from 4.5.–5.0. Thus, many research groups have investigated the use of a variety of hard NP systems for acid-sensitive drug delivery/release through the cleavage of moieties on the surface of a NP, dissolution of the NP core, or dissociation of various capping agents on porous hard NPs.

A number of covalent, acid-labile chemistries have been reported for the attachment of therapeutics to the surface of hard NP carriers.[61-65] Ruan and coworkers conjugated doxorubicin (DOX) to the surface of glioma cell-targeted ~25 nm gold NPs (AuNPs) using a pH-sensitive hydrazone bond, which is naturally cleaved in acidic conditions, to achieve drug delivery through the blood brain barrier (BBB) (Figure 2A).[3] The NPs were also decorated with polyethylene glycol (PEG)-angiopep-2 ligands to simultaneously increase colloidal stability and to target low-density lipoprotein receptor-related protein 1, which is overexpressed in glioma cells. Angiopep-2 has also been shown to be effective for the translocation of cargos across the BBB.[66, 67] *In vivo* biodistribution confirmed improved uptake of the complex after intravenous injection in C6 glioma-bearing mice compared to DOX alone, and survival curves showed a ~2-fold improvement in mean survival time, demonstrating the benefits of pH-dependent drug release. Another example using an acid-labile linker comes from Lee and colleagues, who synthesized 60 nm AuNPs for improved drug delivery.[61] Here the gold nanocarrier was bound to DOX via a 3-[2-pyridyldithio] propionyl hydrazide (PDPH) linker and coated with PEG for stability. *In vivo* studies in 4T1 tumor-bearing mice demonstrated significantly lower tumor volumes for mice treated with the complex compared to free drug. Similar methods of acid-labile chemistries for pH-dependent release from the surface of hard NP carriers have been demonstrated for a

variety of drug systems, including core-shell quantum dots (QDs), gold nanorods (GNRs), and graphene QDs.[62-65]

Drug cargos can also be attached to the surface of hard NP carriers via noncovalent acid-labile interactions.[8, 12, 68, 69] Huang and coworkers bound DOX to graphene oxide (GO) NPs via hydrophobic interactions and π-π stacking.[69] The NPs were further decorated with folic acid (FA) for targeting folate receptors (as they are known to be overexpressed on many types of cancer cells), and with diethylene triamine pentaacetic acid (DTPA) for binding polyvalent metal ions to enable magnetic resonance imaging.[70-72] In acidic conditions, efficient release of the drug is achieved due to the high solubility of DOX, which disrupts the hydrophobic interactions between DOX and GO. Experiments in buffer demonstrated ~40% increase in drug release at pH 5.0 compared to pH 7.0. *In vitro* functionality of the NPs was confirmed using cell viability assays on HeLa cells, which showed increased toxicity after treatment with the complex, compared to free drug. HepG2 cells, on the other hand, which do not express the folate receptor, showed minimal toxicity. In a similar study utilizing noncovalent interactions, Zhang and colleagues complexed the chemotherapeutic daunorubicin (DNR) to ~25 nm titanium oxide (TiO_2) NPs through the combination of keto-phenolate Ti metal affinity and electrostatic interactions between the negatively charged TiO_2 and positively charged drug (Figure 2B).[8] When subjected to low pH, protonation of the drug and neutralization of the TiO_2 NPs resulted in dissociation of the complex and release of the drug. *In vitro* cell viability assays in K562 leukemia cells demonstrated improved apoptosis for the complex compared to free drug, as shown through caspase 3 staining.

Dissociation of the NP core in acidic conditions can also be used to achieve pH-responsive drug release. For example, Liu and coworkers synthesized ~40 nm ZnO NPs wherein DOX is associated with the NP surface through electrostatic interactions. ZnO NPs are ideal for pH-sensitive drug delivery applications as they are stable and nontoxic at physiological pH but dissolve in acidic conditions (pH <5.5). In this configuration, ZnO emission was quenched, and dissociation of DOX from the ZnO surface resulted in increased emission of ZnO, allowing for real-time monitoring of drug release in multidrug resistance (MDR) cells.[73-75] *In vitro* experiments demonstrated improved cellular uptake and increased cell killing in MDR^+ MCF-7 cancer cells compared to free drug as the lower pH of late endosomes/lysosomes facilitated controlled release of the drug far from plasma membrane-resident MDR pumps. As the surface of ZnO NPs is easily modified, the NPs can also be targeted specifically to cancer cells. Cai et al. coated ~6 nm ZnO NPs with PEG, hyaluronic acid (HA, a CD44 targeting moiety), and DOX through a combined electrostatic and metal-drug complex interaction.[73] In situ release experiments showed ~70% drug release after 80 h in pH 5 buffer compared to only ~30% release in physiological pH buffer (7.4). Cytotoxicity experiments in A549 cells showed comparable toxicity for the complex compared to free DOX, thus further demonstrating the use of low pH-mediated ZnO degradation for efficient intracellular drug delivery.

Finally, pH-sensitive drug release from hard NPs can be achieved through dissociation of a capping agent leading to drug release from the core of a porous hard NP.[10, 74, 76, 77] For example, Yang and coworkers synthesized ~130 nm hollow mesoporous upconversion NPs (UCNPs) ($NaYF_4$:YB^{3+}, Er^{3+}) coated with polyethylenimine (PEI) ligands to impart biocompatibility and stability and to protect the NP in acidic conditions.[64]

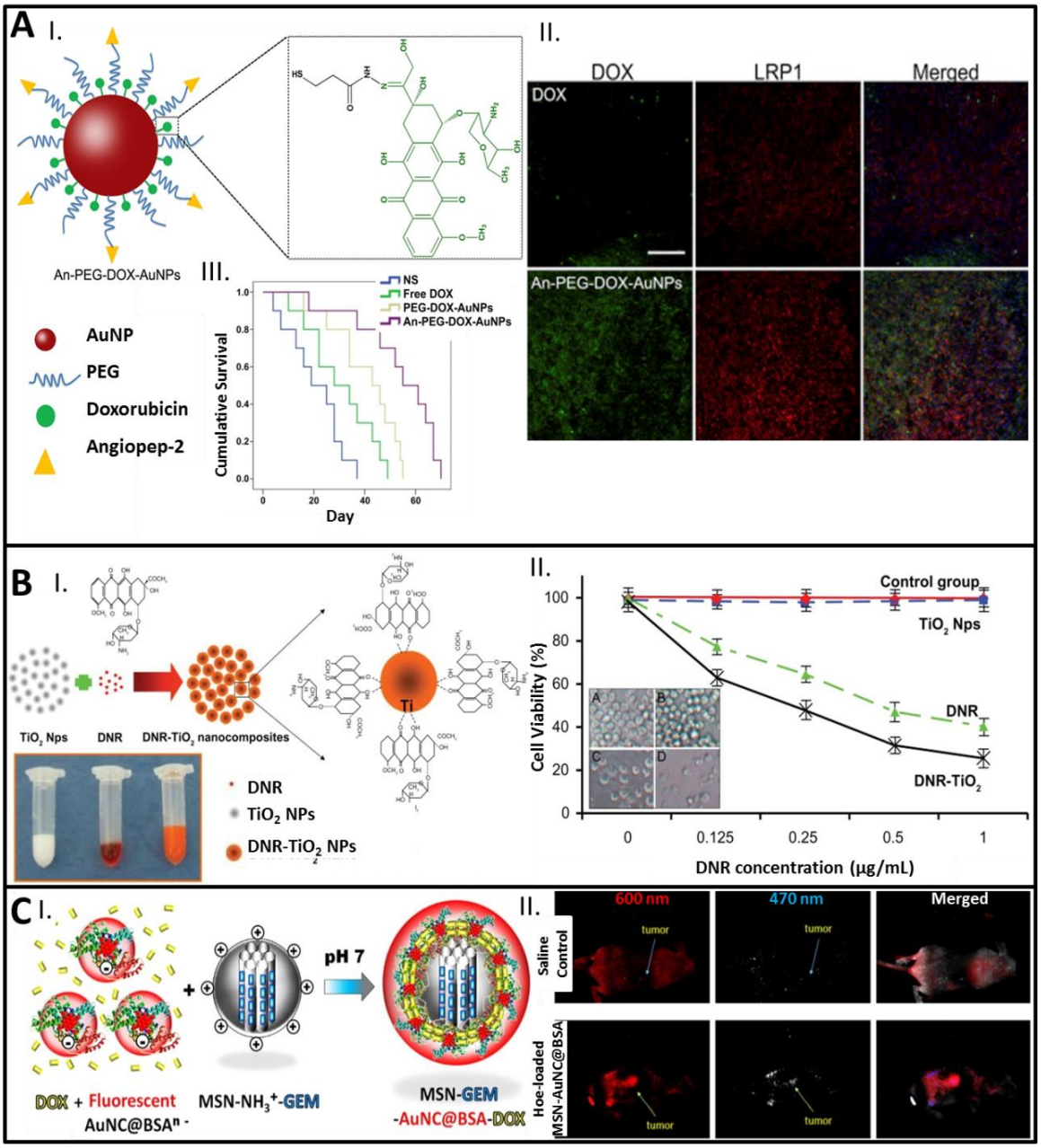

Figure 2: pH-dependent drug delivery from hard NPs. (A) I. Schematic illustration of PEGylated gold NPs (AuNPs) coated with angiopep-2 and appended with DOX via a pH-sensitive hydrazone linker for delivery in C6 glioma bearing mice. II. In vivo DOX accumulation was significantly higher in LRP-1 positive glioma cells 4h after delivery of the complex compared to drug alone. III. Survival studies showed improved survival for mice treated with complex compared to free drug. Reproduced with permission from [3]. Copyright 2015 Elsevier. (B) I. Schematic depiction of titanium dioxide NPs loaded with daunorubicin (DNR) via metal affinity and electrostatic interactions. Low pH disrupts the attachment, facilitating rapid release of the drug. II. In vitro studies in K562 leukemia cells demonstrates higher toxicity of the complex compared to the free drug and minimal side effects of the NPs without drug. Reproduced with permission from [8]. Copyright 2012 Dove Medical Press. (C) I. Schematic of mesoporous silica NPs (MSN) loaded with gemcitabine (GEM), and capped with DOX-loaded Au nanocrystals (AuNC) coated with bovine serum albumin (BSA). II. *In vivo* studies demonstrated improved uptake and fluorescence in MiaPaca-2 tumor-bearing mice. Reproduced with permission from [10].Copyright 2016 Elsevier.

In addition, DOX was loaded in the core and FA was conjugated on the surface for active

cancer cell targeting. After internalization of the complex, low endosomal pH led to protonation of secondary amines along the PEI backbone, resulting in dissociation and dissolution of the PEI chain and pH-dependent release of the drug. Studies done in buffer showed ~30% increase in drug release at pH 5.0 buffer compared to pH 7.4. Additionally, cell viability assays showed comparable toxicity for the targeted complex compared to the free drug. The authors attributed this to DOX's ability to diffuse into cells faster than the endocytosis-mediated internalization of the NPs. Similarly, Croissant et al. used electrostatic interactions between negatively charged gold nanoclusters (AuNCs) conjugated to bovine serum albumin (BSA) and ammonium-functionalized mesoporous silica NPs (MSN) to trap the chemotherapeutic gemcitabine (GEM) in the pores of the MSN (Figure 2C).[10] DOX was incorporated at the AuNC-BSA surface through electrostatic interactions between the drug and BSA. BSA has a pKa around 4.8, so low pH (<5) facilitates release of both drugs through dissociation of the BSA layer from the AuNC-BSA NP, releasing the DOX from the AuNC and the GEM from the pores of the MSN. Buffer studies confirmed the pH-dependent release of both drugs, and cell viability assays in A549 cells showed improved toxicity for dual drug delivery compared to either drug alone. Additionally, use of the fluorescent AuNCs in the shell allowed for *in vivo* tracking and biodistribution studies in MiaPaca-2 tumor-bearing mice and confirmed the preferential uptake of the complex in the tumor compared to other organs.

Redox state

The cellular cytosol is a strong reducing environment with glutathione (GSH) concentrations as high as ~10 mM. Accordingly, disulfide linkages have been used in various formats as the basis of reduction-mediated sensing schemes as well as for drug

delivery.[78-80] In addition, the GSH concentration is often much higher in the extracellular matrix of cancer cells compared to normal blood plasma, and this has been proposed as a mechanism for controlled drug release and also as a potential means by which to preferentially screen for cancer cells within populations of normal cells.[81-83] The most prevalent method for achieving intracellular, GSH-mediated drug release from hard NPs is through the attachment of the therapeutic cargo to the surface of the NP via a disulfide bond. Ding and coworkers fabricated paclitaxel (PTX) dual PTX/PEG conjugates of AuNPs for drug delivery in the presence of both esterases and GSH (Figure 3A).[1] In this system, PTX was bound to PEG via an ester bond and PEG was bound to the surface of the AuNP via a disulfide bond. The ester linkage afforded specificity for esterases present in the cancer cell environment whereas PEG conferred NP stability. *In vivo* studies in Heps tumor-bearing mice showed higher survival and slower tumor growth for the AuNP complex compared to free drug or saline, confirming the therapeutic effect of dual-stimuli release. Additionally, redox-responsive polymers have been used to simultaneously encapsulate hard NPs and entrap drugs, resulting in a hybrid multifunctional NP for GSH-responsive drug delivery. Parida and coworkers coated 50-60 nm GNRs with a redox-responsive block copolymer, PEG-b-poly-N-hydroxylethylacylamide (PHEA), functionalized with lipoic acid (LA) and FA.[84] Also encapsulated was the highly hydrophobic cervical cancer drug, GW627368X, which functions by inhibiting proliferation and inducing apoptosis by interfering with prostaglandin E4 receptor (EP4)/epidermal growth factor receptor (EGFR) interactive signaling. The extracellular environment in the tumor milieu triggers cleavage of the disulfide bond, thus releasing the chemotherapeutic. Use of GNRs enabled PTT (*vide infra*) in combination with drug release

in murine models, resulting in minimal tumor growth for combination therapy, even after 4 weeks. In another example combining PTT and redox-triggered drug release, Zhang and coworkers synthesized mesoporous silica-coated AuNRs loaded with a photosensitizer ($TMPyP_4$), where the MSN pores were gated with sulfide-bound silver (Figure 3B).[6] Close proximity of the photosensitizer in the complex inhibits both its fluorescence and its ability to generate reactive oxygen species (ROS), mediated by energy transfer. The presence of GSH triggers drug release through cleavage of the silver-sulfide bond, resulting in a dual PDT/PTT system. Additionally, attachment of the aptamer AS1411 ensures high targeting specificity to cancer cells expressing nucleolin. In *in vitro* assays, delivery of the NP complex and NIR irradiation demonstrated high toxicity in cancer cells and low toxicity in control cells.

In addition to mediating drug release, high cytosolic GSH can also assist in the reduction/conversion of nontoxic prodrugs into their toxic form. An excellent example of this is reductive elimination of the axial ligands of platinum (Pt)(IV) to form Pt(II) in the potent anticancer drug complex, cisplatin.[12, 75, 85] Although cisplatin is highly effective against a wide variety of cancers, its use is often challenging due to significant off-target toxicity and cellular drug resistance. The Pt(IV) prodrug form of cisplatin, however, has the potential for fewer side effects but is known to have poor uptake efficiency due to its high hydrophobicity. Thus, NP-based strategies for the delivery of the Pt(IV) form of cisplatin have been pursued to improve its solubility, achieve cellular targeting, and overcome drug resistance. Dai and coworkers synthesized $NaYF_4:Yb^{3+}/Er^{3+}$ UCNPs coated with PEI bound to Pt(IV) and further coated with PEG/PEG-FA for stability and targeting [85]. In late endosomes, the low pH facilitated the release of the drug into the reducing cytosol

coupled with the conversion Pt(IV) to the active Pt(II) form and DNA binding in the nucleus. *In vitro* studies in HeLa cells demonstrated higher cell killing at lower concentrations for the conjugate compared to the free drug after 48 hrs. Additionally, the location of the complex could be tracked *in vitro* through fluorescence imaging of the UCNPs. Yu and coworkers demonstrated the use of targeted multifunctional iron oxide NPs (IONPs) to overcome cisplatin drug resistance *in vitro* and *in vivo* (Figure 3C).[12] The ~30 nm IONPs were coated with PEI for stability and conjugated to luteinizing hormone-releasing hormone (LHRH) for targeting cancer cells. Onboard, siRNA directed at suppressing drug resistance and the prodrug Pt(IV) were included. Synergistic effects of the siRNA and cisplatin were demonstrated *in vitro*, where the IC_{50} value for the complex in both drug-resistant and drug-sensitive A2780 ovarian cancer cells was low. The free drug, on the other hand, had a ~2.5-fold higher IC_{50} value for the drug-sensitive cell lines, demonstrating the ability of the complex to overcome drug resistance. Additionally, mice treated with the complex had a significantly lower tumor volume compared to mice treated with free drug, confirming the improved therapeutic benefit of dual-drug delivery. Feng and coworkers reported use of dual-activated 5-8 nm carbon dots (CD) conjugated to a RGD peptide for cellular targeting/uptake and to Pt(IV) for anticancer drug delivery.[86] The RGD peptide was bound to PEG via a benzoic-imide bond such that in acidic environments the PEG was cleaved from the complex, revealing the RGD motif to bind to cells and facilitate endocytosis. Release and activation of the drug is then mediated through the low pH in late endosomes/lysosomes and the reducing environment of the cytosol. *In vitro* studies in MDA-MB-231 cells demonstrated a higher cytotoxicity of the complex when incubated at pH 6.8 versus physiological pH, due to increased uptake after exposure of the

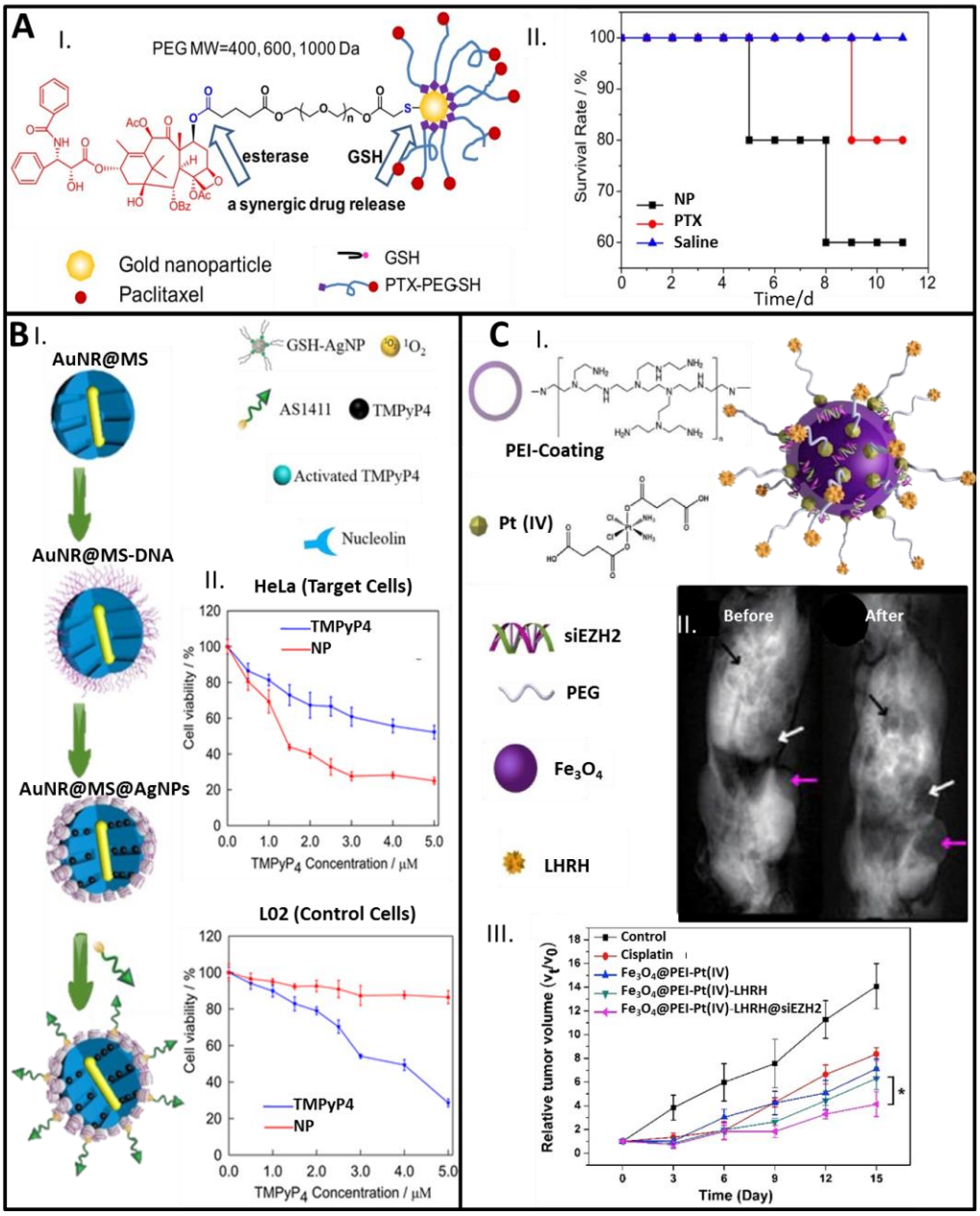

Figure 3: Redox-responsive drug release using hard NPs. (A) I. Schematic of gold NPs capped with glutathione (GSH)- and esterase-sensitive DOX for synergistic release of paclitaxel (PTX). II. Survival studies in Heps xenograft tumor-bearing mice showed improved survival for mice injected with the NPs compared to PTX alone. Reproduced with permission from [1]. Copyright 2013 Elsevier. (B) I. Schematic of mesoporous silica NP (MSN) gated with AuNPs via a sulfide bond and loaded with doxorubicin (DOX) for drug delivery. II. Cell viability assays showed higher toxicity of complex compared to drug in target HeLa cells, but lower toxicity in L02 control cells. Reproduced with permission from [6]. Copyright 2015 ACS Publications. (C) I. Schematic of lutenizing hormone-releasing hormone (LHRH)-targeted Fe_3O_4 NPs coated with a pH-sensitive polymer (PEI) and loaded with Pt(IV), a cisplatin prodrug and siEZH2 (siRNA), to overcome cisplatin resistance. In the cytosol, Pt (IV) is reduced to the more toxic Pt (II) promoting apoptosis and cell death. II. T2 weighted magnetic resonance imaging (MRI) in A2780 cisplatin resistant tumor-bearing mice demonstrated clear contrast enhancement within the tumor site (indicated by arrows) after tail-vein injection of the NP complex. III. Tumor growth studies demonstrated smallest tumor volume for mice treated with the targeted NP complex than for cisplatin alone. Reproduced with permission from [12]. Copyright 2018 Elsevier.

RGD ligand. Comparatively, control cells (MCF-7) that do not express the cognate $\alpha_v\beta_3$ integrin for the peptide showed high viability even at pH 6.8.

Enzymatic cleavage

In addition to the above-mentioned methods of drug release, the cellular environment contains a multitude of enzymes involved in protein digestion (proteases) and ester hydrolysis (esterases), providing another mechanism to actively control cargo release from the surface of hard NP carriers.[87] Protein digestion can occur either through general enzymes found within the cellular environment (such as in endosomes) or through the action of specific enzymes, such as those overexpressed on the membrane or in the cytosol of cancer cells. Cellular esterase enzymes, such as hydrolases, arylsulfatases, and acid phosphatases, are involved in ester hydrolysis of a variety of substrates including ester-link drug conjugates. These enzymes exhibit optimal catalytic activity in endosomes/lysosomes due to the acidic environment found within. As a result, cleavage of the ester bond occurs rapidly and more selectively in low pH compared to neutral environments, proving a ready mechanism for controlled drug release.

Cathepsin-B (CTB), a lysosomal cysteine protease, is known to be overexpressed in many cancer cells and is thus often used for enzyme-responsive drug release.[88-91] One such example is demonstrated by Li and coworkers, who synthesized 40 nm mesoporous silica-coated quantum dots (QDs) loaded with DOX for overcoming MDR (Figure 4A).[4] The NP complex was appended with a nuclear targeting peptide (TAT) and a negatively charged domain consisting of repeating glutamic acid residues. This zwitterionic approach served to enhance NP colloidal stability and the DOX was attached to the QD by a CTB-cleavable peptide linker. After endosomal uptake, CTB cleaved the CTB-responsive peptide,

resulting in release of the negatively charged domain. TAT then targeted the QD to the nucleus and released DOX. Drug release studies in buffer showed improved release both in the presence of enzyme and in acidic conditions (pH 5.5). However, in the presence of enzyme plus a CTB inhibitor, drug release was hindered. *In vitro* cellular uptake demonstrated nuclear localization of both DOX and the QD after 24 hours in both DOX-sensitive (A2780) and DOX-resistant (A2780/ADR) cells. Cell viability assays demonstrated higher toxicity for the complex compared to free drug in multiple CTB-expressing cell lines but lower toxicity in CTB negative cells, thus demonstrating specific response of the complex to CTB. In another study that utilizes CTB, Tian et al. noncovalently attached a photosensitizer, Ce6, bound to a CTB-sensitive peptide (PGFK), to the surface of GO sheets.[91] Coating with DSPE-PEG_{2000}-FA lent stability and cancer cell targeting capabilities to the complex. When in close proximity to the GO sheet, the fluorescence and ROS generation capability of the Ce6 is quenched. After endocytosis, the CTB enzyme cleaved the peptide, resulting in release of Ce6 from the surface, and under 660 nm irradiation, generated ROS, resulting in cell death. *In vivo* distribution in HeLa-tumor bearing mice showed high uptake in the tumor and minimal uptake in other organs. Phototoxicity studies demonstrated a decrease in tumor volume only for the complex plus irradiation; all other controls demonstrated an increase in tumor volume.

In addition to CTB, proteases involved in apoptosis, such as the caspase family of enzymes, have also been used as triggers for drug delivery.[16, 92] Zhao and coworkers (Figure 4B) fabricated UCNPs coated with a caspase-3 cleavable DOX prodrug, a photosensitizer, and cRGD peptide attached to PEG for tumor targeting and stability.[16] NIR irradiation of the UCNP resulted in generation of ROS, triggering the activation of caspase-

3 and release of the drug intracellularly. *In vivo* studies in 4T1 tumor-bearing mice showed a minimal increase in tumor volume for mice treated with complex plus NIR compared to a significant increase for mice treated with drug or NIR plus photosensitizer alone.

Enzymes located on the plasma membrane of cells can also be exploited to control drug release. Furin, a proprotein convertase that cleaves substrates at the Arg-X-Lys/Arg-Arg domain, is known to be overexpressed on the membrane of malignant tumor cells, providing another mechanism for both targeting and controlled release.[93] Jiang and coworkers synthesized a GO-based nanosheet loaded with DOX via pi-pi stacking for furin-dependent drug release.[94] In this system, tumor necrosis factor (TNF)-related apoptosis inducing ligand (TRAIL) was bound to the GO nanosheet via a furin-cleavable peptide attached to a PEG linker. The cytokine TRAIL is known to act on death receptors on the cell membrane for induction of apoptosis and served as a second therapeutic and targeting ligand for the nanocomposite. Upon delivery of the therapeutic, furin on the cell membrane cleaves TRAIL, preventing it from entering the cells. The nanocomposite is then internalized via the endocytic pathway, and the low pH of late endosomes/lysosomes facilitates release of the DOX for nuclear delivery. Release experiments in buffer confirmed furin-dependent release of TRAIL and pH-dependent release of DOX. *In vivo* biodistribution in A549 tumor-bearing mice showed high uptake in tumor, and the complex had decreased tumor volume compared to either drug alone.

Recently, our group reported on the esterase-sensitive release of DOX from the surface of ~5 nm CdSe/ZnS core-shell quantum dots (QDs) (Figure 4C). Here, the DOX moiety was attached to the peptide backbone via an ester bond that is amenable to cleavage by cellular esterase enzymes. Also appended to the surface of the QD was a cell uptake

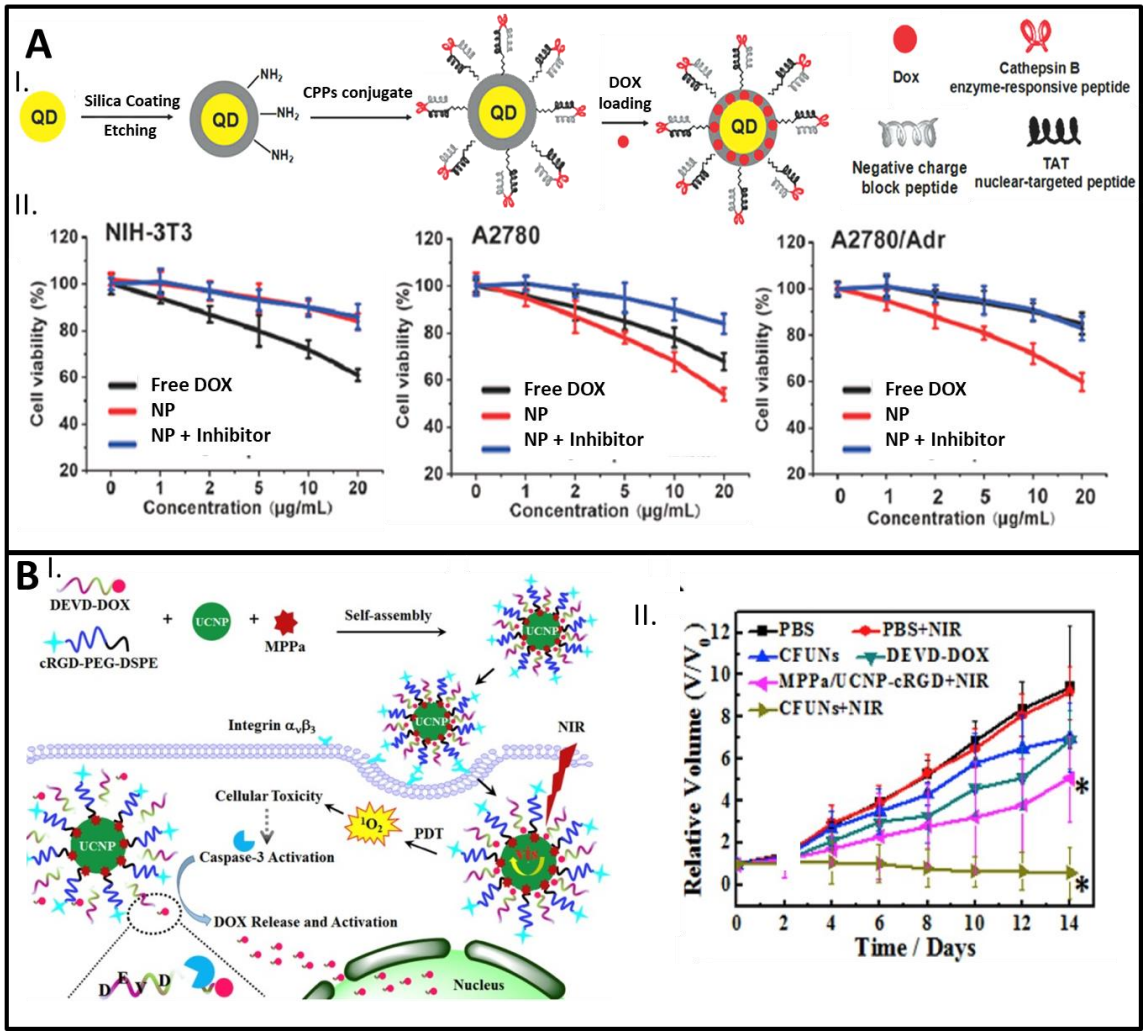

Figure 4: Enzyme-mediated release from hard NPs. (A) I. Schematic illustration of mesoporous silica coated quantum dots (QDs) appended with nuclear targeting peptide (TAT) and cathepsin B enzyme-responsive peptide for overcoming multidrug resistance (MDR) in A2780 tumor cells. II. In vitro cell viability assays in control cells (left) showed minimal toxicity of the NP (red), but high toxicity in both DOX-sensitive (middle) and DOX-resistant (right) cells compared to drug alone. Therapeutic effect of the complex is hindered in the presence of a cathepsin B inhibitor. Reproduced with permission from [4]. Copyright 2014 Wiley-VCH. (B) I. Schematic representation of caspase-sensitive upconversion NPs (UCNPs) capped with cRGD (CFUN) for tumor cell targeting. After internalization into cells, photodynamic therapy (PDT) was used to produce singlet oxygen, resulting in caspase-3 activation and drug release. II. NP delivery plus irradiation (NIR) in 4T1 tumor-bearing resulted in minimal increase in tumor volume after 2 weeks. Reproduced with permission from [16]. Copyright 2017 Elsevier.

peptide, JB434, to facilitate internalization of the QD.[95] In situ experiments in buffer confirmed drug release in the presence of esterase and cytotoxicity assays in HeLa cells demonstrated comparable toxicity to the free drug. Additionally, the use of QD as the scaffold facilitated *in vitro* tracking of the complex over time. Fernando and coworkers

developed MSNs capped with poly(β-amino ester) and loaded with DOX for esterase and pH-dependent release.[96] Drug release studies in buffer resulted in a ~40% increase in DOX release in acidic conditions (pH 5) and a ~50% increase in the presence of esterases, confirming cleavage of the ester bond. Antitoxicity studies in MDA-MB-231 breast cancer cells demonstrated comparable toxicity of the complex to free drug.

Externally-Triggered Drug Release

Magnetic field

Magnetic NP (MNP) drug delivery systems based on hard NP carriers utilize an external magnetic field (MF) to either guide drug delivery or trigger drug release from the NP to the targeted site of action. The most universally accepted type of hard NP used for this application is iron oxide (e.g., Fe_3O_4 and Fe_2O_3), which has been implemented in a variety of uses, including advanced imaging and other biomedical applications, due to its biocompatibility and superparamagnetic properties. In addition to iron oxides alone, ferrites doped with Co^{2+}, Ni^{2+}, and Mn^{2+} have also been developed for magnetic DDS.[8, 97-99] Overall, MNPs are easily incorporated into a variety of DDS, as researchers are able to conjugate drugs directly to the surface of the NP or incorporate them into different nanostructures.

In order to target drug cargo, MNPs can be retained at a region of interest through use of a magnetic field. Jeon and coworkers utilized a system that combined β-cyclodextrin-conjugated superparamagnetic iron oxide NPs (SPIONs) and polymerized PTX in a nano-assembly via multivalent host-guest interactions (Figure 5A).[2] Through use of magnetically guided drug delivery, the NP assembly demonstrated decreased cell viability *in vitro* in three cancer cell lines (HeLa, MCF-7, and CT26), as well as high NP

accumulation within the tumor site and decreased tumor mass in CT26 tumor-bearing murine models. Furthermore, magnetically guided systems can be used to illicit immune responses within the body. Mejias and colleagues encapsulated a ~9 nm magnetite core SPION with dimercaptosuccinic acid as a delivery system for the electrostatically bound antitumorigenic cytokine interferon gamma (IFN-γ).[100] After magnetically targeting the MNP to the tumor site, there was an increase in T cell and macrophage infiltration within the tumor microenvironment, thus providing an antiangiogenic effect resulting in a significant decrease in tumor volume in Pan02 tumor-bearing mice. Combined, these examples demonstrate the versatility of magnetically guided NPs and their potential for developing minimally invasive targeted systems to biological regions of interest.

The use of encapsulating agents to combine MNPs and chemotherapeutics allows the magnetic feature to be applied to multifunctional systems. Lee et al. combined magnetic iron oxide nanocrystals (MIONs) with surface-appended DOX as the therapeutic and with thiol-terminated PEG to facilitate crosslinking.[101] Using magnetically guided brain tumor targeting, the particles were systemically injected and preferentially accumulated to the tumor area in 9L-glioma-bearing rats. During application of an external magnetic field, the particles aggregated, thus increasing the retention of MION clusters within the tumor site, allowing for more effective delivery of chemotherapeutics. In another study, Wei and coworkers developed SPIONs clustered with multiblock polyurethanes (MPU), comprised of PEG and poly(E-caprolactone) PCL, outfitted with a pH-sensitive benzoic-imine linkage that acted as an on-off switch to deliver DOX payloads into tumor cells, as shown in Figure 5B (size, 57 nm).[7] These switchable particles utilize the acidic tumor environment to effectively deliver DOX into the nucleus of HeLa cells. Furthermore, using magnetic

guidance, the NPs demonstrated preferential targeting to specific tumors in murine models implanted with HeLa cell tumors.

Developing multifunctional MNPs for biomedical applications often relies on the magnetic field hyperthermic effect. Compared to other external stimulus techniques, magnetic hyperthermia offers the advantage of localized heating of the tumor tissue, thereby minimizing off-target toxicity. Oh et al. synthesized ~14 nm $CoFe_2O_4$ NPs functionalized with meso-2,3-dimercaptosuccinic acid in order to directly conjugate DOX to the surface of the particle (Figure 5C). Application of an alternating magnetic field (AMF) generated a synergistic effect in MDA-MB-231 cells *in vitro*, combining the toxicity of the chemotherapeutic and hyperthermia of the $CoFe_2O_4$.[14] In addition to direct heating, MNPs can be used to trigger cargo release. In a recent study, Zheng and colleagues developed an AuNR, mesoporous silica and graphene quantum dot (GQD) outfitted with the cell-targeting ligand RGD.[102] Using PTT combined with NIR, the π-π interactions between DOX and the GQD were disrupted, via the hyperthermic properties of the AuNR, and demonstrated differences of release rates with different laser powers. The mesoporous silica also provides a slow release mechanism, which can be coupled with PTT for quick release, in order to control sustained therapeutic efficacy in Hela cells *in vitro*. In another study, Griffete and colleagues used an 11 nm Fe_2O_3 a magnetic particle that was appended to DOX and a molecularly imprinted polymer.[103] Using an AMF, Fe_2O_3 induced local hyperthermia *in vitro* facilitating release of DOX into PC3 cells without causing significant heating to the surrounding media. Hua and coworkers stimulated fluidMAG-CMX particles with covalently appended DOX using an oscillating magnetic field (OMF).[104] During treatment with an OMF, DOX was released from the fluidMAG-CMX particles.

This effect was further demonstrated by growth inhibition in xenograft tumor murine models.

MNPs have also been utilized for controlled release using the combined effects of both MF-induced hyperthermia and pH to release drugs and other biological moieties from the surface while utilizing the particle for magnetic targeting to the area of interest.[103, 105, 106] Alphandery and colleagues recently demonstrated the use of natural endotoxin release in murine glioma models using chains of magnetosomes (CM), a NP that is naturally synthesized from magnetotactic bacteria.[107] Compared to commercially available iron oxide, CM, under alternating magnetic fields, was able to significantly increase survival rates through controlled endotoxin release via magnetic hyperthermia with as little as 10% of the NP occupying overall tumor space. Kaushik and colleagues explored use of magneto-electro carriers (MENCs), which is comprised of $BaTiO_3$@$CoFe_2O_4$ particles, as a method of crossing the BBB noninvasively with the future aim of easily transferring to other drug constructs.[108] It was confirmed that the MENCs could be magnetically guided to the site of interest, and evaluation of toxic side effects and neurobehavioral function in mice injected with the complex showed that the particles did not cause any deleterious impairments. These studies demonstrate the importance of evaluating MNPs for potential toxic effects and the potential constraints hindering use of these NPs in a translational setting.

Photothermal therapy

In recent years, PTT has gained tremendous interest with the use of hard metal NPs, such as Au, Ag, Pt, and Cu, which offer unique advantages due to their absorbance at NIR, ease of surface modification, and ability to engage in hyperthermia/tissue ablation targeted

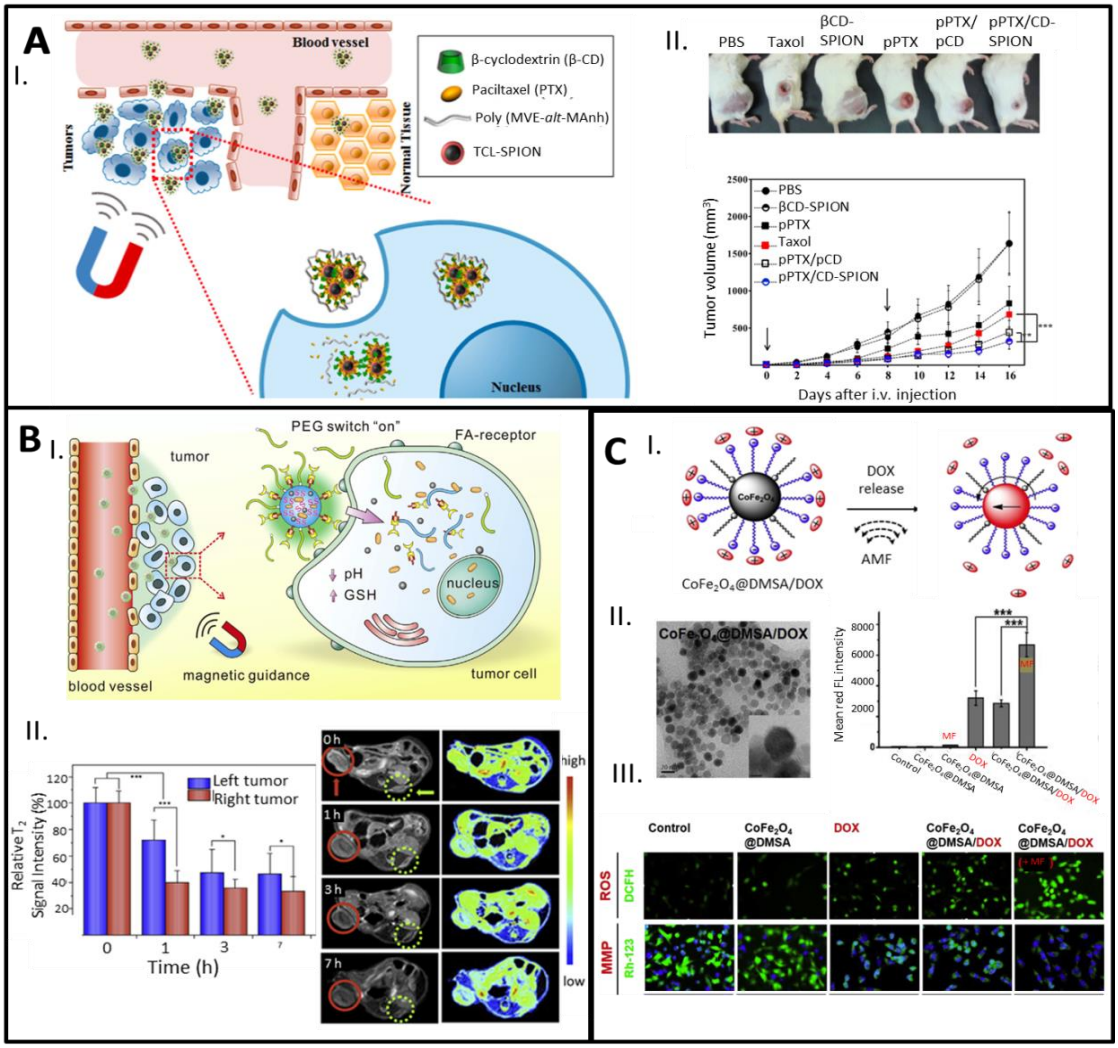

Figure 5: Extracellularly-triggered drug release by applied magnetic field. (A) I. Schematic of the polymerized paclitaxel β-cyclodextran conjugate (pPTX/β-CD)-SPION nano-assembly for magnetic drug delivery/release. II. *In vivo* images (21 days post inoculation) after magnetically guided drug delivery and the tumor volume over 16 days. The arrow indicates injection of sample. Reproduced with permission from [2]. Copyright 2016 Elsevier. (B) I. Schematic of PEG targeting and release properties of multiblock polyurethane nanocarriers with magnetic guidance. II. Relative T2 signal intensity as a function of time of HeLa cell tumors in mice after intravascular injection of NPs loaded with SPIONs and application of an external magnet aligned with the right tumor (left). *In vivo* T2-weigthed MR images of the mice (right). Reproduced with permission from [7]. Copyright 2017 Elsevier. (C) I. Schematic of $CoFe_2O4$@meso-2,3-dimercaptosuccinic acid (DMSA)/DOX NPs for the release of electrostatically assembled DOX induced by alternating magnetic field (AMF). II. TEM of 13 nm CoFe2O4@DMSA/DOX (left). Scale bar, 20 nm; scale bar (inset), 5 nm. Plot of flow cytometry fluorescence intensity of MDA-MB-231 cells incubated with DOX, CoFe2O4@DMSA or CoFe2O4@DMSA/DOX with and without magnetic treatment (right). III. MDA-MB-231 cells after free drug/ NP treatment with or without magnetic field (MF). Reactive oxygen species (ROS) generation was measured with the ROS indicator, 2`,7`-dichlorodihydrofluorescein diacetate, DCFH-DA and loss of mitochondrial membrane potential was measured with Rhodamine 123 (Rh-123). Nuclei are stained with Hoechst 33342 (blue). Reproduced with permission from [14]. Copyright 2017 Elsevier.

to specific tissues/cell. Using a combinatorial approach of PTT and delivery of

chemotherapeutics offers the benefit of providing both dosing and spatiotemporal control at the target site, minimizing off-site effects. Poudel and coworkers used a ~69 nm combinatorial hollow gold nanoshell to load bortezomib and GEM for PTT-mediated drug release in pancreatic cancer cell lines *in vitro* (Figure 6A).[5] With the addition of NIR, particles diffused into the cytosol, enabling efficient drug release in the cell. Wang and colleagues engineered an AuNR with both targeting abilities through use of the peptide sequence RGD and gene delivery through condensation of plasmonic DNA on the surface of the NP.[109] Laser irradiation of the AuNR facilitated both endosomal escape via the proton sponge effect and release of plasmonic DNA once entering into the cytosol of U87 glioma cells. As these examples demonstrate, targeted release via NIR is a unique way to overcome entrapment within endosomes, a common limitation in drug delivery techniques.

Another strategy for delivering hard NPs into tumors for PTT relies on the EPR effect. These particles are designed to accumulate within solid tumors, based on their size, and thus increase retention time, but are ultimately small enough (<5.5 nm) to undergo renal clearance. In addition, NPs with hybrid structures, that often include micelles or liposomes, have the ability to break down after PTT treatment, resulting in effective therapy and limited long-term side effects. These structures differ from the decorated nanoshells, as they typically implement a single nanoparticle for directed drug release from the surface. Rengan and coworkers developed an NP that utilized 5 nm gold seeds on a liposomal surface that induced a photothermal response to facilitate drug release in breast cancer cells *in vitro* resulting in a significant decrease in viability.[110]

Tumor targeting cells that are able to transport large quantities of hard NPs to the tumor site can be used to increase PTT efficiency while minimizing off-target effects, such as

retention of drugs in the liver and kidneys, where many NPs often accumulate in addition to the tumor site. Yanlei Liu and colleagues loaded ~86 nm (length) AuNRs into human-induced pluripotent stem (iPS) cells (Figure 6B).[9] The AuNRs were loaded with the conjugated antibody of CXCR4, which is expressed on the iPS cell surface. The iPS cells possess the ability to migrate to the tumor site, which increases retention time and distribution of the cells within the tumor tissue. After establishing the iPS cells loaded with the AuNR construct within the tumor environment, the tumors were subject to PTT, to induce hyperthermia via the AuNR, thus killing the iPS carrier and the surrounding tumor tissue in MCG-803 tumor-bearing mice. In another study, Zhibin Li and coworkers coated silica AuNRs with BSA in order to increase uptake into macrophages.[111] The Au-loaded macrophages were then directly injected into the tumor, which resulted in an increase in apoptosis upon PTT treatment in addition to a complete regression of the tumor as demonstrated in HepG2 xenografts.

NPs can also provide further control of drug delivery using pH-sensitive moieties.[84, 112] Zhang and colleagues used Au@Sio2 embedded with poly(N-isopropylacrylamide polymer nanocomposites, which were both thermal- and pH-responsive.[113] The polymer undergoes condensation to a hydrophobic globule in the presence of heat via PTT, thus providing the ability to control drug release from the NP, after particle accumulation within the tumor site. *In vivo* studies in 4T1 tumor-bearing mice demonstrated an increase in tumor inhibition rate compared to drug alone. In a similar study using low pH, Luo and colleagues were able to demonstrate the effect of gold-coated liposomes to facilitate pH- and photo-responsive release.[114] Utilizing the EPR effect of the solid tumor, the gold nanoshell-coated

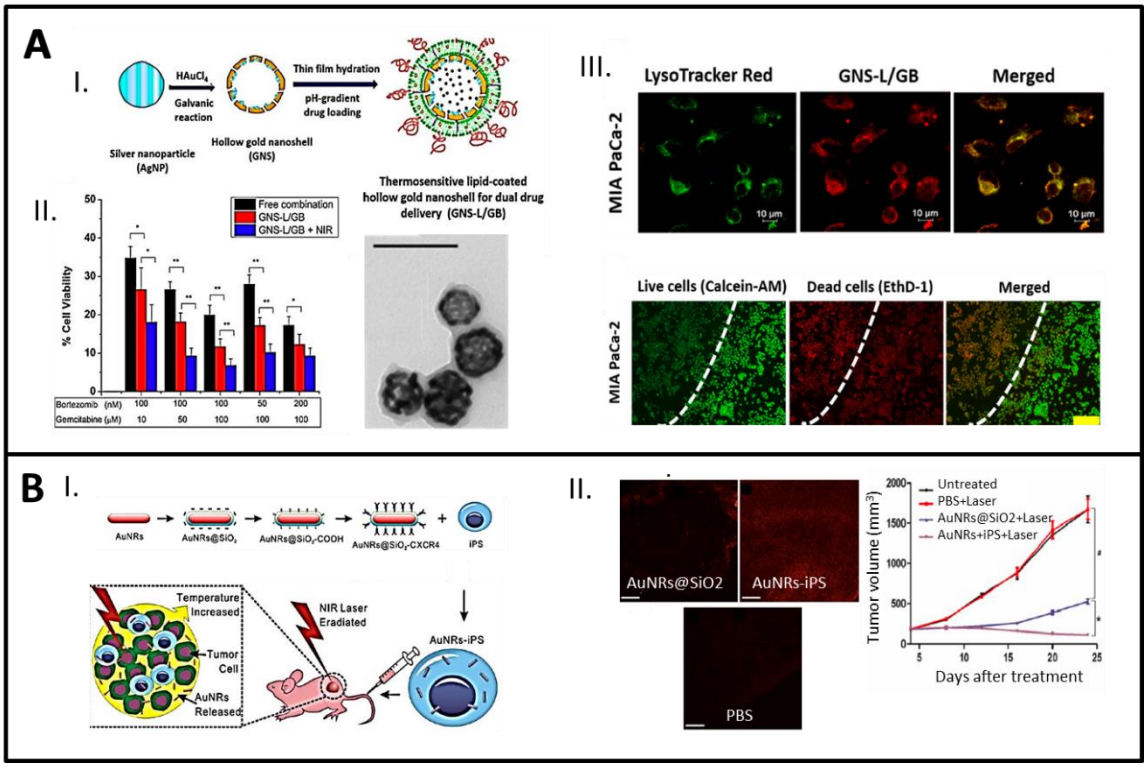

Figure 6: NIR-mediated extracellularly-triggered drug release. (A) I. Synthesis of lipid-coated, hollow gold nanoshells loaded with with bortezomib and gemcitabine (GNS-L/GB). II. Cellular viability of MIA PaCa-2 cells treated with free drug combinations or NP with or without NIR irradiation (left). TEM images of GNS-L (right). III. Confocal microscopy images of fluorescein-labeled NPs in MIA PaCa-2 cells (green) and stained with Lysotracker Red. IV. With or without NIR treatment (dashed line) stained with Calcein-AM (live cells, green) and EthD-1 (dead cells, red). Reproduced with permission from [5]. Copyright 2017 Elsevier. (B) I. Synthesis of AuNRs@SiO2@CXCR4, loaded into Human iPS cells, and injected into mice for NIR treatment. II. Two-photon laser scanning confocal microscopy images of a tumor section 5 days after injection (left). Scale bar, 200 μm. Tumor volume after laser irradiation ($^{\#}P < 0.01$, $^{*}P < 0.05$ (right). Reproduced with permission from [9] . Copyright 2016 American Chemical Society.

oleanolic acid liposomes (GNOL) begin to disassociate due to the lowered pH of the tumor environment. This effect, however, is enhanced in the presence of an 808 NIR laser, which photothermally activates the gold shell to release the drug within the tumor. *In vivo* results in U14 tumor-bearing mice demonstrated slowest tumor growth for mice treated with the GNOL plus laser compared to the controls. To demonstrate the potential for direct drug attachment to solid NPs, Zhang and colleagues appended DNA intercalated with DOX directly onto the surface of an AuNR.[113] The AuNRs are able to release DOX through both low pH within the tumor environment and photothermal effects from the PTT, providing a

synergistic effect with model multidrug resistant (MCF-7/ADR) and drug sensitive (MCF-7) breast cancer cell lines. These results suggest that dual stimuli-responsive release provides an effective method to combat resistant tumors.

Understanding the long-term fate of plasmonic PTT is a critical issue that requires evaluation of biological effects and interactions *in vivo*. To address this, Ali and colleagues investigated the effects of PTT of two different-sized AuNRs conjugated to the chemotherapeutic rifampicin for 15 months after initial administration in a head and neck squamous cell carcinoma xenograft model.[115] Growth studies demonstrated minimal increase in tumor volume for mice treated with the NP plus laser compared to the control. In addition to *in vivo* studies, the group also implemented proteomics experiments to measure differences in protein expression levels in tumor tissues, which indicated that apoptotic-related pathways were significantly regulated after treatment with the NP compared to control groups.

Ultrasound

The use of focused ultrasound has been FDA approved to ablate uterine fibroids and has shown the potential for applications to a variety of diseased states as a targeted noninvasive technique that could be used synergistically with other treatments.[116-118] Hard NPs offer the added benefit of increased stability of the drug during treatment, in addition to high efficacy at the site of interest due to enhanced sono-sensitization. Paris and coworkers developed MSNs that release drug in the presence of ultrasound through coating with a copolymer that was able to open or close upon ultrasound treatment (Figure 7A).[11] At low temperature, the copolymer allowed for loading with DOX to encase the chemotherapeutic and upon ultrasound treatment *in vitro*, significant changes in the

viability, demonstrated controlled release using an external field. Additionally, NPs targeted to the region of interest have greater efficacy at lower powers compared to ultrasound treatment alone.[119] This effect has been shown recently by Chertok and Langer, who loaded heparin-functionalized iron oxide NPs on the surface of microbubbles (MagMB) that are able to circulate systemically due to the presence of heparin, a nonimmunogenic polysaccharide.[120] Upon magnetic field stimulation, the NPs are directed to toward the tumors and found to be concentrated within the tumor vasculature. Furthermore, Cy5.5 dye delivery was triggered with applied ultrasound, resulting in significantly enhanced accumulation at the tumor site in lung carcinoma–bearing mice, thus demonstrating the potential application for enhanced delivery of therapeutics.

The use of focused ultrasound and microbubbles to temporarily disrupt the BBB to enable passage of larger therapeutics for treatment of brain diseases has the potential for a noninvasive and reliable method for drug delivery with clinical trials in progress [121-123]. Fan and colleagues encapsulated SPION and DOX within microbubbles for enhanced targeting across the BBB.[124] The NPs facilitated a 2-fold increase in delivery of DOX to tumors in C-6 glioma-bearing mice in addition to the ability to be imaged using magnetic resonance imaging (MRI) due to the presence of the SPION. Magnetic resonance–guided focused ultrasound (MRgFUS) can also be utilized for targeted treatment. Timbie and coworkers applied this technique to deliver brain-penetrating NPs outfitted with the chemotherapeutic cisplatin.[125] Treatment in 9L and P98 glioma-bearing mice demonstrated a significant increase in accumulation and decrease in tumor growth for mice treated with the NP complex compared to the control

Irradiation

Radiation therapy, specifically gamma and X-ray, is generally effective in the treatment of solid tumors and is included in many cancer treatment regimens. Researchers have used hard NPs with a high Z number, which can act as radio-sensitizers at the treatment site; this offers the advantage of lower radiation dose, and due to the NPs inherent characteristics provides an opportunity for simultaneous treatment options. AuNPs have also been extensively studied for radiotherapies due to their capability for efficient EPR, which can be used to facilitate NP accumulation within the target area. Kim and coworkers used a core/shell NP to simultaneously deliver AuNPs and DOX coated with pluronic-F68, a triblock copolymer of poly(ethylene oxide)– poly(propylene oxide)–poly(ethylene oxide) (PEO–PPO–PEO) [126]. Delivery in squamous cell carcinoma-bearing mice demonstrated enhanced tumor accumulation 3 days after injection and significant reduction in tumor growth compared to the control. Su and colleagues developed ~45 nm PEG-covered AuNPs conjugated to a cyclic RGD peptide with radioactive iodine-125, as a tumor-targeted radio-sensitizer [127]. Treatment with the NPs directly at the tumor site of NCI-H466 tumor-bearing mice demonstrated significant decrease in tumor volume when compared to radiotherapy alone. These results demonstrate the potential for combinational approaches for tumor reduction. Song and colleagues implemented hollow tantalum oxide (TaO) coupled with the chemotherapeutic drug 7-ethyl-10-hydroxycamptothecin (SN-38) (Figure 7B).[128] X-ray radiation after delivery of the NP in 4TA murine breast cancer cells elicited a radio-sensitization effect from the TaO while inducing cell cycle arrest after SN-38 release. In another application utilizing particles coloaded with a chemotherapeutic, Ma and coworkers coated Bi_2S_3 NPs with mesoporous silica and loaded with DOX (BMSNs)

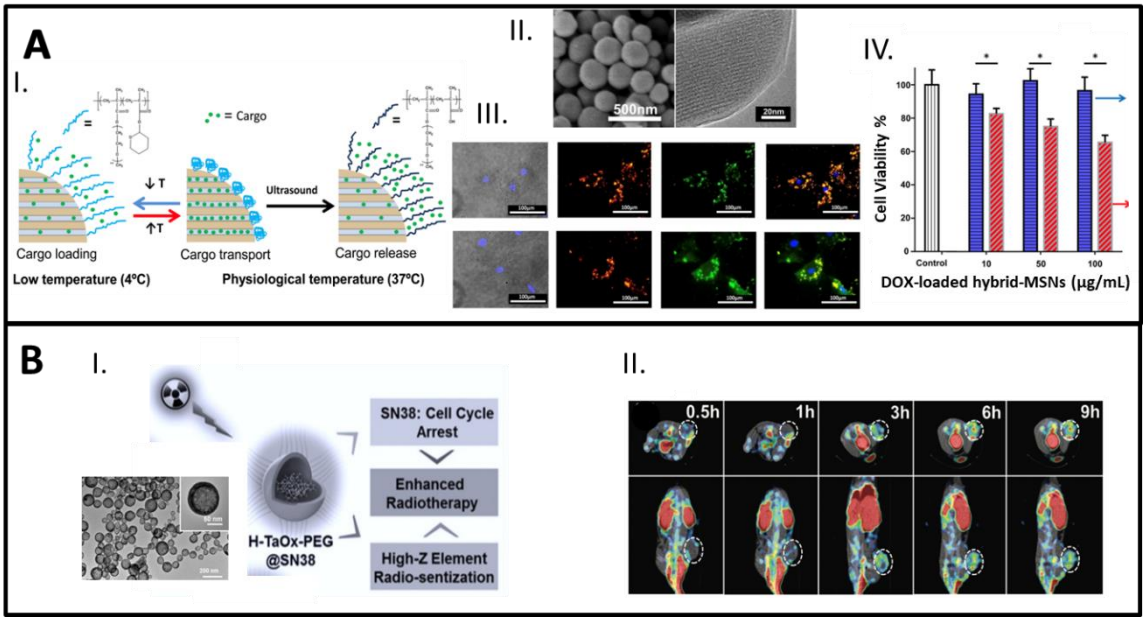

Figure 7: Ultrasound and Radiation triggered release. (A) I. Schematic of the loading and release system of Dox loaded-MSNs. II. SEM images and TEM micrographs of NPs. III. Fluorescence microscopy images of LNCaP cells (nuclei in blue) with RhodamineB-labeled hybrid-MSNs (red) with loaded fluorescein (green) before (top) and after (bottom) ultrasound irradiation. IV. Cytotoxicity assay of LNCaP cells with different concentrations of DOX-MSNs with (red) and without (blue) ultrasound. Reproduced with permission from [11]. Copyright 2015 ACS Nano (B) TEM images of H-TaOx nanoshells. II. SPECT images of a representative 4T1 tumor-bearing post i.v. injection of NP complex. Reproduced with permission from [13]. Copyright 2015 Wiley-VCH.

to establish a significant therapeutic effect against MDR cancer cells. *In vitro* studies indicated that X-ray irradiation was significant enough to result in synergistic cytotoxicity, and *in vivo* treatment resulted in decreased tumor sizes compared to the controls.[13] Additionally, under the effects of interstitial phosphorus-32 (P-32)-enriched gelatin chromic phosphate colloid as an alternate method of radiotherapy, delivery of both P-32 and BMSNs simultaneously demonstrated increased toxicity against PC3 cells compared to no significant toxicity with P-32 alone. These results suggest that combinatorial treatments with chemotherapy and interstitial radiotherapy are a promising treatment regimen for MDR cells.

Conclusion

Advances in the development and understanding of actively controlled release from the

surface of hard NPs have the potential to improve therapeutic efficacy, due to the inherent beneficial properties of these NPs. As clinical use of NPs currently relies on soft NPs and passive methods of actuation, there is low spatiotemporal control over drug release. Active actuation using novel "smart" DDS, however, has the potential to controllably release drug cargo, thus minimizing toxic side effects to healthy tissue, which overcomes the limitations of traditional therapy. Thus the goal of the work presented in this dissertation is to use a model hard NP system in order to address some of the current challenges facing use of hard NMDD and to develop a fundamental understanding controlled release from hard NPs.

Chapter 3: Intracellularly-Actuated Quantum Dot-Peptide-Doxorubicin Nanobioconjugates for Controlled Drug Delivery via the Endocytic Pathway[† 95]

Introduction

Due to the multitude of side effects that result from non-specific systemic delivery of drugs, imaging agents, and other cargos, there has been a lot of interest in controlling the release of NP-associated cargo in order to better modulate toxicity. We address this issue here in the context of a prototypical hard NP carrier, a QD, which is used to control the intracellular delivery and release of the chemotherapeutic DOX. The prototypical system used here has direct relevance to cancer therapy and the fundamental lessons learned here can be transferable to drug cargos directed against other therapeutic targets.

DOX is an FDA-approved cancer therapeutic that has been shown to be effective for the treatment of a variety of cancers.[129] It functions by intercalating into DNA, inhibiting the action of topoisomerase II (the enzyme responsible for unwinding supercoiled DNA), thus inhibiting DNA replication and eventually leading to cell death.[129-131] However, the repeated, systemic administration of DOX is problematic due to its significant nonspecific uptake by non-cancerous cells and off-target toxicity. One of the primary side effects of the systemic administration of DOX is cardiac toxicity, which limits the utility of this otherwise very potent anti-cancer drug.[132-134] Thus, there is wide interest in understanding to what extent DOX toxicity can be modulated once delivered to cells.

[†]Reprinted with permission from Sangtani, A., Petryayeva, E., Wu, M., Susumu, K., Oh, E., Huston, A.L., Lasarte-Aragonés, G., Medintz, I.L., Algar, W.R., Delehanty, J.B., (2017). Intracellularly Actuated Quantum Dot–Peptide–Doxorubicin Nanobioconjugates for Controlled Drug Delivery via the Endocytic Pathway. *Bioconjugate Chemistry*, 29(1), 136-148. Copyright 2018 American Chemical Society.

The delivery of NPs into cells primarily occurs via the endocytic pathway, usually through the attachment of a cell-penetrating peptide (CPP), leading to sequestration of NPs within vesicles and ultimately limiting their therapeutic capabilities.[135-139] Thus, the chief challenge currently facing the implementation of hard NPs in therapeutic drug delivery is the design of drug attachment chemistries that can be actively triggered for temporal control over drug release. In developing a hard NP-mediated, actively triggered cargo delivery system, there are several desirable characteristics that the system should ideally possess. These include: (1) ease of NP synthesis, drug introduction, and delivery to cells, (2) intracellular stability and biocompatibility of the native NP (no drug payload), (3) tracking of the NP–drug ensemble for real-time monitoring of drug delivery, (4) the ability to mediate actively triggered drug release, and (5) the ability to controllably modulate the toxicity of the on-board drug cargo. Of considerable importance here is the method of bioconjugation used to control the number of "copies" of appended active drugs and biologicals on the hard NP surface. Approaches here have ranged, for example, from the use of electrostatic and hydrophobic interactions[140] to the covalent attachment of discrete numbers of antibodies to the surface of colloidal AuNPs. Equally important is the method used to affect drug release and there are several examples demonstrating the controlled release of drug cargos from the surface of hard NPs.[141, 142] For example, Gollavelli et al. bound the photosensitizer, silicon napthalocyanine bis (trihexylsilyloxide) ($SiNc_4$), noncovalently to magnetic and fluorescent graphene nanocarriers.[143] Photoirradiation with a halogen lamp caused activation of the drug resulting in generation of reactive oxygen species, leading to cell death. Similarly, Niu et al. developed channeled mesoporous silica nanocomposites containing UCNPs and Au nanocrystals noncovalently associated with the

cancer chemotherapeutic, doxorubicin (DOX).[144] NIR laser excitation of the UCNPs caused a plasmonic-enhanced release of DOX from the Au nanocrystals. While both examples demonstrate active actuation, they are dependent upon the application of an external light stimulus, which is limited in terms of its depth of tissue penetration[145] and can have potential phototoxic effects away from the point of drug delivery. Alternatively, hard NP systems, wherein drug release is triggered by intracellular processes, could circumvent these issues.

In this study, we have used a luminescent semiconductor QD as a prototypical hard NP to develop a multifunctional hard NP–peptide-drug conjugate platform for combined cell uptake and drug delivery. Our primary goal was to evaluate methods of intracellularly-triggered actuation to overcome limited drug release due to sequestration of NP-appended drugs within endosomes. Here, the QD serves as a central scaffold onto which are self-assembled multiple copies of a CPP to drive uptake via endocytic pathway. Also attached to the QD are drug attachment peptides bearing various chemical linkages (ester, disulfide, and hydrazone) that are responsive to intracellular stimuli (esterases, reducing conditions, and low pH, respectively) for the purpose of active release of DOX from endosomal compartments. Both the CPP and drug-attachment peptides are appended to the surface of the QD using histidine-mediated metal affinity, which allows for ratiometric tuning of the number of peptides on the QD surface.[146] This allows for the controlled tuning of the CPP: drug cargo peptide ratio, enabling the use of a minimal number of CPPs while maximizing the concentration of delivered drug. Finally, the fluorescence of the QD scaffold and DOX cargo enables real-time monitoring of the intracellular location of the ensemble construct and its dissociation.

We present photophysical characterization of the QD–[peptide–DOX]–CPP system both in buffered solution outside the cellular environment and when interfaced with cells *in vitro*. Our data clearly demonstrate that the toxicity of the drug can be controlled by changing the chemistry used to append the peptide–DOX cargo to the surface of the QD. Analytical gel electrophoresis and dynamic light scattering (DLS) demonstrated the successful ratiometric assembly of the constructs and microplate-based Förster resonance energy transfer (FRET) studies confirmed functionality of the peptidyl linkages. Cellular delivery and uptake experiments tracked the residence of the complexes in the endocytic pathway and distinct differences among the various peptide–DOX conjugates are noted. Cytotoxicity studies were performed to determine the modulation of drug toxicity by varying the linkages. After endosomal uptake, the disulfide linkage showed negligible DOX release, while the hydrazone linkage showed a modest degree of time-dependent release of the drug. The ester linkage, however, demonstrated release kinetics and accompanying cellular toxicity that were comparable to free DOX delivered from bulk solution. We interpret our findings in the context of previous studies that have utilized various attachment chemistries to mediate active drug release, particularly from the surface of hard NP carriers. The work described here details basic concepts for the design of "smart" hard NP materials for intracellularly triggered, active release of surface-appended drug cargos. Additionally, our results point to important design considerations that must be taken into account when designing NP systems for delivery of drugs via the endocytic pathway.

Materials and Methods

Materials

Dulbecco's phosphate buffered saline (D-PBS), Dulbecco's Modified Eagle's Medium containing 25 mM HEPES (4-(2-hydroxyethyl)-1-piperazinethanesulfonic acid) (DMEM-HEPES), phosphate buffered saline (PBS), and nickel-nitrilotriacetic acid (Ni-NTA) agarose resin were obtained from ThermoFisher, (Carlsbad, CA). 96-well cell culture cluster microtiter plates were purchased from Corning-Costar (Corning, NY). Doxorubicin hydrochloride (DOX), *N,N*-dimethlyformamide (DMF), dimethyl sulfoxide (DMSO), Tris-borate-ethylenediaminetetraacetic acid (EDTA) buffer solution, *N*-hydroxysuccinimide (NHS), diisopropylcarbodiimide, 4-(dimethylamino)pyridine (DMAP), *N,N*-diisopropylethylamine (DIPEA), tris(2-carboxyethyl)phosphine hydrochloride (TCEP), tetrahydrofuran (THF), 3,3′-dithiodipropionic acid di(*N*-hydroxysuccinimide) ester (DSP), and imidazole were acquired from Sigma. All other materials/reagents were obtained as noted in the text.

QD synthesis

CdSe-ZnS core-shell QD nanocrystals with emission maxima centered at 520 and 545 nm were synthesized using a high temperature reaction of organometallic precursors and were rendered hydrophilic by exchanging the native trioctylphosphine/trioctylphosphine oxide (TOP/TOPO) capping shell with CL4 or dihydrolipoic acid DHLA-$(PEG)_{750}$-OMeligands, respectively, as described previously.[147, 148] The QDs are identified by their wavelength of maximum emission, e.g., a sample of 545 nm QDs designates a population of QDs which exhibits maximum photoluminescence centered at 545 nm.

Transmission electron microscopy

Structural characterization of as-prepared QDs was carried out using a JEOL JEM-2100 FE-TEM, field-emission gun transmission electron microscope. Samples were prepared by spreading a drop (~5 μL of 1 μM QD solution in deionized water) of the filtered QD dispersion (0.25 μm Millipore filter) onto ultrathin holey carbon support film on a 300 mesh Au grid (Ted Pella, Inc.) and letting it dry. Individual particle sizes were measured using a Gatan Digital Micrograph (Pleasanton, CA); average sizes along with standard deviations were extracted from analysis of ~100 nanoparticles.

Synthesis of peptides and peptide-DOX conjugates and characterization

For synthesis of all peptide-DOX conjugates (*vide infra*), the sequence of the peptide used was GNNGAAAA-Aib-AAAA-Aib-GLGHHHHHH-amide (Biosynthesis, Inc.) where Aib is alpha aminoisobutyric acid and the amide blocks the C-terminal carboxyl group. In all cases, the doxorubicin used was doxorubicin hydrochloride. The *N*-terminal amine on the peptide is available and reactive for conjugation to the cognate modified DOX as described below.

DOX-amide peptide. The *N*-terminal primary amine on the peptide was conjugated to the primary amine on DOX. The peptide was first pre-bound to Ni (II)-NTA purification media. The bound peptide was then activated with a 500-fold excess of the homobifunctional linker BS^3, bis(sulfosuccinimidyl)suberate (ThermoFisher), which was dissolved in 70% PBS/30% DMSO and passed over the media using 5 mL syringes 20 times. The activated peptide was washed with PBS and then exposed to 100-fold excess DOX dissolved in 70% PBS/30% DMSO for 15 mins by also passing over the media with syringes. The labeled peptide was then washed with PBS, eluted from the Ni-NTA media

with 300 mM imidazole in 30% DMSO and desalted as described previously.[149]The DOX-labeled peptide was further purified and the conjugation confirmed using an Acquity ultra performance liquid chromatograph (UPLC H-Class) System equipped with a SQ2 Mass Spectral Detector (Waters, Milford, MA) as described elsewhere.[150]

DOX-disulfide peptide. The *N*-terminal primary amine on the peptide was first converted to a disulfide-COOH by sequential reaction of the peptide with DSP and borate buffer. The converted peptide was purified on Ni-NTA agarose media and then reacted with NHS and diisopropylcarbodiimide to conjugate the converted –COOH on the peptide to the primary amine on DOX. The resulting product was purified on Ni-NTA media.

DOX-ester peptide. Glycolic acid (10 mmol) and NHS (11 mmol) were dissolved in 30 mL of THF, the flask purged with argon, and cooled in an ice bath. diisopropylcarbodiimide (11 mmol) in 20 mL of THF was added dropwise to the reaction mixture, which was further stirred for 4 h at room temperature. The product was recrystallized from isopropanol at –20 ^{o}C overnight, collected by filtration, washed with ether, redissolved in 15 mL of dichloromethane and the filtrate collected and dried under vacuum to yield glycolic acid-NHS ester. The peptide was dissolved in 100 μL of anhydrous DMF and mixed with 50 μL of 0.1 M solution (5 μmol) of glycolic acid-NHS ester. The reaction mixture was stirred for 4 h at room temperature and then diluted with 5 mL of PBS (pH 7.2) and purified using Ni-NTA as described above. The purified peptide from the previous step was dissolved in 200 μL of DMF and mixed with succinic acid (17.2 mg, 0.147 mmol) dissolved in 800 μL of DMF. Diisopropylcarbodiimide (2 μL, 13 μmol) and DMAP (0.82 μmol) where then added and the reaction was stirred at room temperature overnight. The reaction mixture was diluted with 5 mL of PBS (pH 7.2) and purified with

Ni-NTA. The purified peptide-ester-COOH was dissolved in 200 μL of DMF and mixed with 3.87 μL of a 0.129 M solution of diisopropylcarbodiimide (0.5 μmol) in DMF and 2.4 μL of a 0.209 M solution of NHS (0.5 μmol) in DMF. The reaction was stirred for 2 h at room temperature. After this time, 1 mg of DOX dissolved in 600 μL of DMF and 5 μL of DIPEA were added and the reaction left in the dark to mix at room temperature overnight. The reaction mixture was diluted to 5 mL with PBS and purified on Ni-NTA media.

DOX-hydrazone peptide. The *N*-terminal primary amine on the peptide was first converted to a thiol (-SH) function by sequential reaction with DSP and TCEP. The modified peptide was then purified using Ni-NTA media. Hydrazone-maleimide-functionalized DOX (suitable for reaction with the –SH on the modified peptide) was generated by reaction of DOX with *N*-[ε-maleimidocaproic acid] hydrazide, trifluoroacetic acid salt (Thermo Fisher).[151] The product was recrystallized from acetonitrile and dried *in vacuo*. The peptide-SH was dissolved in 100 μL of DMF and mixed with the purified DOX-hydrazone-maleimide (600 μL of DMF) and reacted overnight. The reaction was diluted with PBS and the resulting product was purified on Ni-NTA media.

JB434. The CPP, JB434, (R_9GGLA(Aib)SGWKH_6) used in this study is described elsewhere.[152] The polyarginine tract (R_9) that mediates cellular uptake is separated from the polyhistidine tract (H_6) (for peptide self-assembly to the QD surface) by a linker domain (GGLA(Aib)SGWK). Peptide synthesis was performed using Boc-solid phase peptide synthesis, purified by HPLC and characterized by electrospray ionization mass spectroscopy.[47, 153]

Assessment of QD-peptide-DOX bioconjugate assembly and functionality

To confirm the successful assembly of the peptide-DOX conjugates to the QD, gel electrophoresis (1% agarose) was performed on the QD alone and the QD-peptide-DOX complexes. To the individual wells of an agarose gel were added 520 nm CL4–capped QDs (5 pmol) that was pre-assembled (20 min at RT) with varying ratios of peptide-DOX (up to 60/QD). All samples were prepared in PBS buffer. Electrophoresis was performed for 30 minutes at 95 volts/10 cm. A BioRad ChemiDoc XRS+ imaging system was used to image the gels. Dynamic light scattering (DLS) analysis was also performed to confirm successful bioconjugate assembly. Measurements were carried out using a ZetaSizer NanoSeries equipped with a HeNe laser source (λ = 633 nm) (Malvern Instruments Ltd) and analyzed using Dispersion Technology Software (DTS, Malvern Instruments Ltd). 545 nm PEG_{750}-OMe-capped QDs (30 nM) were pre-assembled with a ratio of 50 peptide-DOX for 2 h at RT and then loaded into disposable cells, and data were collected at 25°C. All the samples were prepared in 0.1x PBS buffer pH 7.4. For each sample, the autocorrelation function was the average of five runs of 10 s each and then repeated three to six times. CONTIN analysis was then used to determine number *versus* hydrodynamic size profiles for the dispersions studied.[154]

The functionality of the assembled QD-peptide-DOX conjugates was assessed using a microplate-based Förster resonance energy transfer (FRET) assay. 520 nm CL4–capped QDs (7.5 pmol) were assembled with a varying ratio of peptide-DOX conjugates (up to 40 per QD) in PBS for 20 min at RT. QDs with emission at 520 nm were used for this assay as there is significant spectral overlap between the QD's emission and DOX absorbance. The QD-peptide-DOX conjugate system was excited at 400 nm (Tecan Infinite

M1000) and spectra was collected between 450-650 nm. Appropriate control solutions of QD donor alone and DOX acceptor alone were included to correct for the effect of the various incubation conditions on QD donor photoluminescence (PL) and direct excitation of the DOX acceptor, respectively. Results were analyzed using Excel and FRET efficiency was calculated using the following equation:

$$FRET_E = 1 - \left(\frac{F_{da}}{F_d}\right)$$

where F_{da} is the fluorescence intensity of the QD donor (d) in the presence of the DOX acceptor (a) and F_d is the fluorescence intensity of the QD donor (d) alone. After FRET between the QD donor and DOX acceptor was confirmed, 520 nm CL4–capped QDs (7.5 pmol) were assembled with a ratio of 30 peptide-DOX. QD-peptide-DOX assemblies were then subjected to reducing conditions (for DOX-disulfide), esterase enzyme (for DOX-ester), or acidic pH (for DOX-hydrazone). A ratio of 30 peptides per QD was used because preliminary studies showed efficient FRET at this peptide:QD ratio. For DOX-disulfide, 10 mmol of TCEP, a reducing agent, was added after complex formation. For DOX-ester, 0.03 µmole of esterase from porcine liver (Sigma) was added to solution after complex formation. For DOX-hydrazone, the pH of the solution was reduced to ~5.0 by adding HCl after complex formation. The DOX-amide was used as a control for each condition.

Cellular culture

HeLa cells (American Type Culture Collection (ATCC)) were cultured in complete growth medium (Eagle's Minimum Essential Medium (MEM; ATCC)) supplemented with 10% (v/v) heat inactivated fetal bovine serum (ATCC), 1% (v/v) antibiotic/antimycotic (Sigma) and 1 mM sodium pyruvate (Sigma). Cultures were maintained in T25 flasks and incubated

at 37ºC under a 5% CO_2 humidified atmosphere and passaged every 2-3 days at 80% confluency. All cells used in this study were used between passages 3 and 15.

Cellular delivery of QD-JB434-peptide-DOX conjugates

For delivery experiments, HeLa cells were seeded on MatTek™ 14 mm dishes (Ashland, MA) that were pre-coated with 30 µg/mL fibronectin (ThermoFisher) for 2h. Cells were seeded at 6.5×10^4 cells/mL and allowed to adhere overnight. Prior to addition of materials for cellular delivery, the cells were washed twice with DMEM-HEPES. Initial cell delivery experiments were performed to determine the optimal QD concentration and the minimum number of JB434 cell uptake peptides required to mediate efficient labeling of endosomes with minimal cytotoxicity.[47, 152] QDs (at concentrations of 100 nM or 200 nM) were assembled with varying ratios of JB434 peptide (up to 25 per QD) in DMEM-HEPES for 30 min at RT. The QD-JB434 complexes were incubated on cell monolayers for 1 h at 37ºC. The cells were washed twice with D-PBS and fixed using 4% paraformaldehyde then imaged using confocal microscopy (*vide infra*). Image analysis was used to plot the pixel intensity of selected regions of interest vs. QD concentration. This analysis revealed that a concentration of 200 nM QD and a ratio of 15 peptides per QD provided sufficient cellular uptake, while still leaving ample room on the QD surface for peptide-DOX conjugates. For DOX delivery, 200 nM QD was complexed with JB434 peptides (15 peptides per QD) and with peptide-DOX (30 peptides per QD) in DMEM-HEPES for 30 minutes at RT.[47, 152, 155] The complexes were then incubated on cells for 2 h at 37ºC. After 2 h, the cells were washed twice with DMEM-HEPES and incubated with 100 µg/mL of endosomal marker (transferrin conjugated to AlexaFluor-647 (AF647-Tf))

for 30 min at 37ºC. Cells were washed twice with DPBS and fixed with 4% paraformaldehyde and then imaged.

Quantification of cellular cytotoxicity

Cellular cytotoxicity was determined using the CellTiter 96® AQueous One Solution Cell Proliferation Assay (Promega, WI).[156, 157] This assay is a colorimetric method for determining the number of viable cells after incubation with a material of interest. HeLa cells were seeded in a 96-well tissue culture microplate at a density of 5000 cells/well (doubling time ~24hrs) and allowed to grow overnight. QDs were assembled with JB434 peptides (15/QD) and with peptide-DOX at ratios varying from 2.5/QD to 40/QD in DMEM-HEPES for 30 minutes at RT (corresponding to DOX concentrations ranging from 0.5 µM to 8 µM). QD complexes were then incubated on cells for 2 h at 37ºC. After incubation, the QD-containing solution was replaced with complete media and the cells were allowed to proliferate under standard culture conditions for 72 h. To each well, 20 µL of a solution containing a tetrazolium compound, 3-(4,5-dimethylthiazol-2-yl)-5-(3-carboxymethoxyphenyl)-2-(4-sulfophenyl)-2H-tetrazolium (MTS), was added and incubated with the cells for 6 h. Viable cells convert the MTS into a formazan product that absorbs at 590 nm. Absorbance was read at 590 nm and 700 nm (for background subtraction) using a Tecan Infinite M1000 dual monochromator multifunction plate reader equipped with a xenon flash lamp (Tecan). Results were reported as a percentage of cellular viability, normalized to control wells of cells cultured alone. QD alone, JB434 peptide alone, and QD-JB434 complex (all at the same corresponding concentrations) were included as controls.[156, 157]

Microscopy and image analysis

All imaging was performed using a Nikon A1RSi Laser Scanning Confocal Imaging system. The following imaging settings were used (laser excitation/ dichroic/ emission range): QD, 405 nm/488 nm/500-550 nm; DOX, 561 nm/561 nm/570-620 nm, AF647-Tf, 639 nm/640 nm/663-738 nm. Each channel was imaged sequentially to prevent bleed-through between the channels. Quantification of cellular uptake of QDs and colocalization analysis was done using NIS-Elements AR (ver. 4.30.02). Images were prepared for publication using the same software. Colocalization analysis was done using Pearson's correlation coefficient (PCC) and was used to determine colocalization between QD and DOX, QD and AF647-Tf, and DOX and AF647-Tf. PCC, which ranges from -1 to 1, measures the strength of the linear relationship between two variables.[158] It can be applied to a variety of systems, but in the work described herein, it is used to measure the overlap in signal between the two channels being tested. For image analysis, images were taken as stacks to encompass the whole cell volume and colocalization analysis was conducted on the entire stack.

Results and Discussion

Rationale of QD-peptide-DOX cell uptake/drug delivery system

Our goal in this study was to develop a hard NP-based bioconjugate drug delivery platform that could cumulatively do the following: 1-enter cells *via* the endocytic pathway; 2-allow for tunable control over drug cargo concentration in the formed conjugate; 3-actively release the appended drug cargo to the cytosol from within endosomes in response to intracellular stimuli; 4-avail real-time tracking of both the NP carrier and the drug

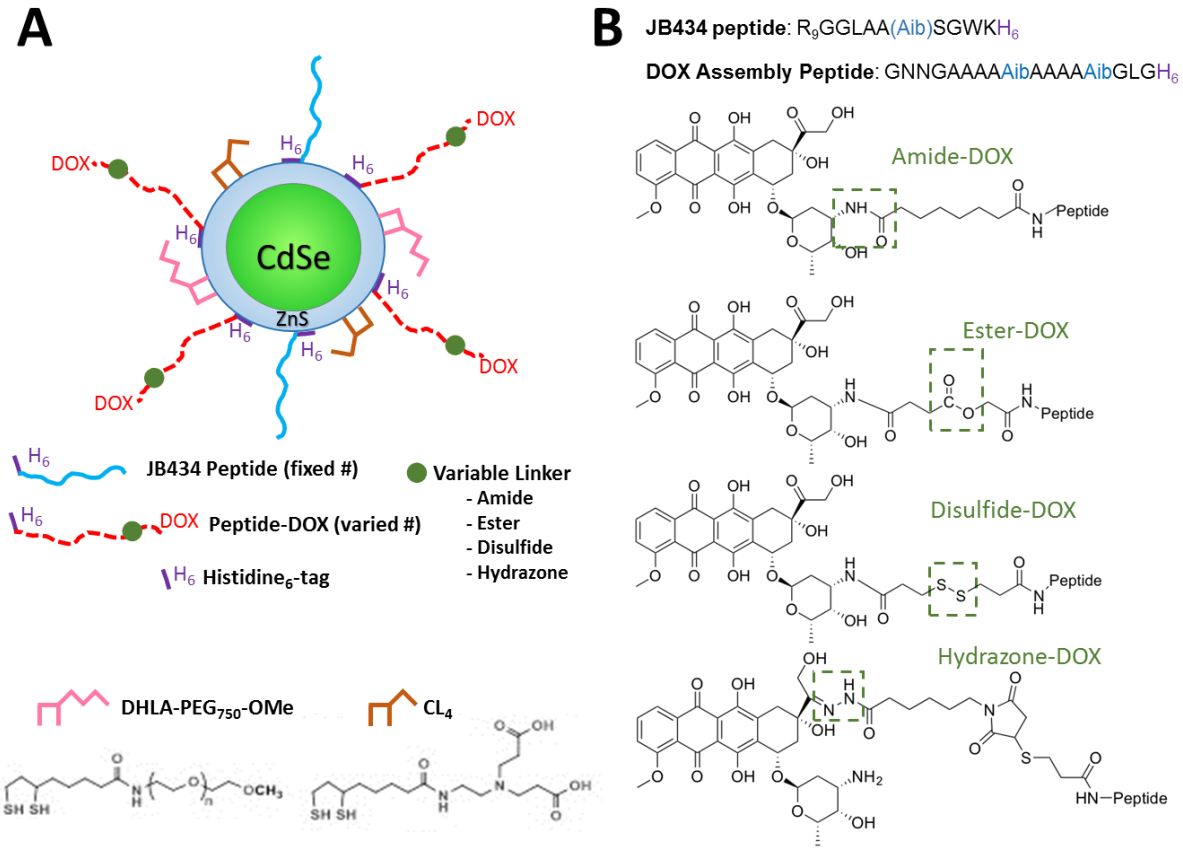

Figure 8: Schematic of the QD-peptide-DOX bioconjugate system. A) Schematic of CdSe-ZnS core-shell QD capped with either DHLA-PEG$_{750}$-OMe or CL4 ligands. QDs are appended with a fixed number of JB434 cell uptake peptides and a varying number of peptide-DOX conjugates. PEGylated QDs were used for cell delivery experiments while CL4-capped QDs were used to functionally test the reactivity of the cell-responsive chemical linkages as described in Methods. **B)** Peptide sequences and chemical structures of the various peptide-DOX conjugates used herein. The JB434 cell uptake peptide has been described elsewhere.[15] The linkage of DOX to the *N*-terminal glycine of the assembly peptide varies between amide, ester, disulfide, and hydrazone. In both peptides, the *C*-terminal his tag on the peptide mediates self-assembly to the surface of the QD.

payload, and 5-elicit minimal cytotoxicity prior to drug release. To achieve this, we employed a QD as a central scaffold onto which was assembled two different species of peptide (Figure 8A). The first peptide used was a CPP, JB434, to drive cellular uptake of the bioconjugate via the endocytic pathway. This peptide, comprised of the sequence R$_9$GGLAA(Aib)SGWKH$_6$, is based on the HIV-TAT peptide, bears an *N*-terminal polyarginine tract (R$_9$) to promote electrostatic interactions with the negatively-charged cell surface, and has been used extensively for the cellular delivery of various NP materials.[15, 155, 159, 160] The second peptide species was a drug assembly peptide with the

sequence GNNGAAAA(Aib)AAAA(Aib)GLGH_6 to which was attached (at the *N*-terminal glycine residue) the chemotherapeutic, DOX, through various reactive/cleavable chemical linkages. Importantly, both peptides have at their *C*-terminus a six-histidine motif (H_6) that drives the self-assembly of the peptide to the QD surface via metal affinity coordination to the ZnS shell.

The polyhistidine-based assembly process plays two important roles in the context of the drug delivery system. First, it allows for ratiometric control over the number of each peptide species assembled to the QD surface. This concept has been demonstrated extensively in previous studies on the interfacing of QD-peptide conjugates with cells.[47, 48, 152, 161-165] This control is critical as it allows for optimal balance between a minimal number of CPPs while allowing for the cellular delivery of a range of DOX concentrations in the form of DOX appended to drug assembly peptides (*vide infra*). Second, we have previously shown the QD:his-peptide association to be stable within the endolysosomal pathway for up to 3 days in cultured cells.[15, 152, 155] This feature, coupled with the fluorescence emission of the central QD scaffold and the DOX cargo, enables time-resolved tracking of the NP-drug assemblies throughout the drug delivery process.

The specific reactive linkages used to attach DOX to the drug assembly peptide included disulfide, ester, and hydrazone linkages as well as a nonreactive amide linkage, used as a control (Figure 8B). These chemistries were specifically chosen to take advantage of various cellular physiological states to mediate the release of DOX from the QD surface. Disulfides can be efficiently reduced by the high cytosolic GSH concentration (~10 mM).[79, 82, 166, 167] Ester linkages can be cleaved by cellular esterases such as those found in

Table 1: Physicochemical properties of peptides used in this study

Properties/Sample	DOX Assembly Peptide	Amide-DOX	Disulfide-DOX	Ester-DOX	Hydrazone-DOX	JB434
Molecular weight	2146.30	2829.99	2866.06	2831.92	2987.19	3159.36
pI[2,3]	8.2					13.0
Peptide charge at pH 7.4[2,3]	0.6					10.5
Hydrophobicity Index[1,3]	-0.26					-2.29

[1]Determined using GPMAW protein bioinformatics tool (www.expasy.org), [2]Determined using PepCalc peptide calculator (www.pepcalc.com), [3]Calculated by substituting alanine (Ala) for aminoisobutyric (Aib)

endosomal compartments.[96, 168] Hydrazone linkages can be hydrolyzed by the low pH environment found in the endolysosomal pathway.[169-171] Additional information on the physicochemical properties of the peptides used herein can be found in Table 1.

Assessment of QD-peptide-DOX assembly and functionality

We first sought to confirm the successful assembly of the DOX delivery peptides to the QD surface. To do this experiment, we used 520 nm QDs capped with CL4 ligands. This ligand bears two carboxyls and imparts sufficient negative charge to the QD surface such that they migrate towards the positively-charged anode during gel electrophoresis. Figure 9A shows the results of gel electrophoresis analysis of these QD complexes assembled with increasing ratios of peptide-DOX. It was apparent that, across all four peptide linkage chemistries, the degree of migration of the complexes toward the anode tracked inversely with increasing numbers of peptide-DOX assembled onto the QD surface, indicating successful attachment of peptides to the surface of the QDs.[162-164, 172] Figure 10 shows TEM images of the QDs used in this study.

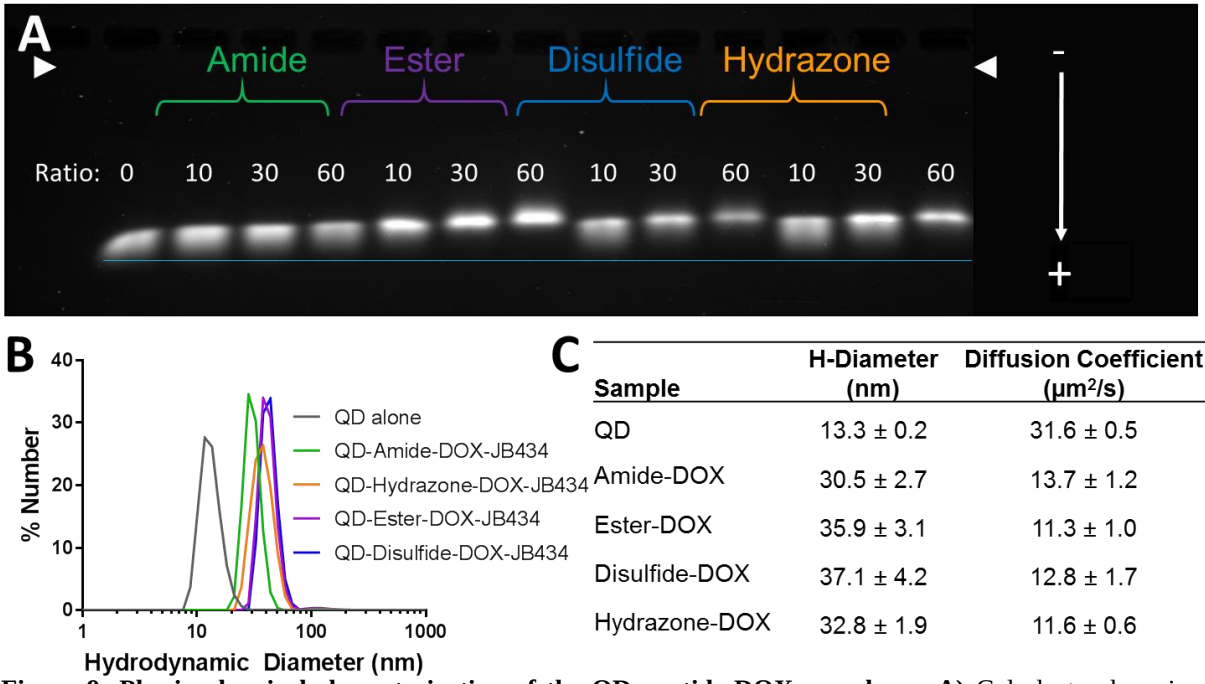

Sample	H-Diameter (nm)	Diffusion Coefficient ($\mu m^2/s$)
QD	13.3 ± 0.2	31.6 ± 0.5
Amide-DOX	30.5 ± 2.7	13.7 ± 1.2
Ester-DOX	35.9 ± 3.1	11.3 ± 1.0
Disulfide-DOX	37.1 ± 4.2	12.8 ± 1.7
Hydrazone-DOX	32.8 ± 1.9	11.6 ± 0.6

Figure 9: Physicochemical characterization of the QD-peptide-DOX complexes. A) Gel electrophoresis of CL4-capped QDs assembled with increasing ratios of peptide-DOX bearing different chemical linkages. White arrows indicate the location of sample loading wells. The blue line shows the location of the migration front of the QDs alone. **B, C)** Size distribution, average hydrodynamic diameter, and diffusion coefficient of DHLA-PEG_{750}-OMe-capped QDs and QD-peptide-DOX complexes containing 50 peptide-DOX/QD as measured by DLS. QD-peptide-DOX complexes were allowed to form for 2 h prior to analysis.

As a second method of confirmation of attachment, we performed DLS analysis on the 545 nm QD-peptide-DOX conjugates. [157] In this instance, the QDs were capped with DHLA-PEG_{750}-OMe ligands. Ultimately PEGylated QDs would be employed for the cellular drug delivery experiments and it was critical to confirm that the terminal polyhistidine motif of the peptide-DOX conjugates could coordinate to the QD surface with this ligand. As shown in Figure 9B, when ~50 peptide-DOX were complexed with the QDs for 2 h, a significant increase in the hydrodynamic diameter of the resulting assemblies was observed. In addition, there was a reduction in the diffusion coefficient for each of the QD-peptide-DOX complexes (Figure 9C). This result is consistent with our multiple previous studies that have shown the efficient self-assembly of a myriad of peptide species

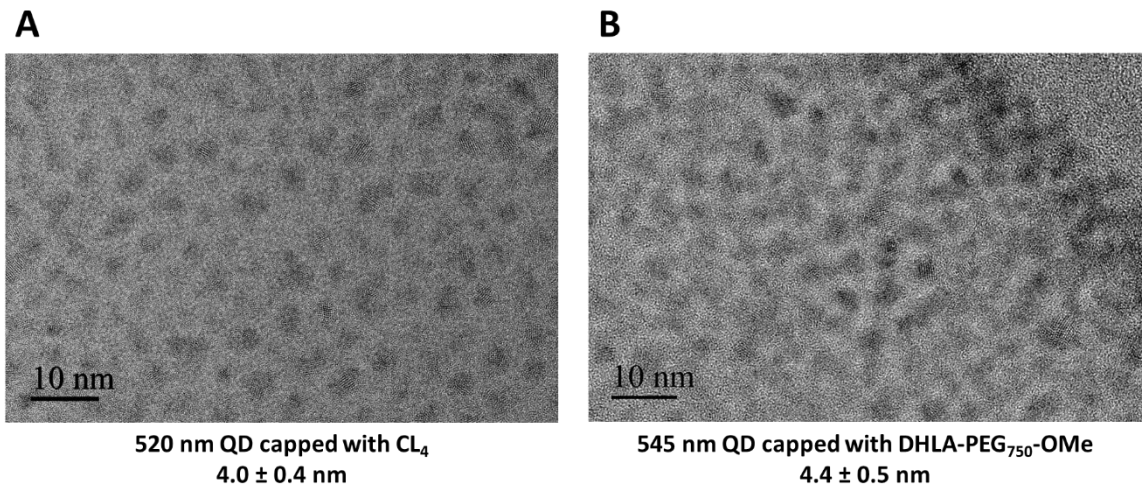

Figure 10: Transmission electron micrographs (TEM) of QD samples used in this study. TEM analysis of A) 520 nm-emitting QDs capped with CL_4 and B) 545 nm-emitting QDs capped with DHLA-PEG_{750}-OMe. The average diameter of the 520 nm and 545 nm QDs were 4.0 ± 0.4 nm and 4.4 ± 0.5 nm, respectively**.**

conjugated to the surface of PEGylated QDs via metal affinity coordination interactions.[15, 152, 155, 157, 161]

We next assessed the responsivity of the QD-peptide-DOX assemblies to their intended respective cellular stimuli/conditions. To accomplish this, a FRET-based assay system was developed wherein the peptide-DOX was assembled onto a QD donor that was suitable for the pendant DOX acceptor. Here, 520 nm-emitting QDs capped with CL4 ligands were used as 1) they are bright (Quantum yield (QY) = 0.4), 2) their emission has significant spectral overlap with DOX absorption, and 3) their small size (dia. 4.0 nm ± 0.4; see SI figure S1) and short CL4 capping ligands afford efficient FRET from the QD donor to the DOX acceptor (Förster Radius (R_0) = ~3.5 nm) (Figure 11A). Upon assembly to the QDs, the peptide-DOX species exhibited FRET efficiencies that were higher than that seen for QD with the free drug. Interestingly, the FRET efficiency for the hydrazone-DOX (~40%) was higher than that of the other three linkages (disulfide, ester and amide, ~20%), suggesting closer association of the DOX moiety to the QD surface in the context

of this peptide (Figure 8, Figure 11C). The attachment of DOX at a different site on the drug and the accompanying spacer could result in folding that reduces the donor-acceptor distance by bringing the DOX closer to the QD surface, yielding the increased observed FRET efficiency. Functional assays showed the hydrazone- and ester-DOX conjugates to be functional in response to their respective stimuli. Lowering of the pH from 7.4 to 5.0 resulted in a ~20% decrease in FRET efficiency for the hydrazone construct while for the esterase construct, incubation with a porcine esterase enzyme reduced the FRET response by more than 50% (Figure 11D). The disulfide-DOX conjugate system, however, showed a negligible decrease in FRET in response to incubation with the reducing agent TCEP (data not shown). In this instance, the free thiol-terminated DOX generated via reduction could potentially rebind to the QD surface, maintaining efficient FRET.[173]

Quantification and optimization of cellular uptake of QD-JB434 conjugates

Having confirmed the controlled assembly of the complexes and the functionality of the various chemical linkages, we next sought to determine the optimal QD concentration required for uptake and visualization of the QD-peptide complexes in living HeLa cells. Here, it was necessary to balance a sufficient number of JB434 CPPs, to facilitate cellular uptake, with adequate doses of DOX in the form of peptide-DOX, to enable cell death. For this purpose we employed 545 nm QDs (final concentration, 200 nM) capped with DHLA-PEG_{750}-OMe because PEGylation is known to improve the

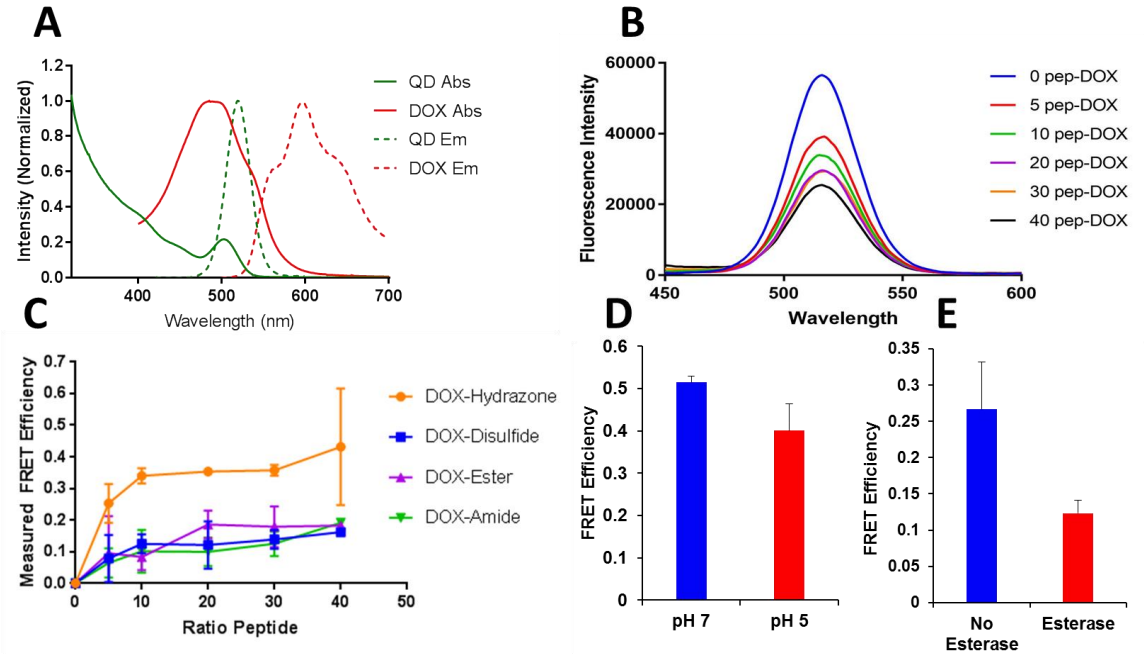

Figure 11. Spectral properties of QD and peptide-DOX and functional responsivity of QD-peptide determined by FRET. A) Normalized absorption and emission spectra of 520 nm-emitting CL4-capped QDs and DOX in water. The calculated R_0 for the FRET pair is 3.5 nm. B) Spectral response showing ratiometric-dependent FRET quenching of QD by hydrazone-DOX. C) Experimentally determined FRET efficiency for the various QD-peptide-DOX systems. Experimentally determined FRET efficiency for (D) QD-hydrazone-DOX complex in neutral (pH 7.4) and acidic (pH 5) environments and (E) QD-ester-DOX in the presence and absence of esterase. The experiment was performed using assemblies that had 30 peptide-DOX per QD. All experiments were done in triplicate.

biocompatibility and stability of the QD in physiological environments and has been shown to minimize nonspecific binding for a variety of NPs.[174, 175] The slightly larger 545 nm QDs were chosen as the delivery scaffold for the present study as they afford sufficient surface area to balance the delivery peptides with the peptide-DOX drug cargo (see Figure 10 for TEM images). In previous studies, we have shown that the maximal number of peptides that can be assembled through his-mediated interactions onto the surface of 545 nm QDs is ~50 ± 10 peptides.[164] Occupying the QD surface with ~15 JB434 peptides affords loading of as many as 35-40 peptide-DOX peptides which corresponds to solution DOX concentrations as high as 8 μM (for 200nM QD). This concentration is ~5-10-fold above the reported IC_{50} for free DOX in many cultured cell lines, including HeLa cells.[176-178]

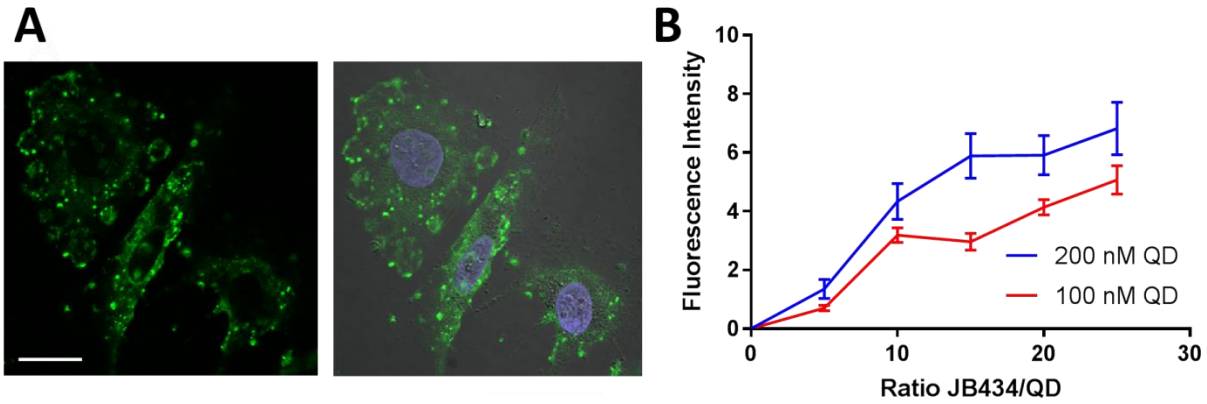

Figure 12: Initial quantification of cellular delivery and uptake of QD-JB434 complexes. A) HeLa cells were incubated with pre-formed QD-JB434 complexes at QD concentrations of either 100 nM or 200 nM and varying JB434 ratio (0 – 25) for 1 h at 37°C. Images were obtained using confocal laser scanning microscopy. Scale bar, 20 µm. **B)** Comparative quantitative analysis of QD uptake. Fluorescence pixel intensities per cell were determined by drawing an ROI around the plasma membrane of individual cells. Plot shows the average pixel intensity ± SEM as a function of increasing ratios of JB434 per QD for ~30 - 40 cells.

Thus, these ratios would be sufficiently high to cause cell death after incubation with the QD-peptide-DOX complexes.

As evidenced by Figure 12 we observed robust, bright cellular labeling at a concentration of 200 nM QD appended with a ratio 15 JB434 peptides per QD. Similar observations have been made for other cell uptake peptide-QD complexes.[47] Additionally,

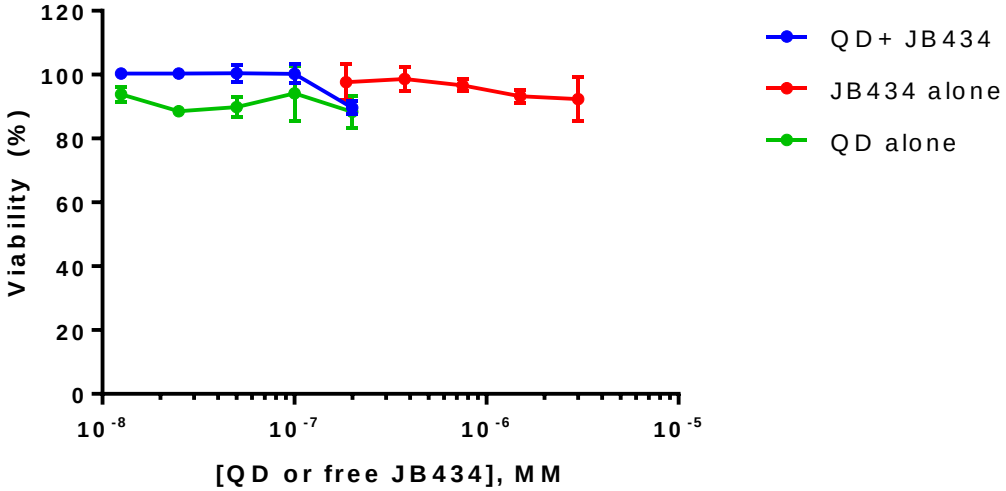

Figure 13. Quantification of cytotoxicity of QD, JB434, and QD-JB434 bioconjugates. Average cell viability of $PEG_{750}OMe$-capped QD, JB434 or QD-JB434 bioconjugates. QD, JB434, or QD-JB434 bioconjugates were incubated on HeLa cells for 2 h followed by 72 h proliferation and viability was determined by MTS assay. For the QD + JB434 plot a ratio of 15 JB434/QD was used. The data is presented as a percent cell viability ± S.D. of wells performed in quadruplicate relative to control cells.

cytotoxicity studies performed on the QD-JB434 conjugates showed minimal cell death using this combination of QD concentration and JB434 ratio (>90% cell viability (Figure 13)). These results are consistent with previous studies which have shown minimal toxicity of QDs at the given ratios over a period of 72 hrs.[47, 152, 156].

Cellular uptake and fate of QD-peptide-DOX-JB434 conjugates

Having determined the optimal ratio of CPP:QD necessary to facilitate endosomal uptake, we next sought to ascertain the fate of the conjugates after internalization via the endocytic pathway. Confocal imaging and comparative colocalization analysis was performed to determine the simultaneous location of the QD carrier, DOX, and the endosomal compartments for the four different QD-peptide-DOX conjugates. For these studies, 545 nm DHLA-PEG_{750}-OMe-capped QDs (200 nM) appended with 15 copies of the JB434 cell uptake peptide and 30 copies of the peptide-DOX conjugate was used. Endosomes were labeled with an AlexaFluor 647-transferrin conjugate (AF647-Tf). We examined the intracellular distribution of the complexes after 2 h incubation with cells. Clear differences among the four peptide-DOX constructs were noted, in terms of both the colocalization of the QD signal and the DOX signal with the endosomes as well as the colocalization of the QD and DOX signals with each other.

Figure 14 shows representative images of HeLa cells to illustrate the nature of the various signals upon cellular delivery. The amide-DOX peptide construct showed a significant degree of punctate DOX signal that was highly colocalized with the punctate QD signal (Pearson's correlation coefficient (PCC) = 0.71) and the AF647-Tf endosomal marker signal (PCC = 0.68) (see Table 2 for full colocalization quantification analysis). This result is not unexpected given the stability of the amide bond used to attach DOX to

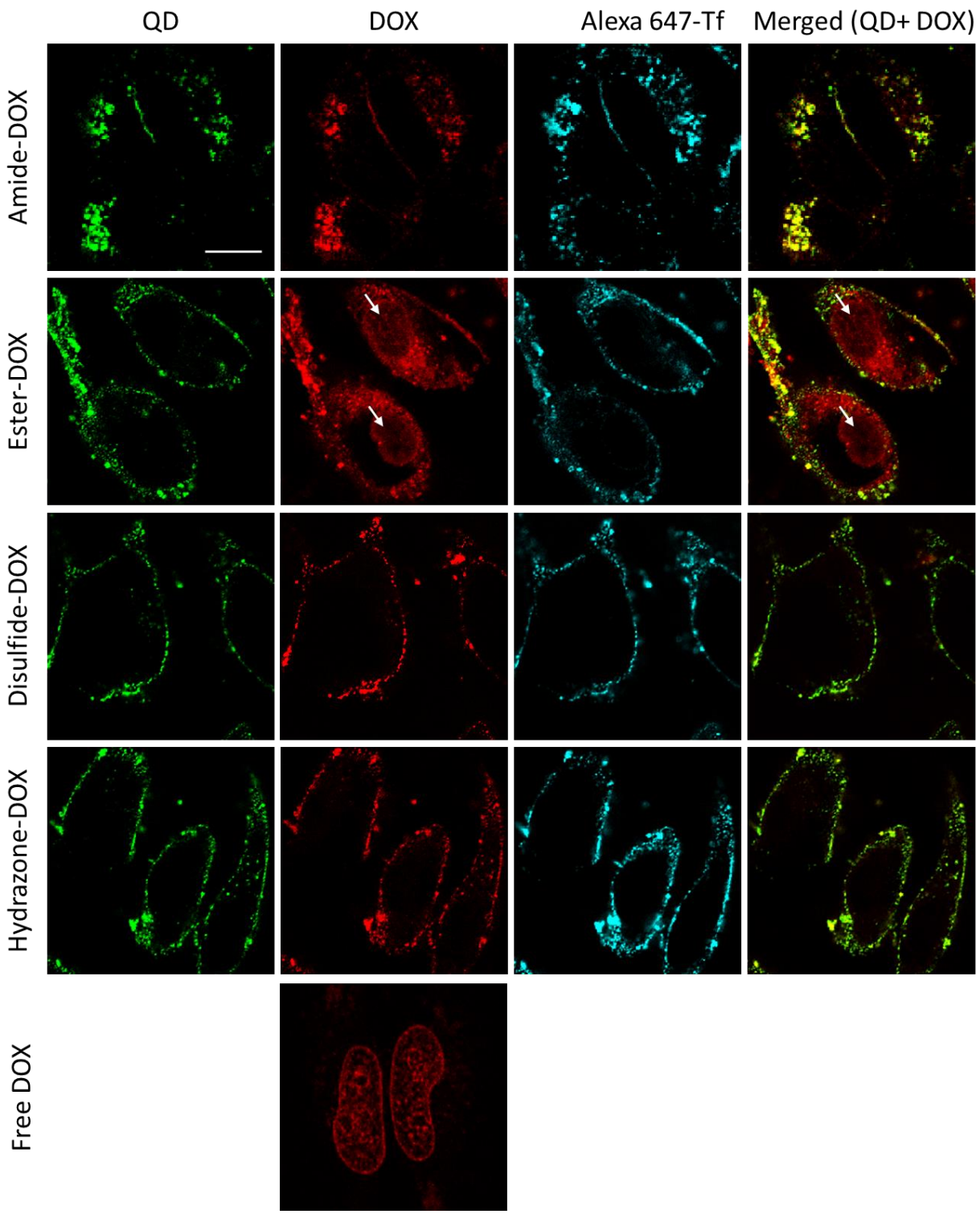

Figure 14: Cellular uptake and distribution of QD-peptide-DOX-JB434 complexes in HeLa cells. HeLa cells were incubated with pre-formed complexes (incubated at RT for 30 min to mediate QD-peptide assembly) for 2 h at 37°C and subsequently stained with endosomal marker Alexa647-Transferrin (Tf) (100 µg/mL) for 30 min at 37°C. Images were obtained using confocal laser scanning microscopy. Shown are fluorescence images of the QD (green), DOX (red), Alexa647-Tf (cyan) and merged QD and DOX channels. Images shown are representative of ~40 cells per peptide-DOX variant. White arrow indicates nucleus. Scale bar, 10 µm.

Table 2: Colocalization analysis of endosomes and NPs using PCC*

	Amide-DOX	Ester-DOX	Disulfide-DOX	Hydrazone-DOX
QD-Dox	0.71 ± 0.07	0.60 ± 0.09**	0.78 ± 0.08	0.82 ± 0.05
Endo-Dox	0.68 ± 0.09	0.47 ± 0.15****	0.73 ± 0.08	0.73 ± 0.08
Endo-QD	0.70 ± 0.13	0.66 ± 0.12	0.76 ± 0.09	0.73 ± 0.10

***PCC-Pearson correlation coefficient**

the peptide backbone and the fact that previous work has shown that the his-mediated attachment of the peptide to the QD is stable in endocytic compartments for up to three days in cultured cells.[152] Similar trends were observed for the hydrazone-DOX and disulfide-DOX linkages where a significant degree of overlap between the QD and DOX signals (PCC = 0.78 and PCC = 0.82, respectively) was observed. Similarly, for both linkages, the degree of overlap of the DOX with the endosome signal was high (PCC = 0.73), demonstrating that DOX was sequestered in endosomal compartments. That the disulfide linkage showed essentially no release of DOX from within endosomal compartments is consistent with the oxidizing environment found in early endosomes which is topologically equivalent to the oxidizing environment of the extracellular milieu.[179] Further, disulfide bonds have been shown to be stable even in the acidic environment (~pH 5.0) of endocytic compartments.[179] The lack of release seen with the hydrazone-DOX as this 2 h time point was somewhat surprising given that this bond is known to be cleaved in the pH range of 3-6[169, 171, 180]and multiple studies have demonstrated the utility of the hydrazone linkage to release NP-appended cargos from within endosomal compartments via acid-induced cleavage.[171, 181-183] Indeed, our plate-based FRET assay demonstrated the acid-labile nature of this linkage outside of the context of cells.

Nevertheless, the fact that we saw minimal release of the hydrazone-appended DOX from the QD surface strongly suggests that it is the context of the NP itself (NP material, ligand coating, steric shielding of the hydrazone linkage, cellular environment vs. in buffer etc.) that plays a critical role in acid lability of the bond within cellular environments. This result is consistent with previous studies where, in the context of endosomal compartments, chemoselectively-ligated cell uptake peptides bearing hydrazone bonds were used for cellular QD delivery. The peptides maintained their function in cultured COS-1 cells, even 48 h after delivery, providing strong evidence that the peptide integrity remained intact.[155] Thus, our findings with the hydrazone-DOX peptide in the current study are not wholly unexpected and strongly suggest that in the context of the hard NP QD platform and under a relatively short incubation period, the hydrazone bond remains intact.

Evidence from the literature also points to the fact that the environment of the NP (buffer vs. cells) can play a key role in determining the kinetics of hydrazone bond cleavage. Xiong *et. al.* developed DOX-loaded micelles assembled from copolymers that were crosslinked with hydrazone, yielding stimuli-responsive NPs. In buffer at pH 5.0, the micelles showed nearly 90% release of DOX after 48 h. Cytotoxicity studies, however, showed an attenuated cell killing effect compared to free DOX, suggesting a less efficient cleavage of the hydrazone bond in the context of cells. Studies have also shown that the efficiency of hydrazone bond cleavage can vary based on the composition of the NP and mixed results have been reported in the literature in terms of release of hydrazone-attached cargos. Lee *et al*. synthesized AuNPs conjugated to DOX via a hydrazone bond and coated with PEG to improve biocompatibility and stability of the complex. Release kinetic studies

performed under acidic conditions (pH 4) showed a significant decrease in DOX release (~4-fold) for AuNPs coated with PEG compared to AuNPs without PEG. Additionally, cell viability studies showed more potent cell killing for free DOX compared to the NP form, even after 72 h, demonstrating the role played by cellular context in attenuating hydrazone bond cleavage.[61] Prabaharan *et al.* synthesized AuNPs coated with a hydrophobic poly (L-aspartate-DOX) inner shell and folate-conjugated PEG outer shell, where DOX was conjugated to the inner shell via a hydrazone linkage. When studying release kinetics of DOX from the surface of the AuNPs, it was determined that conjugates showed ~40% release of DOX after 4 hrs.[171] Similarly, Savla *et al.* developed QDs coated with ligands terminated with carboxyl groups and conjugated to mucin1 aptamer, for targeting capabilities, and DOX via a hydrazone bond. Release kinetic studies for these NPs, however, showed only ~30% release after 4 h in acidic buffer.[62] Patil and coworkers, on the other hand, developed poly(β-L-malic acid) based nano vehicles with PEG conjugated to the surface along with DOX, which was attached via a hydrazone linkage. In pH 5.0 buffer, the complexes showed ~65% release of drug after 4 h.[170] Taken together, these results demonstrate that the composition of the NP can indeed play a significant role in hydrazone-linked cargo release.

Of the four linkages, the ester-DOX linkage was the only one that showed a significant degree of separation of the DOX signal from both the QD (PCC = 0.60) and the endosomal marker (PCC = 0.47). Concomitant with this was the appearance of strong DOX staining in the nucleus for the ester-linked DOX that was not observed for any of the other QD-peptide-DOX assemblies (Figure 14). These findings are consistent with previous findings demonstrating ester-based hydrolysis in the endosomes/lysosomes of cells due to

the presence of acid hydrolases, such as acid phosphatases and cholesteryl ester acid hydrolases.[184, 185] Previous studies using the ester linkage for drug attachment to other NPs have shown similar efficiencies in cleavage.[185] For example, Fernando *et al.* developed MSNs loaded with DOX and capped with poly(β-amino ester). Release kinetics demonstrated a significant release of DOX in the presence of esterase compared to the control and cell viability assays showed comparable toxicity of the complex to free DOX delivered from bulk solution.[96] Similarly, Zhou *et al.* conjugated camptothecin (CPT) to poly(ethylene glycol-*co*-anhydride) via an ester bond as an esterase-sensitive drug carrier for cancer therapy. In buffer, it was determined that the complexes were relatively stable in the absence of esterase, but were efficiently hydrolyzed in the presence of esterase in a manner that was dependent on pH. Additionally, cytotoxicity assays demonstrated comparable cell killing capabilities of the complex to free CPT at low concentrations and promoted cell death of the complex at higher drug concentrations.[168] Cumulatively, our data provide strong evidence that in the context of the QDs, the ester linkage is sufficiently available for cleavage by the esterases present within the endolysosomal pathway and that endosomal release and nuclear accumulation are clearly evident under the 2 h experimental window used here.

Cytotoxicity of QD-peptide-DOX-JB434 conjugates

In addition to the intracellular optical tracking of DOX release from the QD-peptide-DOX bioconjugates, the comparative functional implications of DOX release were also confirmed by cell viability assays. Cellular proliferation assays were performed in which the delivery/incubation conditions emulated those of the delivery/imaging

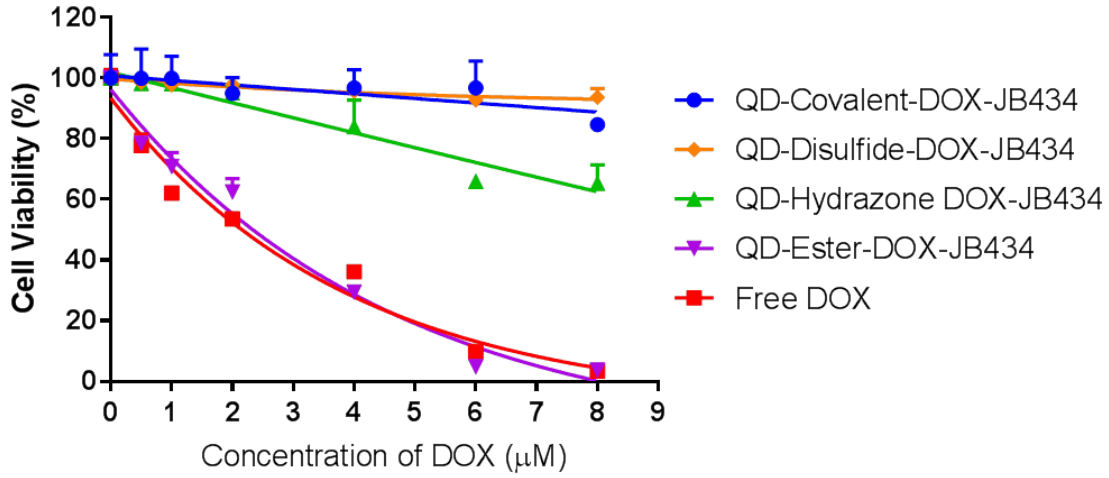

Figure 15: Quantification of cytotoxicity of QD-peptide-DOX-JB434 bioconjugates. Average cell viability of PEG_{750}-OMe-capped QD-peptide-DOX-JB434 bioconjugates with fixed JB434 concentration (15 JB434 per QD) and varying peptide-DOX concentrations. QDs (200 nM) were incubated on cells for 2 h incubation followed by 72 h proliferation. Viability was determined by MTS assay. Plot shows average cell viability at DOX concentrations ranging from 0 to 8 μM. The data is represented as a percent cell viability ± S.D. of wells performed in quadruplicate relative to control cells incubated with QD-JB434 alone (no peptide-DOX).

experiments described above followed by a 72 h period to allow for cell division. As DOX is known to elicit its toxicity through the induction of apoptosis and the generation of reactive oxygen species [186, 187], processes that can take several cell divisions to manifest their effects, we chose the 72 h time point at which to assay DOX toxicity as it provided an optimal experimental window to allow for cellular proliferation. QDs decorated with 15 copies of JB434 were further appended with varying ratios of peptide-DOX conjugates (from 2.5 to 40 per QD) such that the DOX concentration incubated with the cells spanned the range of 0.5 μM to 8 μM. This range was purposefully selected to encompass the known IC_{50} of free DOX in cultured cells (1-2 μM).[176-178] Figure 5 shows the resulting cytotoxicity plots for the various QD-peptide-DOX constructs. Consistent with previous literature reports, free DOX exhibited an IC_{50} of ~2 μM. In general, the toxicity results for the QD-peptide-DOX conjugates mirrored those observed for the colocalization studies in that the amide-DOX and disulfide-DOX showed negligible toxicity, consistent with the lack of

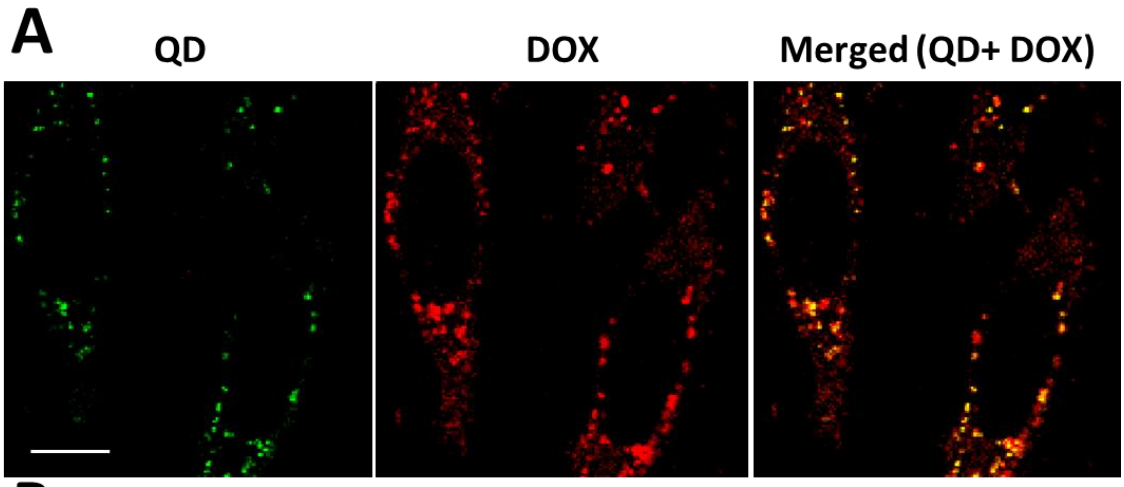

B

Colocalization Analysis of DOX and QD using PCC*

	2 h	8 h
QD-Dox	0.82 ± 0.05	0.62 ± 0.13

***PCC-Pearson correlation coefficient**

Figure 16. Cellular uptake and distribution of QD-peptide-hydrazone-DOX-JB434 complexes in HeLa cells after 8 h. A) HeLa cells were incubated with pre-formed QD-peptide-hydrazone-DOX-JB434 bioconjugates (incubated at RT for 30 min to mediate QD-peptide assembly) for 2 h at 37°C followed by proliferation in complete media for 6 h at 37°C. Images were obtained using confocal laser scanning microscopy. Shown are fluorescence images of the QD (green), DOX (red), and merged QD and DOX channels. Images shown are representative of ~40 cells. Scale bar, 10 µm. **B)** PCC value for colocalization of QD and hydrazone-DOX after 2 h and 8 h. P-value <0.0001.

DOX release and its sequestration in endosomes (Figure 15). As discussed previously, this result is due to the stability of the amide bond and oxidizing environment of endosomes, respectively. That the hydrazone-DOX elicited a modest degree of toxicity (IC_{50} = ~5 µM) suggests that the longer time frame used for the cell proliferation assays (2 h initial incubation on cells followed by a 72 h proliferation period), facilitates the cleavage of a percentage of the hydrazone-linked DOX. In this context, the endosomal compartments would have a longer time to acidify and release DOX, resulting in nuclear accumulation of DOX that was not apparent in the 2 h time window used for fluorescence imaging. Indeed, imaging performed at longer time points, for example at 8 h, did begin to show a

statistically significant separation of the DOX signal from the QD carrier signal that was indicative of a slower rate of cleavage of the hydrazone bond (Figure 16). Combined, these results suggests a slower method of drug release for the hydrazone linkage compared to the more immediate "burst" release seen for the ester-DOX linkage.

The ester-DOX linkage, on the other hand, showed similar toxicity to the free DOX, suggesting that the ester bond is rapidly cleaved upon internalization. This result fits with the functionality studies done in buffer, as well as with the fluorescence studies, which showed clear signs of cleavage of the linkage and nuclear delivery after 2 h. Though the ester-DOX and free DOX show similar toxicities, the use of a NP carrier to facilitate delivery can ultimately have implications within the context of the cell type. For example, multidrug resistance (MDR) is a known limitation of drug delivery, where membrane-resident pumps work to remove free drug from cells. This is particularly true for DOX, where MDR pumps can effectively lower the efficacy of free DOX.[188-190] Delivery of drugs as a NP complex via the endocytic pathway, on the other hand, could potentially mitigate the rapid MDR-mediated efflux of DOX delivered from bulk solution. Taken together, our data demonstrate the ability to modulate DOX toxicity by delivering it as an ensemble complex using the CPP-decorated QD as a carrier through the endocytic pathway.

Conclusion

The overall goal in this study was to ascertain the degree of control that can be achieved in NMDD by varying the intracellularly-responsive chemical linkage used to attach the drug cargo to the surface of a hard NP. It has become generally accepted that the primary route of cellular NP uptake is endocytosis, whether the NP is appended with a targeting/uptake agent or not.[191] Differences in the rate of NP endocytosis primarily occur

as a function of NP size and shape, surface coating, and presence of various moieties (peptides and drugs) used to facilitate entry into the endocytic pathway. Compared with other means of cellular delivery, such as microinjection (which has low throughput) or the use of transfection agents (which can be toxic to the cells), the delivery of NPs via the endocytic pathway is the most facile route for cellular entry, yet the endosomal sequestration of the NP–drug cargo complex poses a considerable challenge for the delivery of drugs to the rest of the intracellular environment.(1) Hence, there is a critical need for the controlled release of drugs (and other cargos) from NP carriers from within the endocytic pathway.[15]

Here, we have designed a series of peptide–DOX formulations that are appended to QD–cell uptake peptide conjugates that are destined for endocytic uptake. In this configuration, each formulation differs in the nature of the chemical attachment of the DOX moiety to the central QD carrier. The stimuli-responsive linkages (ester, disulfide, and hydrazone) were chosen specifically for their ability to be cleaved through intracellular stimuli, resulting in the controlled modulation of toxicity of the drug that is driven by intracellular physiology. By using histidine-mediated metal affinity to self-assemble both the cell uptake peptide and peptide–DOX to the surface of the QD, we have shown the ability to control the ratio of each peptide species, thus allowing us to tune the concentration of drug delivered to cells. Importantly, from our data, it was evident that the nature of the linkage has a profound effect on both the efficiency of drug delivery and the kinetics of DOX cargo release.

Compared to the delivery of DOX from bulk solution, the ester linkage showed comparable toxicity and clear signs of nuclear delivery after 2 h. The hydrazone linkage,

however, showed intermediate toxicity, and the disulfide linkage and control amide linkage showed minimal toxicity. For the disulfide linkage, the results were not unexpected, as endosomal compartments are known to be an oxidizing environment. Interestingly, the hydrazone and ester linkage both showed reactivity in plate-based assays done in buffer, but within the cellular context, there were differences in activity that were not expected. The ester linkage showed efficient cleavability, which was observed intracellularly in terms of both nuclear accumulation and concomitant cytotoxicity. Intracellular delivery of the hydrazone linkage, however, exhibited minimal release from within endosomes after 2 h and moderate toxicity after 72 h. This points to a slower drug release time for the hydrazone linkage, compared to release from the ester linkage. This attribute can potentially be beneficial for sustained, yet differential, release profiles of multiple drugs from the same NP carrier.

Cumulatively, our data points to the importance of design considerations one needs to take into account, particularly in the context of hard NP carrier systems delivered via the endocytic pathway. Namely, the chemical nature of the attachment of the drug cargo to the hard NP surface plays a profound role in the ultimate efficiency of drug release, particularly within the cellular environment. Going forward, the findings of this study can be used to design NP composites with more complex architectures that use a combination of the presented methods of drug release. For example, it is well-known that the extracellular tumor environment is highly acidic (pH of ~5–6)[62, 169, 170, 183], and cancerous cells often over-express esterases compared to normal cells.[48, 192-194] A combination of the linkages presented here, such as the hydrazone–DOX and ester–DOX, could facilitate development of multifunctional particles that exhibit dual release in response to multiple stimuli. Our

work shown here demonstrates that careful consideration must be given to the design and display of these linkages if they are to be used in combination to facilitate efficient and controlled drug release.

Chapter 4: Nanoparticle-Peptide-Drug Bioconjugates for Unassisted Defeat of Multidrug Resistance in a Model Cancer Cell Line[‡195]

Introduction

Multidrug resistance (MDR), the ability of cancer cells to overcome the activity of therapeutic drugs and reduce their efficacy, is a major challenge in the treatment of a number of recurrent cancers. Blood cancers and solid tumors including breast, ovarian, lung and lower gastrointestinal tract cancers are among the most prevalent examples of cancers that display resistance to chemotherapeutics.[196-198] MDR arises through a number of pathways including drug inactivation, suppression of apoptosis, and the active efflux of drugs from the cell by membrane-resident pumps.[199] The latter is mediated through the action of ATP-binding cassette (ABC) drug efflux transporters (*e.g.*, P-glycoprotein (P-gp)) and breast cancer resistance protein (BCRP)) which utilize energy from ATP hydrolysis to expel drugs out of the cell, severely limiting the utility of common cancer drugs such as DOX and PTX.[200, 201] Nanoparticles (NPs), however, have shown increasing utility in a variety of drug delivery applications, including those aimed at mitigating MDR. NPs' small size (<100 nm) affords efficient tissue penetration and they can be synthesized/modified to have excellent biocompatibility. Additionally, their multifunctionality and drug loading capability have made them attractive vehicles for the delivery of a myriad of drug cargos.[161, 202-205]

‡ Reprinted with permission from Sangtani, A., Petryayeva, E., Susumu, K., Oh, E., Huston, A.L., Lasarte-Aragonés, G., Medintz, I.L., Algar, W.R., Delehanty, J.B., (2019). Nanoparticle–Peptide–Drug Bioconjugates for Unassisted Defeat of Multidrug Resistance in a Model Cancer Cell Line. *Bioconjugate Chemistry*. Copyright 2019 American Chemical Society.

Recently, strategies employing NP-based therapeutics for overcoming MDR have emerged including: 1) the combinatorial delivery of multiple anticancer drugs in an effort to overwhelm the effectiveness of MDR pumps; 2) the use of NP-nucleic acid hybrids to down-regulate expression of efflux pumps or to promote apoptosis; and 3) the delivery of the NP-drug complex in combination with MDR pump inhibitors.[206, 207] Examples include the work of Tian and colleagues who stabilized upconversion NPs with the surfactant α-tocopherol polyethylene glycol succinate (TPGS), a common P-gp inhibitor, to demonstrate a ~8-fold decrease in the IC_{50} of DOX in MDR-positive MCF-7 cells compared to drug alone.[208] Similarly, Yi and coworkers demonstrated a ~7-fold decrease in IC_{50} of DOX in DOX-resistant MCF-7 cells upon delivery of folate-coated micelles containing DOX and the P-gp inhibitor, tariquidar, compared to free DOX.[209] Xue and coworkers synthesized lipid-coated hollow mesoporous silica NPs co-loaded with a P-gp expression-inhibiting mRNA, miR-375, and DOX, resulting in a significant decrease in IC_{50} in MDR-positive HepG2 cells.[210] While effective, these aforementioned strategies are not without liabilities including off-target toxicity or the need for genetic transfection. Thus, NP-based drug delivery systems that can efficiently defeat the activity of MDR pumps without the need for exogenous drugs or can do so without concomitant toxicity are highly desired.

With this goal in mind, herein we sought to significantly extend our work from Chapter 3, where we demonstrated the use of a multifunctional QD/cell-uptake peptide/drug-release peptide bioconjugate to controllably modulate the toxicity of DOX.[95] As mentioned before, QDs are bright, luminescent semiconductor nanocrystals that possess many optical properties that are tied directly to their size and material composition that

make them ideal for use as a prototypical scaffold. In the system utilized herein, the central QD serves as a scaffold upon which two species of peptide are attached: (1) JB434, a cell-uptake peptide that mediates QD internalization via the endocytic pathway and (2) a peptide-DOX conjugate in which the DOX was attached via a cleavable linker for controlled intracellular drug release.[15] In the previous study, of the three cleavable linkers tested (ester, disulfide, and hydrazone), the QD bioconjugate with the ester linkage (QD-ester-DOX) displayed cellular toxicity and nuclear accumulation that were comparable to free DOX in a DOX-sensitive cell line (HeLa), indicating rapid cleavage of the ester linkage by endosomal esterases. Our working hypothesis in the current study, therefore, was that the sequestration of the QD/cell-uptake peptide/drug-release peptide complex within endosomes could effectively 'hide' the attached DOX cargo from plasma membrane-resident MDR pumps in a multifaceted spatiotemporal approach where (1) DOX is physically trafficked away from the plasma membrane (spatial), and (2) DOX is released closer to the nucleus, its target destination, in a time-dependent manner (temporal), as depicted schematically in Figure 17.

We present characterization of the QD-ester-DOX/JB434 system when interfaced with MDR+ cells *in vitro.* Our data clearly demonstrate that delivery of the drug as part of NP bioconjugate significantly augmented its uptake and toxicity in MDR cells. Cellular delivery and uptake experiments confirmed significantly higher uptake of the complex compared to free drug in MDR+ cells, and nuclear delivery of DOX in the complex after 48 h. Additionally, colocalization analysis demonstrated cleavage of the ester linkage and separation of DOX from the QD over time. Finally, cell proliferation assays were performed to confirm ability of the complex to overcome MDR pumps. Cell viability in

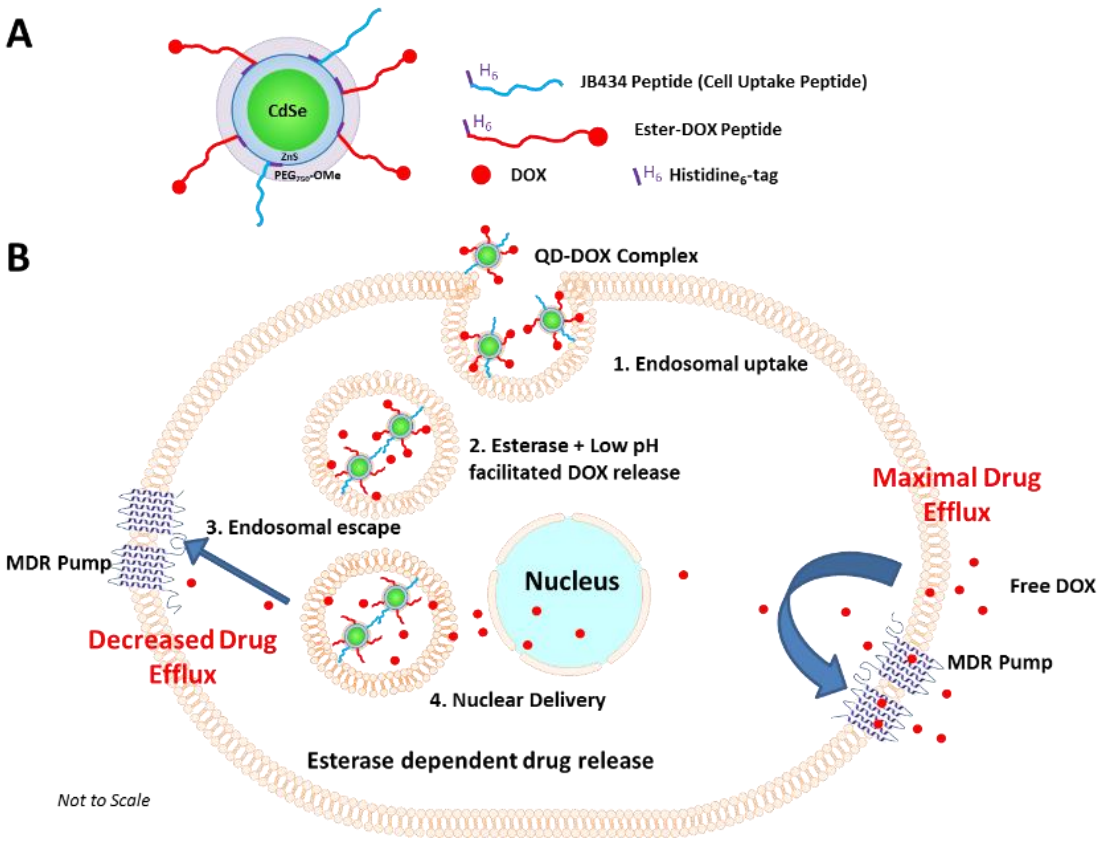

Figure 17: Schematic depiction of QD-ester-DOX bioconjugates for overcoming drug efflux pumps in multidrug resistant (MDR+) cells. (A) Representation of QDs appended with ester-DOX peptide (30 copies/QD) and JB434 cell uptake peptide (15 copies/QD). Both peptide species are assembled to the QD surface by polyhistidine (H6) metal affinity interaction with the ZnS shell. (B) Free DOX enters cells from bulk solution by crossing the plasma membrane where it interacts with MDR pumps and is effluxed out of the cell. QD-ester-DOX bioconjugates facilitate cellular uptake of DOX via endocytosis, which sequesters DOX away from MDR pumps and promotes the time-resolved release of DOX away from plasma membrane. Combined, these two facets create a spatiotemporal strategy to defeat MDR that is independent of the use of drugs that incapacitate MDR pumps.

MDR-cells showed comparable toxicity between the free drug and complex. However, cytotoxicity in MDR+ cells demonstrated significantly augmented toxicity of the complex compared to free drug. We interpret these findings in the context of previous studies, as the system utilized herein is one of the few examples of NP-mediated drug delivery that achieves defeat of MDR pumps without the need for exogenous drugs. As before, the work described here details basic concepts in use of controlled release from hard NPs and points

to important considerations when designing NP systems for overcoming MDR in cancer cells.

Materials and Methods

Materials

RPMI-1640 Media, Dulbecco's phosphate buffered saline (D-PBS), phosphate buffered saline (PBS), Live Cell Imaging Solution (LCIS), and nickel-nitrilotriacetic acid agarose resin (Ni-NTA) were obtained from ThermoFisher, (Carlsbad, CA). V-bottom and flat-bottom 96-well cell culture cluster microtiter plates were purchased from Corning-Costar (Corning, NY). Doxorubicin hydrochloride (DOX), *N*,*N*-dimethlyformamide (DMF), dimethyl sulfoxide (DMSO), Tris-borate-EDTA buffer solution, *N*-hydroxysuccinimide (NHS), diisopropylcarbodiimide (DIC), 4-(dimethylamino)pyridine (DMAP), *N*,*N*-diisopropylethylamine (DIPEA), Tris(2-carboxyethyl)phosphine hydrochloride (TCEP), tetrahydrofuran (THF), and imidazole were acquired from Sigma. All other materials/reagents were obtained as noted in the text.

Quantum dot synthesis

CdSe-ZnS core-shell QD nanocrystals capped with DHLA-polyethylene glycol $(PEG)_{750}$-OMe ligands were synthesized as described previously. [147, 148] The QDs exhibit maximum photoluminescence centered at 545 nm. Size was confirmed by TEM.[95]

Synthesis of peptides and characterization

DOX-ester peptide. The DOX-ester peptide was synthesized as described previously. [95] The sequence of the peptide used was GNNGAAAA-Aib-AAAA-Aib-GLGHHHHHH-amide (Biosynthesis, Inc.) where Aib is α-aminoisobutyric acid and the amidation blocks the C-terminal carboxyl group. The DOX used was doxorubicin

hydrochloride. The *N*-terminal amine on the peptide was conjugated to the cognate modified DOX. Conjugation of DOX to the peptide was done as described previously. [95] Briefly, the peptide was dissolved in anhydrous DMF and mixed for 4 h at room temperature (RT) with glycolic acid-NHS ester. The product was then diluted with PBS and purified using Ni-NTA agarose resin. The purified peptide was dissolved in DMF and mixed with succinic acid. Diisopropylcarbodiimide and DMAP where added and the reaction was mixed overnight at RT. The reaction mixture was diluted with PBS and purified using a Ni-NTA agarose resin. The purified peptide was dissolved in DMF and mixed with diisopropylcarbodiimide and NHS for 2 h at RT. After this time, DOX dissolved in DMF and DIPEA was added and the reaction was left in the dark to mix at RT overnight. The reaction mixture was diluted with PBS and purified with Ni-NTA as before.

JB434. Synthesis of the cell uptake peptide, JB434, (R_9GGLA(Aib)SGWKH_6; Biosynthesis, Inc.) used in this study is described elsewhere.[152] The peptide contains a polyarginine tract (R_9) that facilitates endocytic uptake, a polyhistidine tract (H_6) that mediates self-assembly to the surface of the QD surface, and a linker domain (GGLA(Aib)SGWK). [152, 153]

Cell culture

NCI-H69 cells (DOX-sensitive, non-adherent, American Type Culture Collection (ATCC HTB-119)) were cultured in complete growth medium (RPMI-1640) supplemented with 10% (v/v) heat inactivated fetal bovine serum (ATCC) and 1% (v/v) penicillin/streptomycin (Sigma). Cultures were maintained in suspension in T75 flasks and incubated at 37 ^{o}C under a 5% CO_2 humidified atmosphere. Media was refreshed every 2-3 days and cells were passaged every 7 days. H69AR cells (DOX-resistant, adherent,

ATCC CRL-11351) were cultured in complete growth medium (RPMI-1640) supplemented with 20% (v/v) heat inactivated fetal bovine serum (ATCC) and 1% (v/v) Penicillin Streptomycin (Sigma). Cultures were maintained in T75 flasks and incubated at 37^{o}C under a 5% CO_2 humidified atmosphere and passaged every 3-4 days at 80% confluency. All cells used in this study were between passages 2 and 15.

Cellular delivery of QD-ester-DOX-JB434 conjugates

For cellular delivery experiments, H69AR cells were seeded on MatTek^{TM} 14 mm dishes (Ashland, MA) that were pre-coated with 30 µg/mL fibronectin (ThermoFisher) for 2h. Cells were seeded at 6×10^4 cells/mL and allowed to adhere overnight. Prior to addition of materials for cellular delivery, the cells were washed twice with serum free media. QDs (200 nM) were assembled with JB434 peptide (15 peptides per QD) and ester-DOX peptide (30 peptides per QD, final DOX concentration 6 µM) in serum free media for 30 min at RT. [152, 155] The complexes were then incubated on cell monolayers for 2 h at 37 ^{o}C. Control cells were incubated with free DOX at the same concentration (6 µM). After 2 h, the cells were washed twice with LCIS and retained within an environment-controlled incubation chamber while being imaged using confocal microscopy (*vide infra*). Fluorescence signal intensity of DOX was calculated by drawing a region of interest (ROI) around individual cells. The data were statistically analyzed by a two-tailed Welch's *t*-test at the 95% confidence interval using Graphpad Prism 7.03 software (La Jolla, CA). After imaging, the LCIS was replaced with complete media, and the cells were returned to the incubator and imaged at 8 h and 48 h. After 48 h, the cells were stained with a live cell nuclear marker (NucBlue; ThermoFisher) for 20 min at RT.

Quantification of cellular cytotoxicity

Cellular cytotoxicity was determined using the CellTiter 96® AQueous One Solution Cell Proliferation Assay (Promega, WI).[156, 157] This colorimetric assay determines the number of viable cells after incubation with a material of interest through conversion of the tetrazolium compound (MTS) into formazan by live cells. NCI-H69 cells were seeded in a v-bottom 96-well tissue culture microplate at a density of 2×10^4 cells/well and H69AR cells were seeded in a flat-bottom 96-well tissue culture microplate at a density of 3×10^3 cells/well. Both cultures were allowed to grow overnight. QDs were assembled with JB434 peptides and with ester-DOX peptides (*vide supra*) in serum free media for 30 min at RT. QD complexes were then incubated on cells for 2 h at 37°C. As controls, free DOX, QD alone, and QD-JB434 complexes were also included at corresponding concentrations. After incubation, the QD-containing solution was replaced with complete media and the cells were allowed to proliferate under standard culture conditions for 72 h. For non-adherent cells, to replace solution, the cells were spun down at 3000 rpm for 5 min. After 72 h, 20 µL of a solution containing MTS was added to each well and incubated with the cells for 4 h. Non-adherent cells were transferred to a flat bottom 96-well tissue culture microplate and absorbance for both cell lines were read at 600 nm and 800 nm (for background subtraction) using a Tecan Infinite M1000 dual monochromator plate reader equipped with a xenon flash lamp (Tecan). Results were reported as a percentage of cellular viability, normalized to control wells of cells cultured alone.[156, 157] The data were statistically analyzed by a two-tailed Welch's *t*-test as before.

Microscopy and image analysis

All imaging was performed using a Nikon A1RSi Laser Scanning Confocal Imaging system. The following imaging settings were used (laser excitation/dichroic/emission range): NucBlue, 405 nm/405 nm/425-475 nm; QD, 405 nm/488 nm/500-550 nm and DOX, 561 nm/561 nm/570-620 nm. Each channel was imaged sequentially to prevent bleed-though between the channels. All imaging settings (i.e. laser power, gain, exposure time) were kept consistent between experiments. Quantification of DOX uptake and colocalization analysis was done using NIS-Elements AR (ver. 4.30.02). Fluorescence signal corresponding to DOX uptake was calculated by drawing a ROI around individual cells (n = 30 cells), and then averaging data across all cells. Images were prepared for publication using the same software. Colocalization was statistically analyzed by a two-tailed Welch's t-test at the 95% confidence interval using Graphpad Prism 7.03 software.

Results and Discussion

Time-resolved cellular uptake and fate of QD-ester-DOX-JB434 complexes

To assess this hypothesis, we first investigated the cellular internalization and distribution of free DOX and the QD-ester-DOX complexes in the MDR pump-expressing cell line, H69AR (human small cell lung carcinoma), which is ~50-fold more resistant to DOX compared to the parental cell line, H69.[211] All materials and methods can be found in the supplementary information. H69AR cells were incubated (for 2 h at 37 °C) with 200 nM 545 nm-emitting QDs that were preassembled with 30 copies of the ester-DOX peptide (6 μM DOX) and 15 copies of the cell-uptake peptide, JB434. Previous studies have demonstrated that the maximum number of peptides that can be appended through

histidine-mediated binding to 545 nm QDs is ~50 peptides.[164] As a control, cells were incubated under the same conditions with 6 µM free DOX. Live cell confocal laser scanning imaging was performed immediately after incubation with the QD-ester-DOX conjugates or free DOX (2 h) and after a 6 h incubation period in complete media (8 h). H69AR cells incubated with the QD-ester-DOX bioconjugates showed significantly greater cellular accumulation of DOX compared to cells incubated with free DOX (Figure 18). To confirm that the observed differential DOX loading between the QD-ester-DOX conjugate and free DOX in the H69AR cell line was due primarily to the cells' drug efflux activity, control experiments were performed wherein we compared the mean fluorescence intensity of free DOX uptake in H69AR cells to two DOX-susceptible cell lines (the parent H69 cell line and HeLa cells). When incubated with 6 µM DOX, both DOX-susceptible cell lines exhibited a significantly higher (~1.8-fold) degree of DOX internalization

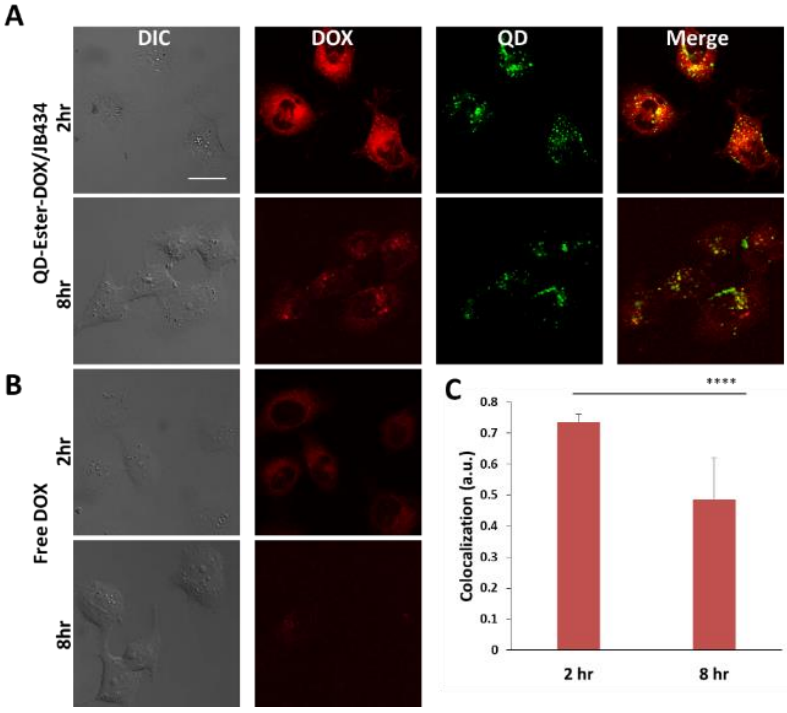

Figure 18: Time-resolved cellular uptake and distribution of QD-ester-DOX/JB434 conjugates and free DOX in H69AR cells. Cells were incubated for 2 h with either (A) 200 nM QDs complexed with JB434 (15/QD) and ester-DOX (30/QD) or with (B) free DOX (6 µM DOX in all cases). Images were acquired using confocal microscopy at 2 h and 8 h. Shown are representative images: differential interference contrast (DIC), DOX fluorescence (red), QD fluorescence (green), and merge of QD and fluorescence (yellow). Scale bar is 20 µm. (C) Graph shows colocalization between DOX and QD after 2 h and 8 h. Data was obtained using Pearson's colocalization coefficient. (n = 30 cells ± SD). A statistically significant difference in colocalization was noted between 2 h and 8 h (****, $p<0.0001$).

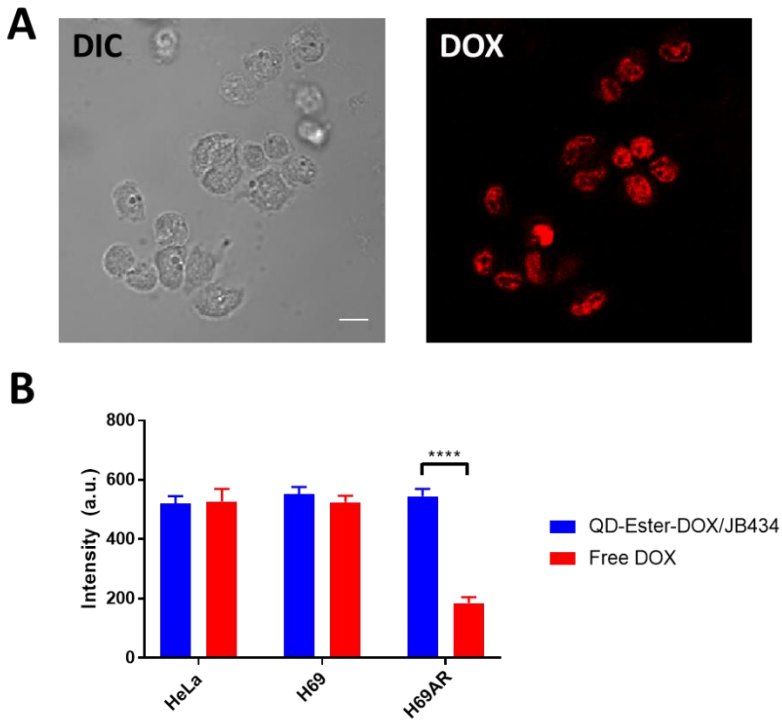

Figure 19. Cellular uptake of DOX in H69 (DOX-susceptible) cells. A) Cellular uptake of free DOX in H69 cells. Cells were incubated for 2 h with 6 µM free DOX and images were taken using confocal microscopy. Shown are representative images of DIC and DOX (red). Scale bar is 20 µm. (B) Quantification of the mean fluorescence signal from DOX after 2 h delivery to H69, H69AR and control HeLa cells. Fluorescence signal was calculated by drawing a region of interest (ROI) around individual cells (n = 30 cells). A statistically significant difference in mean fluorescence intensity was noted between H69AR cells compared to H69 and HeLa cells ($p < 0.0001$; ****).

compared to the DOX-resistant cells (Figure 19). As expected, colocalization analysis (Pearson's correlation coefficient (PCC)) revealed separation of the QD and DOX fluorescence signals over the 8 h time period, indicating an increase in release of DOX from bioconjugate. Interestingly, we observed no significant nuclear accumulation of DOX for either treatment group, which is likely attributable to a slower DOX release rate for the ester conjugate and the low retention of free DOX in the H69AR cell line. This was confirmed by imaging the cells at 48 h after the initial 2 h incubation time (Figure 20) where H69AR cells treated with the complex demonstrated clear signs of nuclear accumulation (PCC=0.438; cells counterstained with NucBlue®) compared to cells treated with free DOX. Additionally, late endosomes/lysosomes are known to be localized in the area surrounding the nucleus, thus a portion of the DOX from the QD-ester complex was perinuclear, further facilitating nuclear delivery. This nuclear/perinuclear accumulation

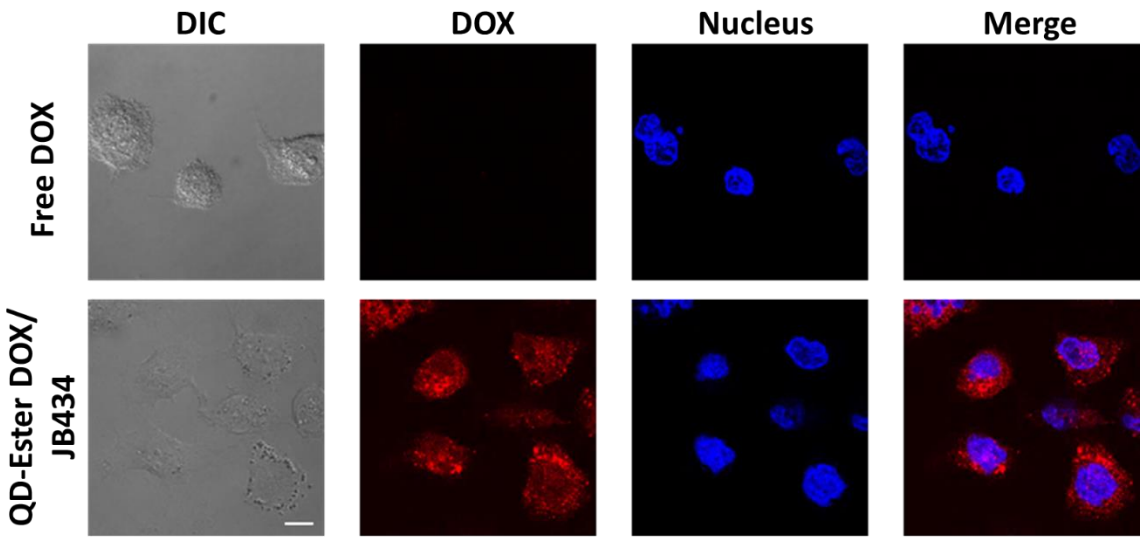

Figure 20: Cellular distribution of DOX after 48 h. After 2 h delivery of complexes or free DOX and 48 h culture in complete media, H69AR cells were stained with NucBlue®, a live cell nuclear stain, for 20 min and imaged using confocal microscopy. Shown are representative images of DIC, DOX (red), nucleus (blue) and DOX plus nucleus (merge). Scale bar is 20 nm. PCC was used to determine colocalization between DOX and NucBlue (n= 30 cells ± SD). White arrows indicate perinuclear location of DOX.

time is consistent with other solid/hard NP systems that have utilized intracellular mechanisms for drug release.[212]

Quantification of cellular cytotoxicity of QD-ester-DOX-JB434 complexes

Having characterized the cellular localization kinetics of the QD-ester-DOX conjugates in H69AR cells, we next used a cellular viability assay to ascertain the anti-proliferative effect of DOX delivered in the form of the QD-ester-DOX conjugate compared to the free drug. H69 and H69AR cells seeded to the wells of a microtiter plate were treated with the conjugate or free DOX as described for the imaging studies with QD alone and QD complexed with only the cell uptake peptide included as controls. Following an initial 2 h incubation with the materials and subsequent removal, the cells were cultured in complete media for 72 h to allow for proliferation, after which an MTS tetrazolium reagent was added to the wells. As shown in Figure 21, QDs alone and the QD-JB434

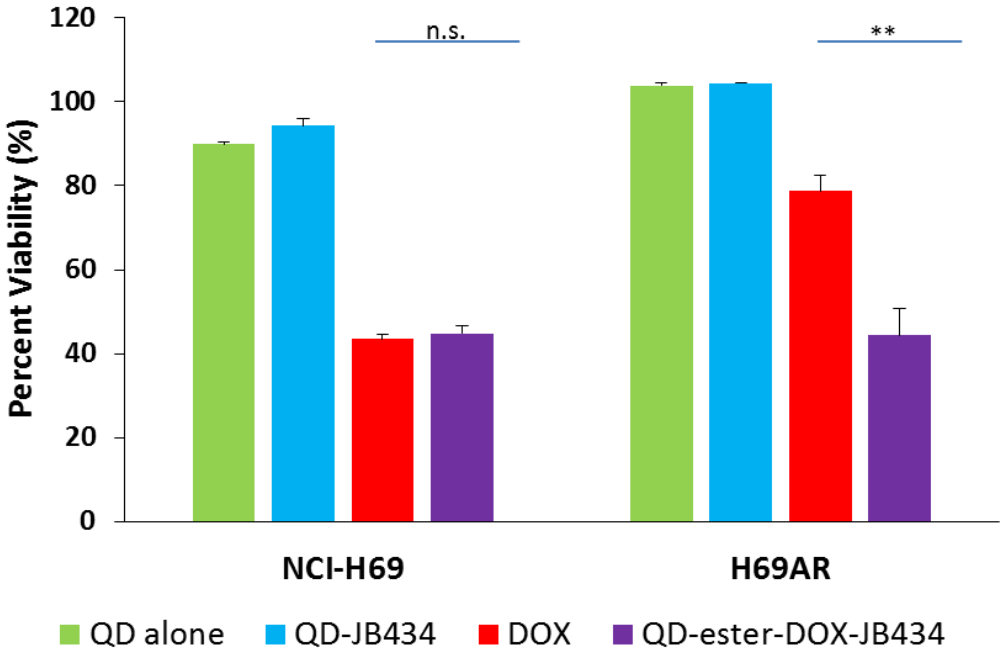

Figure 21: Cytotoxicity of QD-ester-DOX-JB434 bioconjugates compared to free drug. Cell proliferation of NCI-H69 (DOX-sensitive) and H69AR (DOX-resistant) cells after incubation with complexes vs. free drug was determined by MTS. Cells were incubated with QDs (200 nM) assembled with JB434 (15/QD) and ester-DOX (30/QD) for 2 h followed by a 72 h culture period in complete media. Graph shows percent cell viability ± SD of wells performed in quadruplicate relative to control cells incubated with serum-free media. Free DOX, QD and QD-JB434 were included as controls. A statistically significant difference in toxicity was noted between free DOX compared to the bioconjugate in DOX-resistant cells ($p<0.001$;**, n.s.- not significant)

complex showed minimal toxicity in both cell lines, confirming the biocompatibility of the QD delivery system.[95, 156] As expected, the free DOX and QD-ester-DOX peptide complex had similar toxicity in the DOX susceptible cell line (H69), which agrees well with our previous results in HeLa cells (also DOX-sensitive).[95] In DOX-resistant H69AR cells, however, there was a ~40% improvement in cell killing for the QD-ester-DOX bioconjugate system compared to free drug, clearly demonstrating the ability of the QD complex to bypass the activity of the MDR pumps without the need for co-delivery of other agents.

Conclusion

Our results reported here are one of the few examples of a NP-based drug delivery system to achieve significant defeat of MDR pumps without the need for augmentation using exogenous MDR pump-incapacitating drugs or nucleic acids. Other studies utilizing various NP composites to overcome MDR have demonstrated similar results but they have required co-delivery with other agents aimed at abrogating MDR pump activity. For example, Li *et al.* showed a ~60% decrease in cell viability (compared to free DOX) in A2790 ovarian cancer cells bearing MDR pumps after delivery of their folic acid-conjugated polymeric NPs containing DOX and BCL2-inhibiting siRNA.[213] Oliveira *et al.* demonstrated a 40% increase in toxicity after delivery of solid lipid NPs co-loaded with DOX and the P-gp inhibitor TGPS in MDR-positive MCF-7 cells.[214] Similarly, Zeng and colleagues reported a 20% decrease in MDR-positive cell viability after delivery of polyester dendritic NPs compared to free drug.[215] Still, other systems have required unusually long incubation times with the targeted cells to achieve the desired therapeutic effect. Such is the case, for example, in the nuclear-targeted mesoporous silica coated QD system described by Li *et al.* where a 24 h incubation time was required for sufficient NP uptake.[4] Similarly, Wang and colleagues required up to a 72 h incubation period to enable sufficient uptake of their AuNP/DOX complexes.[212] In our system, we were able to achieve a ~40% increase in cell killing in MDR-positive cells with only a 2 h incubation time with the QD complex. This significantly shorter delivery time is driven by the highly efficient cell-uptake activity afforded by the JB434 cell-uptake peptide.

The QD scaffold-based system described herein is a facile, traceable platform that affords multiple benefits in the ensemble drug delivery system. These include: (1) bright

QD fluorescence for bioconjugate tracking, (2) tunable drug loading that is controlled through ratiometric assembly of peptide-drug conjugates to the QD surface, (3) easy entry of the ensemble complex into the endocytic pathway, (4) negligible toxicity of the drug-free conjugate, and (5) spatiotemporal control of drug release that effectively defeats the effects of MDR pumps. This system represents a new paradigm in NP-mediated drug delivery and will likely lead to new therapeutic approaches for the successful treatment of MDR-positive cancers.

Chapter 5: Proof-of-Concept of an Extracellularly-Actuated Nanoparticle-Peptide-Photosensitizer Bioconjugate for Targeted Membrane Delivery and Improved Photodynamic Therapy

Introduction

Photodynamic therapy (PDT) is an emerging modality for treating certain types of disease and is currently used in the clinic as the fourth line of treatment for cancer. In PDT, photoexcitation of a photosensitizer (PS) drug facilitates electron or energy transfer to the surrounding oxygen molecules resulting in generation of reactive oxygen species (ROS), such as singlet oxygen ($^1O_2$) or free radicals (O_{2-}), causing oxidative damage and eventually leading to cell death.[216, 217] The PS is minimally toxic in the absence of light and consequently PS accumulation in non-specific tissues confers minimal systemic toxicity.[218] In addition, the activating light is non-ionizing (in contrast to light used in radiotherapy) meaning the effect on tissues in the absence of the PS is minimal.[218] In general, PDT is a relatively inexpensive, noninvasive form of therapy, thus providing an attractive clinical alternate to traditional drug therapy.

One common class of PS drug used for PDT is porphyrins.[219] Porphyrins are complex, highly conjugated aromatic molecules with chemically stable structures.[220] There are several FDA-approved formulations of porphyrin and porphyrin derivatives including Photofrin®, Metvixia®, and Visudyne®, all of which have been used for the treatment of various types of cancers.[216-218, 221] While useful for clinical treatment, porphyrins have certain limitations that hinder their overall therapeutic efficacy, namely: 1) they are highly hydrophobic and 2) they are typically delivered non-specifically to cells. The

hydrophobicity of porphyrins pose a major roadblock in the treatment of cancers as low aqueous stability of the drug can result in aggregation in physiological conditions.[222] Additionally, it has been shown that the subcellular localization of a PS can determine its therapeutic efficacy in PDT.[223-226] The singlet oxygen that results from energy transfer after excitation of the PS diffuses only tens of nanometers, such that damage produced is limited to the subcellular location of the PS. Uptake of porphyrins usually limits them to endosomes or the cellular cytosol, whereas directed delivery to the membrane of cells can potentially be used to enhance the cytotoxic effect of ROS via spatially-localized lipid peroxidation of the plasma membrane resulting in peroxyl radicals.[222, 223, 227, 228]

As mentioned in the previous chapters, QDs offer many benefits when used as a central scaffold for NMDD. The surface of QDs can be coated with various hydrophilic ligands, significantly improving the water solubility of appended cargos. The surface is also amenable to attachment of various targeting ligands, as demonstrated in Chapters 3 and 4, where a cell uptake peptide was used to facilitate internalization into endosomes. Additionally, due to their large quantum yield, high photostability, and size-tunable photoluminescence, QDs are ideal Förster resonance energy transfer (FRET) donors, as described in Chapter 3. Hence, by attaching both a porphyrin and a targeting moiety to the surface of the QD, the photosensitizer can be specifically targeted to the membrane of cells and excited by the QD in a FRET configuration in an effort to improve the efficacy of the targeted drug.

In the past, several schemes have been developed to improve the therapeutic efficacy of a porphyrin, chlorin e6 (Ce6).[229-233] Li and coworkers loaded Ce6 onto iron oxide nanoclusters functionalized with polyethylene glycol for targeted delivery using a

magnetic field. *In vivo* results demonstrated minimal increase in tumor volume for mice treated with the NP-Ce6 conjugate compared to a large increase for mice treated with drug alone.[229] Similarly Dou and colleagues showed an improvement in therapeutic efficacy of Ce6 when conjugated to an upconversion NP.[233] Other strategies utilize delivery with oxygen-generating dots to improve therapeutic efficacy in the hypoxic tumor microenviornemnt.[231, 234] While these studies utilize hard NPs for NMDD and show an improvement in therapeutic efficacy, ours is the first study to explore membrane targeting of Ce6 with a hard NP to augment cytotoxicity.

In this study, we use a QD as a prototypical hard NP scaffold to show a proof-of-concept multifunctional hard NP–peptide-photosensitizer conjugate platform for combined membrane targeting and PDT (Figure 22). Our primary goal was to evaluate augmented therapeutic efficacy of the PS when delivered in combination with a QD and a membrane labeling peptide. Here, the central QD serves several purposes: 1) a scaffold for attachment of a membrane labeling peptide, JB858, 2) a scaffold for attachment and improvement of aqueous solubility of a PS, chlorin e6 (Ce6) and 3) a donor molecule to engage in FRET with the Ce6 acceptor. In this system, JB858 is self-assembled, via histidine-mediated metal affinity (described in Chapter 3) and is used to drive membrane tethering of the QD via insertion of the peptide into the lipid bilayer. Also attached to the QD is the well-known, widely used PS, Ce6. The Ce6 is attached directly to amine-terminated QD ligands using EDC conjugation chemistry. Finally, the fluorescence of the QD scaffold and Ce6 cargo enables real-time monitoring of the localization of both the QD carrier and the PS cargo present in the ensemble construct.

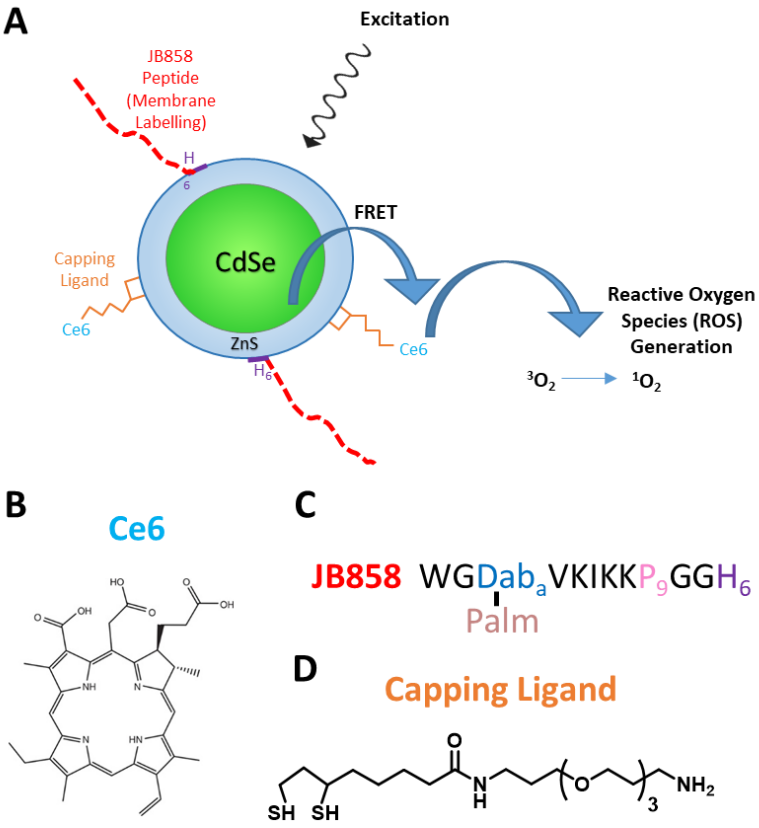

Figure 22: Schematic of the QD-JB858-Ce6 FRET system. A) Schematic of CdSe-ZnS core-shell QDs capped with DHLA-PEG$_{750}$-Ome and a DHLA-PEG-Amine ligand. The amine ligand of the QDs are conjugated to chlorin e6 (Ce6) and a membrane tethering peptide, JB858. Direct excitation of the QDs facilitates fluorescence resonant energy transfer between the QD and Ce6 which leads to generation of reactive oxygen species (ROS) by the Ce6. B) Chemical structure of the Ce6. C) Peptide sequence of JB858. D) Chemical structure of the amine terminated capping ligand. Chemical structure of the methoxy ligand is shown in Figure 8.

We present photophysical characterization of the QD–peptide–Ce6 system in buffered solution outside the cellular environment. Analytical gel electrophoresis and UV/VIS absorbance spectra demonstrated successful assembly of the constructs and long-term stability and fluorescence spectra confirmed FRET between the QD and Ce6. Cellular delivery experiments tracked the residence of the complexes on the plasma membrane of cells, confirmed the maintenance of FRET *in vitro*, and demonstrated an increase in lipid peroxidation and augmented destruction of the plasma membrane for cells treated with the conjugate compared to Ce6 alone. Finally, cytotoxicity studies were performed to

determine the comparative toxicity of Ce6 delivered as a QD complex versus as free PS drug. After excitation with the laser, the QD-JB858-Ce6 complex showed augmented toxicity indicating the benefit of the delivery Ce6 to the plasma membrane. Our *in vitro* data clearly demonstrates that the toxicity of the PS can be augmented by localized delivery to the membrane of cells. The work described here details basic concepts for the design of hard NP materials for externally-triggered actuation of surface-appended drug cargos. The principles developed here can be taken into consideration when developing other NP-based drug delivery systems for the overall improvement of other PDT-based therapeutics.

Materials and Methods

Materials

Dulbecco's phosphate buffered saline (D-PBS) and phosphate buffered saline (PBS), were obtained from ThermoFisher, (Carlsbad, CA). 96-well cell culture cluster microtiter plates were purchased from Corning-Costar (Corning, NY). Doxorubicin hydrochloride (DOX), Dimethyl sulfoxide (DMSO), Tris-borate-EDTA buffer solution, *N*-hydroxysuccinimide (NHS), and 1-Ethyl-3-(3-dimethylaminopropyl)-carbodiimide (EDC) were acquired from Sigma. All other materials/reagents were obtained as noted in the text.

Quantum dot (QD) synthesis

CdSe-ZnS core-shell QD nanocrystals with emission maxima centered at 545 nm were synthesized using a high temperature reaction of organometallic precursors and were rendered hydrophilic by exchanging the native trioctylphosphine/trioctylphosphine oxide (TOP/TOPO) capping shell (hydrophobic ligands) with 85% DHLA-polyethylene glycol $(PEG)_{750}$-OMe and 15% of a short amine ligand (structure shown above in Figure 22), as described previously. The QDs are identified by their wavelength of maximum emission,

so a sample of 545 nm QDs designates a population of QDs which exhibits maximum photoluminescence centered at 545 nm.

Conjugation of QD to chlorin e6 (Ce6)

The primary amine of the DHLA-PEG-NH2 ligands on the QD was conjugated to the carboxyl on the Ce6 (Frontier Scientific Inc.) using EDC/NHS chemistry. QD (1.9 μM) was added to EDC (50 mM), NHS (5 mM), and Ce6 (9.5 uM dissolved in DMSO) in a 1.5x PBS solution and left to stir in the dark at r.t. After 2 h, the reaction was moved to 4^{o}C and left covered overnight. The QD-Ce6 complexes were then purified by centrifugation (3 times) at 1400 x g using a 10K centrifugal filter (Amicon). Conjugation and aqueous stability of the complex was confirmed through UV/vis absorbance using a UV-1600PC Spectrophotometer (VWR Inc.). Conjugation was also confirmed by gel electrophoresis on the QD alone and the QD-Ce6 complexes as described in Chapter 3. Briefly, 5 pmol of samples prepared in PBS buffer were added to the individual wells of an agarose gel. The gel was for 15 minutes at 95 volts/10 cm and imaged using a BioRad ChemiDoc XRS+ imaging system. To confirm FRET, fluorescence spectra of the complex, QD, and Ce6 alone was taken using a RF-6000 Spectrofluorophotometer (Shimadzu Scientific Instruments) at fixed concentrations by excitation at 488 nm for indirect excitation of Ce6.

Synthesis of JB858 peptide and characterization

The membrane-targeting peptide, JB858, (WG[Dab][Palm]VKIKKCP$_9$GGH$_6$) used in this study is described elsewhere.[152] The palmitol ([Palm]) is an aliphatic carbon chain which inserts into the membrane bilayer and is attached to the peptide backbone by a diaminobutyrate moiety. The highly positively charged lysines (KIKK) mediate interaction with the negatively charged membrane. The polyhistidine tract (H$_6$) at the *C*-

terminus mediates peptide self-assembly to the QD surface. Peptide synthesis was performed by Bio-Synthesis Inc. using Boc-solid phase peptide synthesis, purified by HPLC and characterized by electrospray ionization mass spectroscopy.[47, 153]

Cell culture

HeLa cells (American Type Culture Collection (ATCC)) were cultured in Eagle's Minimum Essential Medium (MEM; ATCC) and human embryonic kidney cells (HEK) were cultured in Dulbecco's Modified Eagle's Medium (DMEM; ATCC). Both media were supplemented with 10% (v/v) heat inactivated fetal bovine serum (ATCC), 1% (v/v) antibiotic/antimitotic (Sigma) and 1 mM sodium pyruvate (Sigma). Cultures were maintained in T25 flasks and incubated at 37°C under a 5% CO_2 humidified atmosphere and passaged every 2-3 days at 80% confluency. All cells used in this study were used between passages 3 and 15.

Plasma membrane delivery of QD/JB858/Ce6 bioconjugates

For membrane labeling experiments, HEK 293T/17 cells were seeded on MatTek™ 14 mm dishes (Ashland, MA) that were pre-coated with 30 µg/mL fibronectin (ThermoFisher) for 2h. Cells were seeded at 2×10^5 cells/mL and allowed to adhere overnight. Prior to addition of materials for cellular delivery, the cells were washed twice with DMEM-HEPES. QDs-Ce6 complexes (200 nM) were assembled with JB858 peptides (30 per QD) in DMEM-HEPES for 45 min at RT. The cell monolayers were incubated with QD-JB858-Ce6 for 45 min at 37°C and then colabeled with 8 µM of a plasma membrane marker (Lissamine Rhodamine B 1,2, dihexadecanoyl-sn-glycero-3-phosphoethanolamine (Rhod-PE); ThermoFisher) for 10 min at RT. Cells were then washed twice with LCIS (live cell imaging solution, ThermoFisher) and imaged using confocal microscopy (*vide*

infra). Image analysis and Pearson's correlation coefficient was used to confirm QD, e6 and membrane marker colocalization.

Fluorescence lifetime imaging microscopy (FLIM)

To confirm FRET *in vitro,* FLIM was used to determine the lifetime of the QD alone, Ce6 alone, QD in the QD-Ce6 complex and Ce6 in the QD-Ce6 complex. For FLIM studies, HeLa cells were seeded at a concentration of 8×10^4 cells/mL and allowed to adhere overnight. JB858 was complexed to QD and QD-Ce6 (ratio 30) and QD-JB858, QD-JB858-Ce6, and Ce6 alone were delivered to cells. FLIM was done using an ISS™ FastFlim Imaging System (Champaign, IL) interfaced with a Nikon A1RSi confocal microscope (*vide infra*). Phasor plot analysis was used to determine the lifetimes of the QD and Ce6 and well as the contribution of QD and Ce6 in the QD-Ce6 complex.

Lipid peroxidation mediated by QD/JB858/Ce6 bioconjugates

For lipid peroxidation studies, HeLa cells were seeded at a concentration of 8×10^4 cells/mL and allowed to adhere overnight. Complexes were formed and delivered as described above. After delivery, cells were colabeled with 1 μM of a lipid peroxidation senor (BODIPY™ 581/591 C11, ThermoFisher) for 30 min at 37°C. Cells were then washed with LCIS and placed in an incubation chamber to be imaged using confocal microscopy. QD-JB858 complexes and Ce6 alone at corresponding concentrations were used as controls. This probe detects peroxyl radicals, such as those caused by lipid peroxidation, wherein oxidation of the polyunsaturated butadienyl portion of the probe results in a shift of fluorescence emission peak from ~590 to ~510, thus a loss in fluorescence emission at ~590 indicates lipid peroxidation. Cells were sequentially irradiated using a 488 nm laser at ~60 mW/cm^2 then imaged for a total of 16 minutes.

Individual cells were selected as regions of interest (n = 40-50 cells) and image analysis was used to determine change in fluorescence. Change in fluorescence intensity of the lipid peroxidation probe after excitation was expressed as the percent decrease compared to the fluorescence intensity at t = 0 min.

Quantification of membrane permeability (dead stain)

Changes in membrane permeability/structure was determined using the dead stain, ethidium homodimer-1 (EthD-1), from a LIVE/DEAD® Viability/Cytotoxicity Kit (ThermoFisher). EthD-1 is a membrane impermeable dye that detects cytotoxicity by entering cells with compromised plasma membranes. Upon entering cells, the dye undergoes a 40-fold enhancement in fluorescence, thus producing a bright red fluorescence in cells with compromised membranes. For this study, the conditions used for the lipid peroxidation experiment were emulated. The only difference was colabeling with EthD-1 (4 μM) instead of the lipid peroxidation sensor. EthD-1 was left in solution during irradiation/imaging so that entry into cells could be tracked over time. After the 16 minute irradiation period, cells were imaged every 30 min for 12 h. As before, individual cells were selected as regions of interest (n = 30-40 cells) and image analysis was used to determine a change in fluorescence. Increased uptake of the dye confirms cell death. Change in fluorescence intensity of the EthD-1 dye was expressed as raw intensity with arbitrary units over time (h).

Quantification of cellular cytotoxicity (MTS)

Cellular cytotoxicity was also determined using the CellTiter 96® AQueous One Solution Cell Proliferation Assay (Promega, WI), which is a colorimetric assay that can be used to determine the number of viable cells after incubation with materials of interest.[156,

[157] HeLa cells were seeded in a 96-well tissue culture microplate at a density of 3000 cells/well (doubling time ~24hrs) and allowed to grow overnight. QD-Ce6 complexes were assembled with JB858 peptides (30/QD) in DMEM-HEPES for 45 minutes at RT QD. Complexes were then incubated on cells for 45 min at 37^{o}C. QD-JB858 and Ce6 at corresponding concentrations with and without irradiation were included as controls. The solution was then replaced with DMEM-HEPES and wells were irradiated with a 488 nm laser for a total of 15 min (laser power ~ 15 mW/cm^2) . Cells were then placed in complete media and allowed to proliferate for 72 h. After 72 h, 20 µL of a MTS solution was added to each well and incubated with the cells for 4 h. Absorbance was read at 600 nm and 800 nm (to correct for background subtraction) using a Tecan Infinite M1000 dual monochromator multifunction plate reader equipped with a xenon flash lamp (Tecan). Results were reported as a percentage of cellular viability, normalized to control wells of cells cultured alone with or without irradiation, respectively.

Microscopy and image analysis

All imaging was performed using a Nikon A1RSi Laser Scanning Confocal Imaging system. The following imaging settings were used (laser excitation/dichroic/emission range): QD, 488 nm/488 nm/500-550 nm; Lipid Peroxidation Sensor/Membrane Marker, 561 nm/561 nm/570-620 nm, Ce6, 405 nm/640 nm/663-738 nm. Each channel was imaged sequentially to prevent bleed-though between the channels. Image analysis and image preparation was done using NIS-Elements AR (ver. 4.30.02).

Statistical analysis

The data were statistically analyzed by the univariate analysis of variance (ANOVA) using GraphPad Prism 7.0 software for Windows (La Jolla, CA). Average

values were calculated ± standard error of mean (SEM). A probability of significance of $p < 0.05$ was accepted.

Results and Discussion

Rationale of QD-JB858-Ce6 drug delivery system

The goal of this study was to develop a hard NP-mediated drug delivery system that could cumulatively do the following: 1-target the NP conjugate to the plasma membrane of cells; 2-generate ROS and enable lipid peroxidation via excitation of an appended photosensitizer in a FRET configuration; 3-improve the overall cell killing through treatment with PDT; 4-avail real-time tracking of the NP scaffold, photosensitizer, and therapeutic, and 5-elicit minimal cytotoxicity prior to laser-induced actuation of the NP complex. To achieve this, we employed a QD as a multifunctional central scaffold to attach a PS and a membrane labeling peptide, JB858 (Figure 22). We chose the PS, Ce6, as it is a well-known and widely used porphyrin and is known to cause ROS generation leading to apoptosis and eventual cell death. JB858, the membrane-labeling peptide, is comprised of the sequence WG[Dab][Palm]VKIKKP_9GGH_6, and facilitates membrane tethering of the QD complexes to cells.. The peptide contains an aliphatic palmitol [Palm] for insertion into the lipid bilayer of membranes, a positively charged lysine tract (KIKK) to facilitate electrostatic targeting to the negatively charged membrane of cells, a polyproline tract (P_9) as a spacer, and a polyhistidine tract (H_6) to drive self-assembly of the peptide to the ZnS shell of the QD surface via metal affinity coordination. Additionally, the QD serves as a FRET donor to the Ce6 acceptor in the QD-Ce6 complex, where excitation of the QD leads to energy transfer to and excitation of the Ce6, resulting in generation of ROS. As discussed in Chapter 3, FRET is a photophysical process where excitation of a donor molecule (QD)

results in non-radiative dipole-dipole energy transfer to an acceptor molecule (Ce6), a process that is dependent upon, in part, spectral overlap between the donor's emission and the acceptor's absorbance as well as the center-to-center distance between the donor and acceptor molecule. Overall, the system serves to show proof-of-concept for augmented PDT when delivery of a photosensitizer in a QD bioconjugate.

Characterization and stability of QD-JB858-Ce6 complexes

Conjugation of the carboxyl moiety on the Ce6 to the amine ligands on the QD surface was done using EDC coupling, as described elsewhere.[235] After conjugation, we first sought to confirm successful assembly of the Ce6 to the QD surface. Figure 23A shows the results of gel electrophoresis analysis of the unconjugated QDs compared to QD-Ce6 complexes. As anticipated, the QD alone showed strong mobility towards cathode, while QD-Ce6 complexes stayed within the well. This is due to the fact that the unconjugated QDs contains free amine ligands that impart positive charge and migration in the gel, whereas in the complex form, the amine is conjugated to the Ce6. As a second method of confirmation of assembly, the complexes were analyzed using UV/VIS absorbance (Figure 23B). The absorption spectrum of free Ce6 has an intensive peak at 403 nm (Soret band) and several weaker Q band peaks at 505 nm, 558 nm, 607 nm, and 652 nm with the most intensive being at 652 nm (QD(I)). When Ce6 is conjugated to the QD, the resulting spectra is not a simple superposition of the QD alone and Ce6 alone spectra. Instead, there is a bathochromic shift in the Q(I) band from 663 nm to 655 nm and a broadening of the Soret

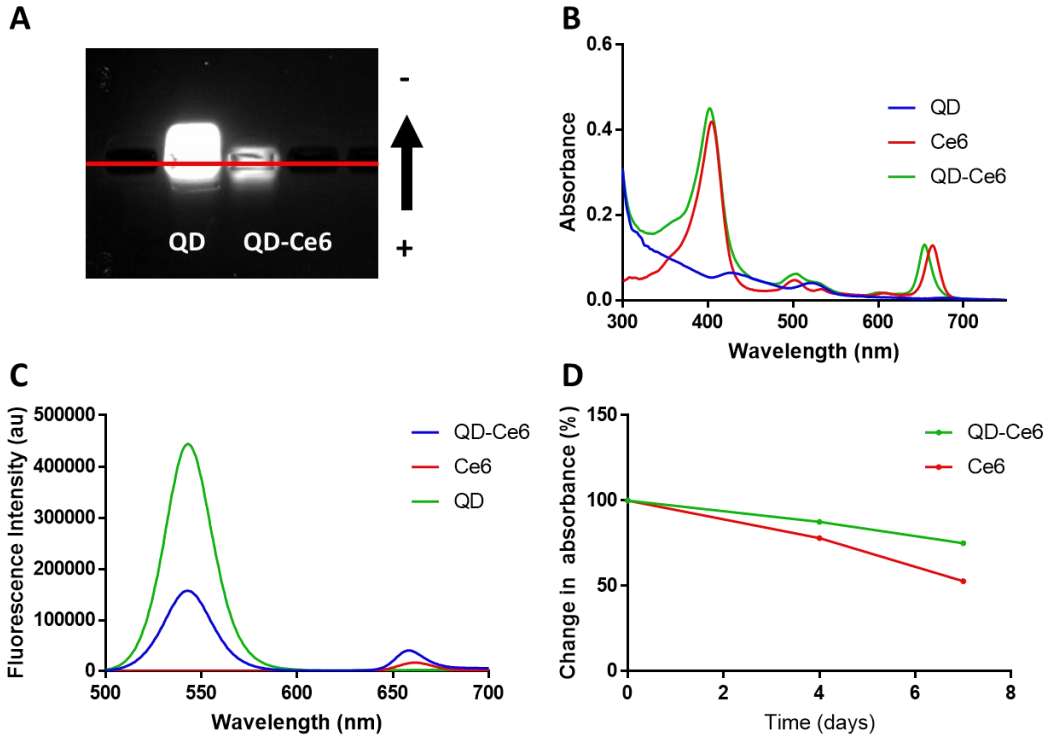

Figure 23: Characterization of the QD-Ce6 FRET system. A) Gel electrophoresis of QDs assembled with Ce6. Red line indicates the location of sample loading wells. B) UV/VIS absorption spectra of QDs alone, Ce6 alone, and QD-Ce6 complexes. C) Fluorescence emission spectra of QD alone, Ce6 alone, and QD-Ce6 complexes excited in a FRET configuration (all excitations done at 488 nm). D) Stability of the QD-Ce6 complex compared to Ce6 alone in aqueous media. Stability was measured as a function of change in percent of absorbance at 655 nm (QD-Ce6) or 663 nm (Ce6 alone).

band (400 nm) which has been reported previously in the literature.[236-239] To confirm FRET between the QD and Ce6, fluorescence spectra was taken at 488 nm excitation. We chose this wavelength due to the fact that here the Ce6 alone has minimal absorbance, while the QD maintains significant absorbance, thus permitting excitation of the QD alone. Although below 375 nm the difference between the QD and Ce6 absorbance is greater than at 488 nm, these wavelengths are toxic to cells, and thus would not be practical for *in vitro* experiments. Fluorescence spectra in Figure 23C shows both a decrease in QD donor fluorescence in the complex compared to QD alone as well as sensitized Ce6 emission confirming FRET. The steady-state experimental FRET efficiency, using the equation from Chapter 3, was determined to be 64%.

In addition to confirmation of complex formation, the stability of the Ce6 when appended to the QD was tested over time. Here, we used UV/VIS absorbance and focused on the Q(I) band at 655/663 nm as the QD has minimal absorbance at this wavelength. Figure 23D shows a percent change in absorbance over time. Even over a one week period it is clear that the Ce6 alone shows a significantly higher decrease in absorbance compared to the QD-Ce6 complex, indicating improved aqueous stability of Ce6 in the conjugate. This difference can be attributed to the hydrophilic PEG coating of the QDs, which lends aqueous solubility to the entire complex.[240, 241]

Plasma membrane labeling of QD-JB858-Ce6 conjugates and in vitro FLIM measurements

Membrane labeling of the QD-JB858-Ce6 complexes was investigated in HEK 293T/17 cells using confocal laser scanning microscopy based on the green emission of the QD, cyan emission of the Ce6 and red emission of the membrane marker, for distinguishing plasma membrane resident NPs vs those inside the cell. After delivery of the QD-JB858-Ce6 conjugates to cells followed by delivery of a membrane maker (Rhod-PE), confocal imaging and comparative colocalization analysis was performed to determine simultaneous location of the QD carrier, Ce6, and the plasma membrane marker as well as to confirm structural integrity of the complex after delivery to cells. As evidenced by Figure 24, the plasma membrane displayed robust labeling with the QD-Ce6 complexes, as confirmed by a Pearson's colocalization coefficient (PCC) of 0.72 ± 0.09 between the QD and membrane marker. This result is consistent with our previous studies utilizing this peptide motif where membrane tethering of QDs was seen for up to 48 hrs in mammalian cells.[15, 242] Additionally, the Ce6 signal was highly colocalized with the QD signal (PCC =

A

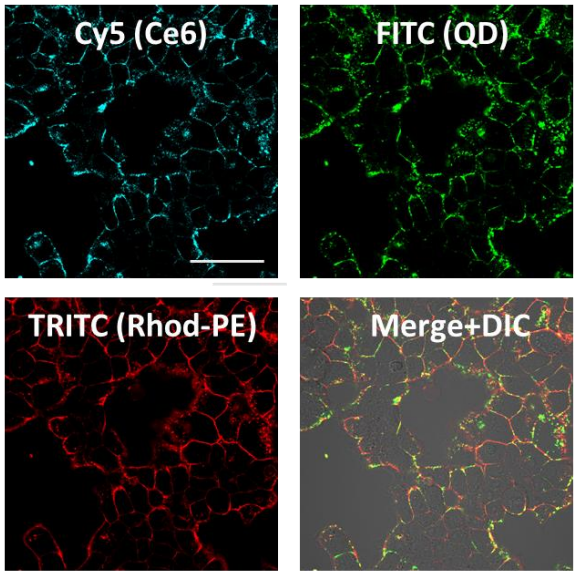

B

Colocalization analysis of membrane and NPs using PCC		
QD-Ce6	QD-Membrane	Ce6-Membrane
.72 ± .05	.72 ± .09	.71 ± .08

Figure 24: Plasma membrane labeling of QD-JB858-Ce6 complexes in HEK cells. A) HEK cells were incubated with pre-formed complexes (incubated at RT for 45 min to mediate QD-peptide assembly) for 45 min at 37°C and subsequently stained with membrane marker Lissamine Rhodamine B (Rhod-PE; 8 µM) for 10 min at RT. Images were obtained using confocal laser scanning microscopy. Shown are fluorescence images of the QD (green), Ce6 (cyan), Rhod-Pe (red) and merged plus transmitted light. Images shown are representative of ~40 cells. Scale bar, 50 µm. B) Image analysis was performed using Pearson's colocalization coefficient (PCC) to determine amount of colocalization between each of the channels. Colocalization is represented as ± SD.

0.72 ± 0.05) demonstrating structural integrity of the complex after delivery and tethering to the plasma membrane.

Table 3: Fluorescence Lifetime (nsec)	
QD	16.9
QD in QD-Ce6 complex	10.6
Ce6	4.8
Ce6 in QD-Ce6 complex	7.7

In addition to confirming membrane delivery of the conjugates, we also determined FRET efficiency after delivery by measuring the change in fluorescence lifetime of QDs *in vitro* using fluorescence lifetime imaging microscopy (FLIM). Table 3 shows FLIM data from samples of QD alone, Ce6 alone, and QD-Ce6 complexes. It is clear that the QD in the complex (10.6 nsec) has a significantly lower lifetime than QD alone (16.9

nsec), whereas Ce6 in the complex (7.7 nsec) has a significantly higher lifetime than Ce6 alone (4.8 nsec). Previous studies have shown similar results where adding Ce6 to QDs in a FRET configuration decreased the lifetime of QD fluorescence.[243, 244] Using the lifetime measurements of the fluorophores in cells and the modified FRET efficiency equation:

$$FRET_E = 1 - \left(\frac{\tau_{da}}{\tau_a}\right)$$

where τ_{da} is the lifetime of the donor in the donor-acceptor complex and τ_d is the lifetime of the donor alone, the FRET efficiency was calculated to be 38%. FRET efficiency differences calculated using emission versus lifetime is not unexpected as the method used to calculate FRET is different.[157] Additionally, this change in FRET efficiency from the steady-state measurements done in a cuvette and calculated using the change in fluorescence of the QD is likely due to the fact that FLIM measurements were done in a different, more complex environment (cells vs. buffer), with different ion concentrations and pH, all of which could contribute to a change in the quantum yield of the QD, resulting in changes in its efficiency of energy transfer to the Ce6 acceptor.[245-247]

Lipid peroxidation mediated by QD-JB858-Ce6 complexes

Having confirmed successful assembly of the complex, effective tethering to the plasma membrane, and FRET within the complex in the context of cells, we next sought to determine the ability of the complexes to produce ROS and facilitate lipid peroxidation. HeLa cells were incubated with Ce6, QD-JB858, or QD-JB858-Ce6 complexes for 30 minutes and then placed in an incubation chamber and imaged using confocal microscopy. For these experiments, we switched to HeLa cells due to the fact that they are a cancer cell line, and thus are a better model for treatment efficacy. Generation of ROS and peroxyl radicals in HeLa cells was recorded and imaged using a red fluorescent probe, BODIPY

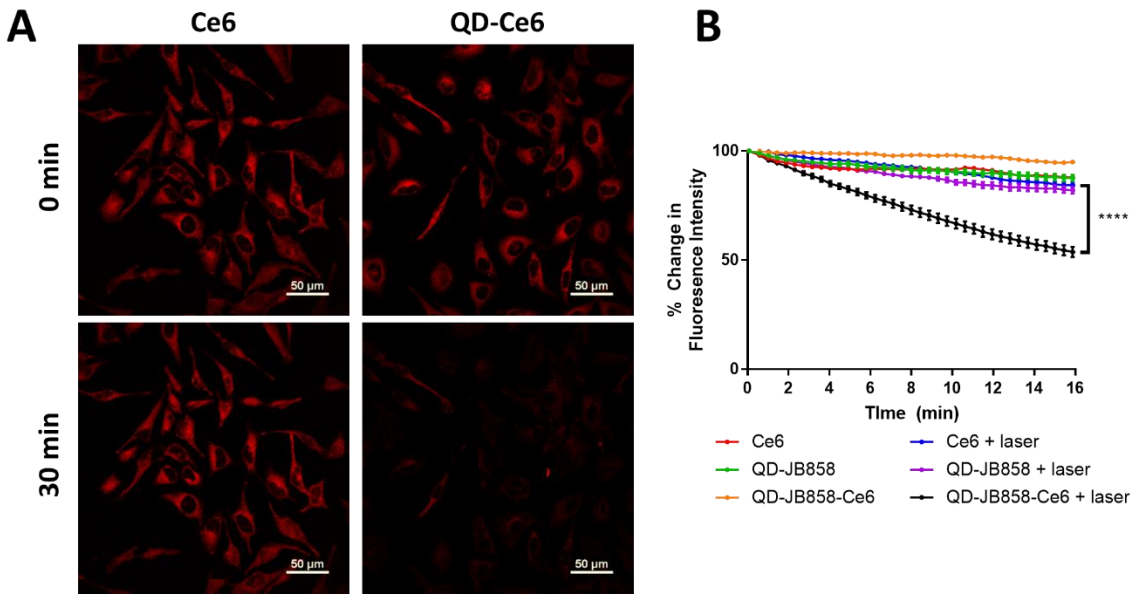

Figure 25: Lipid Peroxidation after treatment with complexes in HeLa cells. A) HeLa cells were incubated with either QD-JB858, QD-JB858-Ce6, or Ce6 alone as before. Cells were colabeled with a lipid peroxidation probe (BODIPY^{TM} 581/591 C11) and then sequentially irradiated for 30 seconds with a 488 nm laser and then imaged using confocal microscopy for a total of 16 minutes. Shown is the change in fluorescence of the probe over the 16 minute period. Images shown are representative of ~40 cells. Scale bar, 50 µm. B) Image analysis was performed to determine the change in fluorescence intensity of the sensor and is plotted as a percent decrease compared to the intensity at t=0. ****,P<0.0001

581/591 C11. The presence of peroxyl radicals causes oxidation of the polyunsaturated butadienyl portion of the sensor, resulting in a fluorescence emission peak shift from ~590 nm to ~520 nm. As the 545 nm QDs have strong emission in the ~520 nm range, we monitored the change in emission in the ~590 nm window, where a decrease in luminescence confirms the presence of ROS/peroxyl radicals indicating lipid peroxidation. Cells were sequentially imaged, then irradiated for 30 seconds with a 488 nm laser at a power of ~60 mW/cm^2 for a total of 20 minutes. In these tests, the QD alone concentration and Ce6 alone concentration was kept the same as that in the complex and QD-JB858, Ce6 alone, and QD-JB858-Ce6 without irradiation were included as controls. As shown in Figure 25, there was minimal change in fluorescence intensity of the probe in cells treated with Ce6 after laser irradiation, indicating minimal generation of peroxyl radicals. This is

due to the fact that Ce6 is spread throughout the cytosol, instead of being localized to the membrane, where lipid peroxidation occurs. Additionally, as the cells were treated with a 488 nm laser, there is minimal direct excitation of the Ce6. For cells treated with the complex, on the other hand, there was a significant decrease in fluorescence intensity of the probe in the red channel, confirming generation of peroxyl radicals. Additionally, minimal change was observed in the fluorescence intensity of the probe after treatment with QD-JB858 plus laser irradiation, confirming peroxyl generation was due to Ce6 on the membrane and not due to the presence of the QDs.

Assessment of changes in membrane permeability/structure

In addition to optical tracking of delivery of the QD-peptide-Ce6 bioconjugates to the plasma membrane and confirmation of cellular lipid peroxidation, changes in membrane permeability/structure after delivery of the QD-JB858-Ce6 conjugate system were examined using a dead stain, ethidium homodimer-1 (EthD-1), from a LIVE/DEAD® assay kit. EthD-1 exhibits a ~40 fold increase in fluorescence when inside cells and it is known to only enter cells with a compromised plasma membrane, thus distinguishing dead cells from viable cells. Staining was performed in a manner where the delivery/imaging conditions emulated those of the lipid peroxidation experiments described above followed by time-resolved imaging using confocal microscopy for 12 h. QD-Ce6 conjugates decorated with 30 copies of JB858 were delivered to HeLa cells for 30 minutes as described above. QD-JB858 complexes without drug were included to evaluate the feasibility of the QD-JB858 bioconjugate as an anticancer platform and Ce6 alone at a corresponding concentration was included to assess changes of the drug alone. All treatments were done with and without laser irradiation to confirm laser effect in ROS generation, lipid

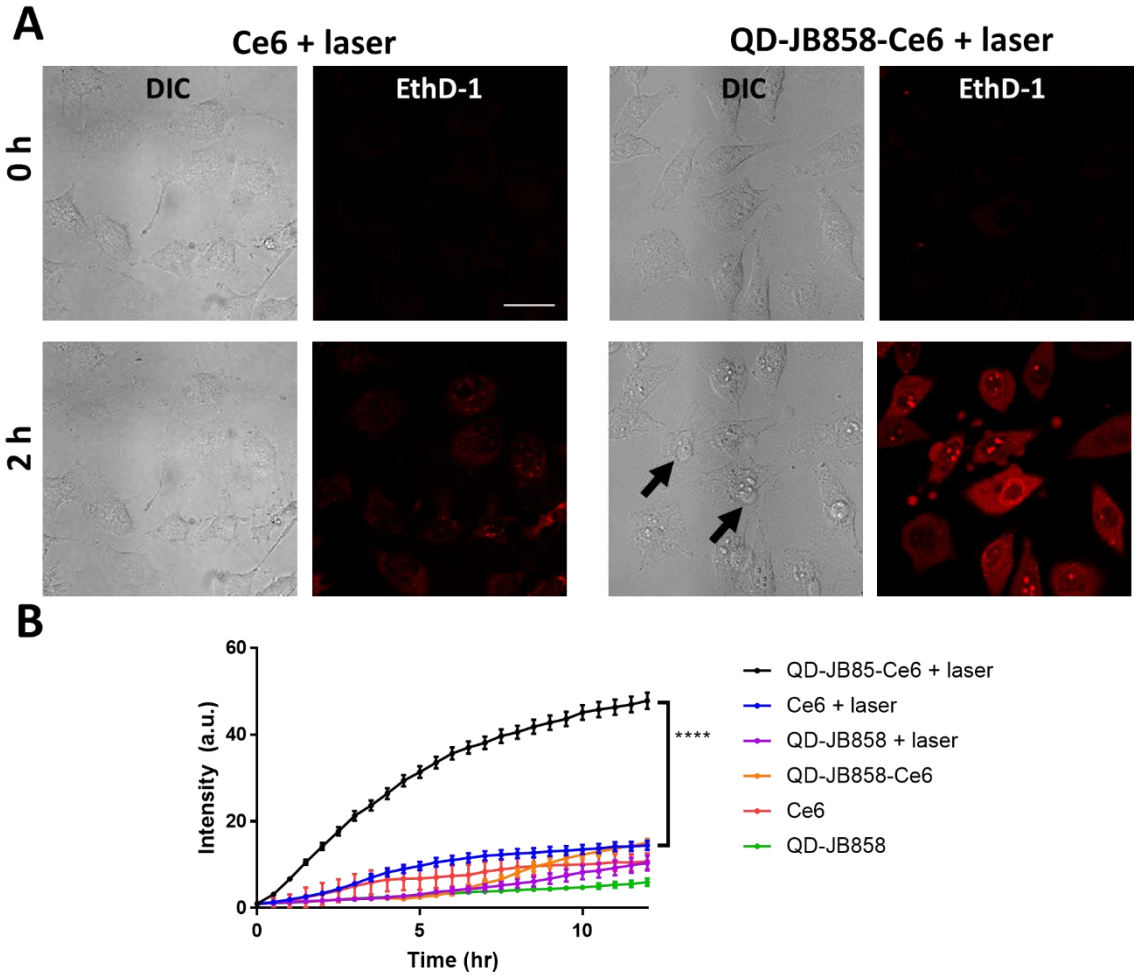

Figure 26: EthD-1 uptake in HeLa cells. A) HeLa cells were incubated with either QD-JB858, QD-JB858-Ce6, or Ce6 alone as before. Cells were colabeled with a dead stain (ethidium homodimer-1 (EthD-1)) and then irradiated for 30 seconds at a time with a 488 nm laser for a total of 16 minutes. After irradiation cells were imaged for 12 h. Shown is the transmitted light (DIC) as well change in fluorescence of the stain (red) over a 2 h period. Images shown are representative of ~40 cells. Scale bar, 50 µm. B) Image analysis was performed to determine the change in fluorescence intensity of the stain and is plotted as arbitrary units. ****; P<0.0001

peroxidation, and improvement of toxicity. After incubation with the constructs, cells were colabeled with EthD-1. After co-staining, the cells were excited as before and then imaged every 30 minutes to determine EthD-1 uptake within the cells. As seen in Figure 26, cells treated with QD-JB858-Ce6 system plus irradiation had significantly higher uptake of the dead stain than cells treated with Ce6 plus irradiation or any of the controls, as expected. Additionally, transmitted light (TD) images of the cells treated with the complex after just 2 h, showed morphological signs consistent with compromised membranes including blebs

in the membrane (protrusion of the plasma membrane that is known to be a marker of cell death)[248]. Previous studies examining delivery of the photosensitizers to the membrane of cells show similar results, both in EthD-1 uptake as well as morphological changes in the membrane.[249-252] Taken together, these results authenticate our lipid peroxidation experiments that demonstrated augmented ROS generation for irradiated cells treated with the complex compared to cells treated with the free drug.

Cytotoxicity of QD-peptide-DOX-JB434 conjugates

Although EthD-1 is used as a dead cell marker, the cellular internalization of EthD-1 is dependent on a change in membrane integrity as it is known to preferentially enter cells with a damaged plasma membrane. As our construct is known to affect the membrane through lipid peroxidation, the significantly improved uptake of the EthD-1 dye is probably attributable to compromised membrane structure prior to cell death. Thus, as an additional method of testing viability that was not dependent on membrane integrity, an MTS cell viability assay was used. MTS is a colorimetric assay that determines cell viability by assessing cellular metabolic activity. Viable cells contain enzymes that reduce the MTS dye into an insoluble formazan product, which has a purple color. Hence, generation of the formazan product is dependent on cellular activity and not on changes in membrane integrity. After initial delivery of the complexes, followed by 15 minutes of irradiation and a 72 h cell culture period to allow for proliferation, MTS tetrazolium reagent, a colorimetric metabolic activity indicator, was added to the wells. As with the EthD-1 viability experiment, all the appropriate controls were included to confirm the effect of the laser and membrane delivery mechanism in augmenting therapy, as well as to verify cytocompatibility of the QD-JB858 system. Figure 27 shows the resulting cytotoxicity

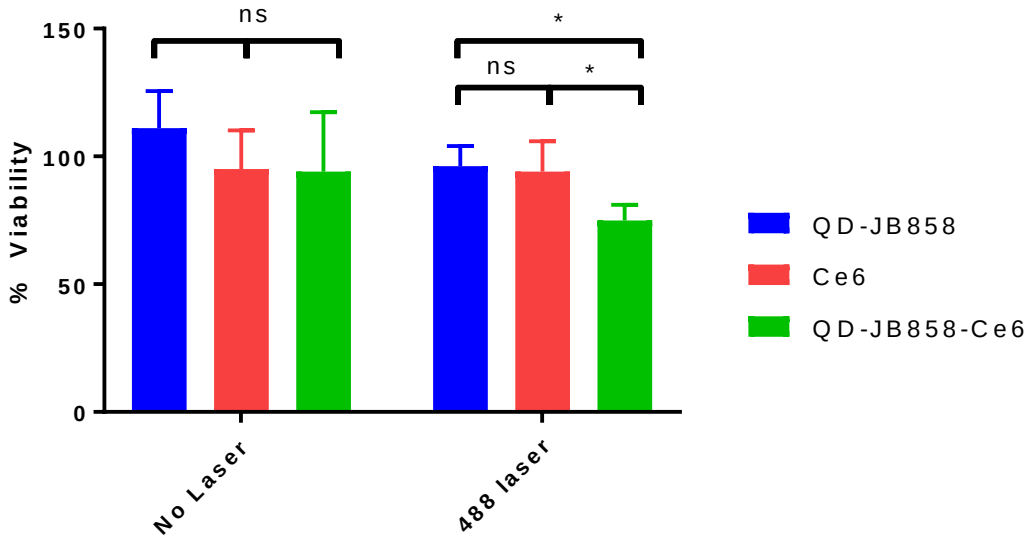

Figure 27: Quantification of cytotoxicity of complexes with and without irradiation. Average cell viability of QD-JB858, Ce6, and QD-JB858-Ce6 bioconjugates with and without laser treatment. Complexes were incubated on cells for 45 min followed by laser irradiation for 15 min and proliferation for 72 h. Viability was determined by MTS assay. Plot shows average cell viability for each construct. The data is represented as a percent cell viability ± S.D. of wells performed in triplicate relative to control cells with and without laser irradiation, respectively. *; $P<0.05$, ns; $P>0.05$

graphs for the various constructs. Laser irradiation of cells alone and delivery of QD-JB858 with and without laser treatment displayed negligible cytotoxicity, proving cytocompatibility of the nanoplatform as well as the laser.[15, 155] Additionally, delivery of both Ce6 alone and QD-JB858-Ce6 bioconjugates alone (without laser irradiation) had high viability. At this laser power, even the Ce6 alone plus laser showed minimal toxicity. The only sample to show significant toxicity was the QD-JB858-Ce6 NPs with laser treatment, confirming the cell-killing effect after delivery in the conjugate form. It is important to note that while the laser intensity used in the MTS experiments were ~4-fold lower than in the EthD-1 uptake study and the lipid peroxidation experiment, we still saw a significant difference in toxicity between laser-irradiated cells treated with Ce6 alone compared to Ce6 in the bioconjugate form. This is consistent with results from both the lipid peroxidation experiments and well as the EthD-1 uptake study. Previous studies

without membrane targeting of the QDs showed comparable toxicity of Ce6 in the complex form compared to free drug. For example, Charron and colleagues synthesized InP/ZnS QDs conjugated to Ce6 using EDC chemistry. *In vitro* delivery in MDA-MB-231 breast cancer cells showed comparable toxicity between the free drug and the hybrid.[253] Similarly, Song and colleagues found comparable toxicity in 4T1 cells treated with polypyrrole (PPy) NPs coated with bovine serum albumin (BSA) and loaded with Ce6 compared to Ce6 alone with an without laser.[254] Additionally, while other studies do show improved therapeutic efficacy of the photosensitizer after delivery with a NP bioconjugate complex, the improvement in therapeutic efficacy is attributed to other factors such as improved uptake or generation of O_2 in a hypoxic environment.[230, 236, 255] Thus, our work shown here demonstrates that delivery of the photosensitizer specifically to the membrane can significantly improve its therapeutic efficacy.

Conclusions

The goal of this project was to show proof-of-concept of a prototypical multifunctional NP-photosensitizer bioconjugate platform for augmented PDT in cancer cells. The complex consists of a central QD for real-time tracking of the complex in cells, aqueous solubility, and FRET excitation of the Ce6 photosensitizer, a targeting peptide for tethering of the NP-complex to the plasma membrane of cells, and a photosensitizer for PDT.

Here, the QD, as a delivery platform imparts several features of note. First, as the QD itself is fluorescent, it enables real-time tracking of the complex in cells. This allows us to determine membrane localization of both the QD and Ce6 and to confirm stability *in vitro.* Second, the QD is highly soluble in aqueous media, thus, it imparts solubility to the

Ce6, a highly hydrophobic drug. Cuvette analysis showed improved solubility of this drug over time, when delivered in conjunction with the QD-JB858 bioconjugate. Third, the QD can be used as a central scaffold to append other biomolecules. In the study, we appended a peptide, JB858, capable of tethering the complex to the plasma membrane of cells. Looking forward, we expect the QD-JB858-Ce6 to be utilized as a multifunctional scaffold to afford drug delivery in addition to mediating lipid peroxidation. A collaborator has recently developed a ROS-responsive chemical linker attached to the chemotherapeutic DOX.[256] Thus, after conjugation to a his-tagged peptide, the second drug could also be appended to the QD scaffold in order to develop a combinatorial ROS-generation/drug delivery therapy system. Finally, we use the QD in a FRET-based system to indirectly excite the Ce6. FRET is facilitated by the overlap between the QD emission and Ce6 absorbance, as well as the high quantum yield of the QD. While in this case, excitation of the QD is actually at a lower wavelength than direct excitation of the Ce6 would be, use of a FRET based system has implications that can be used to augment therapy. QDs are known to be one of the best two photon excitation donors and possess a large two photon absorption cross section, where the wavelength max is size dependent. Two photon absorption of porphyrins is on the order of 1,000 GM (for monomers), whereas two-photon absorption for QDs is on the order of 30,000 GM.[257, 258] Therefore, delivery of this system with FRET excitation could be used to further improve the overall therapeutic efficacy of the drug.

Overall, we have shown augmented PDT of a photosensitizer after delivery in a QD-JB858-Ce6 complex. Cuvette analysis and *in vitro* studies confirmed FRET between the QD and Ce6. Experimental evidence showed both improved stability of the complex in

aqueous media as well as membrane tethering and maintenance of structural integrity of the complex in cells. *In vitro*, the QD-JB858-Ce6 bioconjugates resulted in both improved lipid peroxidation and ROS generation as well as improved cytotoxicity compared to free Ce6, indicating an overall improvement in PDT. The system developed in this study utilizes NMDD to improve the stability and therapeutic efficacy of a well-known photosensitizer, Ce6. The concepts developed here can be applied to other hard NP systems for development of more effective anticancer therapies using PDT.

Chapter 6: Conclusions

Conclusions Overview

The development of an effective hard NMDD system requires the careful consideration of many components including the composition of the NP (hard vs. soft), targeting of the NP to specific cells or cellular organelles, controlled release of cargo from the NP, and stability and biocompatibility of the NP system itself. This project has specifically focused on expanding our understanding of controlled release of appended cargos from hard NP carriers and targeting capabilities of these NP-cargo complexes to specific subcellular organelles. We have examined both intracellularly and extracellularly-actuated systems of drug release and determined important design considerations that need to be taken into account as well as potential applications of such systems *in vitro*. For all the systems described herein, we utilize a QD as a prototypical hard NP due to its optoelectronic properties such as its exceptional luminesce, small size, amenability to surface modification and attachment of biomolecules, and long-term cytocompatibility.

In Chapter 3 and 4, we examined an intracellularly-actuated QD drug delivery system, where release is controlled by the innate cellular environment. First, in Chapter 3, we performed a comparative study of four different internally cleavable linkages in order to modulate the toxicity of a well-known cancer therapeutic, DOX. Here the QD served as a central scaffold onto which was appended both a cell uptake peptide to facilitate internalization within the endocytic pathway, as well as a drug display peptide that was conjugated to DOX via three cleavable linkers (ester, disulfide, hydrazone) and a control non-cleavable linker (amide). As uptake of the complexes was within the endocytic pathway, the presence of esterases and low pH within endosomes/lysosomes can facilitate

cleavage of the ester and hydrazone linkages, respectively, inside endosomes where they would normally be trapped. Thus toxicity studies revealed high toxicity of the QD-ester-DOX-JB434 complex and moderate toxicity of the QD-hydrazone-DOX-JB434 complex. Additionally, localization studies revealed that the ester linkage had "burst-type" release kinetics, where nuclear localization was seen after just 2 h, but the hydrazone showed increased release over an 8 h period, indicating a slower release time. As endosomes are known to be oxidizing environments, the disulfide linkage, which is only cleavable in the presence of reducing agents remained intact and resulted in no toxicity *in vitro.* Clearly, the nature of the linkage has a profound effect on the kinetics of cargo release as well as the efficiency of drug delivery within the cellular environment. The linkage of drug attachment must, therefore, be chosen with care to overcome limitations of uptake within the endocytic pathway of cells. A comparative understanding of these linkages with respect to hard NPs helps to broaden the range of potential applications of such complexes and could lead to designs including combinations of such linkages for the development of higher architecture hard NP drug delivery systems.

Second, in Chapter 4 we utilized the knowledge gained in Chapter 3 to produce a novel NMDD system for overcoming MDR, a phenomenon that is known to severely affect the therapeutic efficacy of many anticancer drugs. Here, we used the ester linkage from Chapter 3 to spatiotemporally control release in MDR positive cells, so that the drug is trafficked away from membrane resident pumps and released closer towards the nucleus, its target destination. While this chapter describes a potential use of the system developed in Chapter 3, it also elucidates potential mechanisms to improve the overall drug therapeutic efficacy in MDR cells. This system is unique in that 1) it does not require the

use of exogenous drugs such as combinatorial chemotherapeutic agents, nucleic acids, or MDR pump inhibitors, all which introduce the potential for off-target toxicity and 2) it requires a short incubation time (2 h) compared to similar systems that utilize much longer incubation times (24-72 h) to achieve comparable defeat of MDR. The novelty of this system and the general concepts discovered, could be used in conjunction with other hard NP systems as a mechanism for overcoming MDR and improving the therapeutic efficacy of drugs in treatment of various cancers.

Finally, in Chapter 5, we used a method of extracellularly-controlled actuation to improve the therapeutic efficacy of an attached drug. This system, overall, is unique from the other two described here as it uses two other properties of the QD: the ability to participate in FRET and its hydrophilicity to improve the aqueous solubility of a hydrophobic drug. Here, a photosensitizer and a membrane targeting peptide were appended to the surface of the QD in order to generate ROS through excitation of the photosensitizer and to direct tethering of the complex to the plasma membrane, where the ROS generated are most effective as they participate in lipid peroxidation. Delivering the Ce6 in conjunction with the QD was shown to significantly improve its aqueous solubility over time. Additionally, lipid peroxidation and cytotoxicity data made it clear that membrane localization of the Ce6 has a profound effect on the therapeutic efficacy of the drug and that excitation in the FRET configuration further separates efficacy of the Ce6 alone compared to Ce6 in the complex. Much like the systems developed and utilized in the other two chapters, concepts from the complex developed here can be used in conjunction with other hard NP systems to improve the overall therapeutic efficacy of PSs for use in PDT.

The work completed as part of this dissertation contributes substantially to our understanding of how to actively control the release of appended cargo from the surface of hard NPs both intracellularly and extracellularly. The work presented here has expanded on knowledge of previous systems that utilize similar concepts as the ones developed here. While internally controlled release of hard NP systems has been shown before, a comparative analysis of different internally cleavable linkages on the same platform has never been done before, as was done in Chapter 3. Additionally, application of such a system for overcoming MDR without the need for exogenous drugs and with a short incubation time has not previously been shown, as was shown in Chapter 4. Finally, Chapter 5, developed a novel FRET-based system for improved PDT by specific delivery to the membrane of cells to improve overall therapeutic efficacy. All the complexes presented herein utilize multifunctional systems that are capable of visualizing the complex in cells, targeting the complex to specific subcellular locations, and controlling therapy, either through release or activation of an appended therapeutic. Additionally, all the systems presented outline basic fundamental design concepts that need to be taken into consideration and that can be applied to other hard NMDD systems for a variety of applications. Overall, we feel the work presented here outlines the potential utility of hard NPs in improving the therapeutic efficacy of NMDD systems and further overcoming the roadblocks in traditional systemic therapy.

Future Directions

As mentioned before, the systems presented here can be applied to other hard nanoplatforms such as AuNPs and metal oxides, however, there is still some understanding that can be achieved using the prototypical NP complex utilized here. For

example, Chapter 3 and 4 developed a bioconjugate capable of controlling release internally and elucidated modulation of toxicity that was dependent on the type of intracellularly cleavable linkage used to release the drug. However, the influence of other factors such as the coating of the NP, size of the NP and cell type were not specifically examined but they likely play a role in determining the efficacy of the QD-drug cargo system *in vitro*. Additionally, the experiments focused on release and cytotoxicity over a 72 h time period (the standard for assays like MTT which was used in the studies detailered here). Yet, from the results of Chapter 3, it was clear that length of time did have an effect on the percentage of drug released. Thus, longer studies could help elucidate more about the role the linkages play in internally controlled drug delivery. In Chapter 5, we developed a bioconjugate capable of engaging in FRET with a PS and generating peroxyl radicals leading to cell death and improvement of the therapeutic efficacy of the drug. It is well known that QDs have a much larger two-photon extinction coefficient when compared to that of many PS.[259, 260] Hence a future study looking at two-photon excitation could further improve PDT. Additionally, recently, a university collaborator developed a ROS-cleavable linkage attached to DOX that can append DOX to the DOX display peptide or to the termini of the QD capping ligands.[256] Consequently testing this linkage in conjunction with the complex developed here could be used to develop a combinatorial PS/drug delivery system that can controllably induce ROS generation while releasing DOX using external stimuli. Finally, all three chapters focused on delivering the complex to subcellular organelles, however, a limitation in current use of NMDD systems is non-targeted delivery in terms of delivery to specific subsets of cells (*i.e.* cancer cells vs. normal cells). Accordingly, a future

project could be focused on utilization of novel peptide sequences for distinguishing between such groups of cells.

Application Outlook

Overall, the objective of this dissertation was to address some of the critical parameters that need to be taken into consideration when designing hard NP systems and to outline proof-of-concept systems for controlled drug delivery. While the systems detailed here help develop a fundamental understanding of actively controlled drug release, the overall goal is eventual translational application of these systems to *in vivo* use. Thus, the goal of this section is to address some of the remaining challenges that need to be addressed in order to apply these systems as therapeutics in the clinic.

All three systems described herein are capable of targeting the hard NP to a specific subcellular location (endosomes in the case of Chapter 3 and 4 and plasma membrane in the case of Chapter 5). However, as the *in vitro* systems used here contain only one cell type, targeting the constructs to specific subsets of cells was not addressed. Hence one future challenge in application of these systems could be targeting specific cells *in vivo*. One potential method to address this limitation could be conjugation/co-delivery with ligands that target specific receptors expressed only on the desired cell.

Another potential pitfall in the application of the first system described is active exocytosis by the same endosomes that helped facilitate cellular internalization of the NP-drug complex. A number of studies have shown the efficient exocytosis of internalized NPs.[261-263] To prevent exocytosis from affecting the therapeutic efficacy of the NP, the drug release rate needs to be monitored to ensure that the drug is released before the vesicles containing the NP-drug complex are exocytosed from the cell. Additionally,

exocytosis can be prevented by co-delivery with certain inhibitors, such as Vacuolin-1, which is a known lysosomal exocytosis inhibitor.[264]

Finally, the hard NP system used here were QDs, which pose some challenges for *in vivo* applications due to their cadmium containing core. While for *in vitro* studies, extensive research has shown that surface ligands and multiple layers of the ZnS shell play a large role in improving biocompatibility and preventing leeching of the Cd from the core, there are much fewer studies examining long term biocompatibility of CdSe/ZnS QDs *in vivo.* Thus for translational purposes, the concepts developed here would need to be translated to a non-toxic QD core, such as CuInS2 or InP, or to other hard NP materials currently in clinical trials such as AuNPs and IONPs.[265]

Appendix

Contribution to Science

Publications

Sangtani, A., Muroski, M. E., and Delehanty, J. B. (2019) Mechanisms of actively triggered drug delivery from hard nanoparticle carriers, in *Targeted nanosystems for therapeutic applications: New concepts, dynamic properties, efficiency, and toxicity* (Sakurai, K., and Ilies, M. A., Eds.), American Chemical Society, Ch. 8, 157-185.

Sangtani, A., Petryayeva, E., Susumu, K., Huston, A.L., Medintz, I.L., Algar, W.R., Delehanty, J.B. (2019). Nanoparticle-peptide-drug bioconjugates for unassisted defeat of multidrug resistance in a model cancer cell line. *Bioconjugate Chemistry*. 30(3), 525-530.

Delehanty, J. B., Das, S., Goldberg, E., **Sangtani, A.**, Knight, D. A., (2018). Synthesis of a reactive oxygen species-responsive doxorubicin derivative. *Molecules*, 23(7), 1809.

Field, L.D., Nag, O.K., **Sangtani, A.**, Burns, K. E., Delehanty, J. B., (2018). The role of nanoparticles in the improvement of systemic drug delivery. *Therapeutic Delivery*, 9(7), 527-545.

Sangtani, A., Petryayeva, E., Wu, M., Susumu, K., Oh, E., Huston, A.L., Lasarte-Aragonés, G., Medintz, I.L., Algar, W.R., Delehanty, J.B., (2018). Intracellularly actuated quantum dot–peptide–doxorubicin nanobioconjugates for controlled drug delivery via the endocytic pathway. *Bioconjugate Chemistry*, 29(1), 136-148.

Sangtani, A., Nag, O. K., Field, L. D., Breger, J. C., & Delehanty, J. B., (2017). Multifunctional nanoparticle composites: progress in the use of soft and hard nanoparticles for drug delivery and imaging. *Wiley Interdisciplinary Reviews: Nanomedicine and Nanobiotechnology*, 9(6), e1466. ***(Featured on journal)***

Rowland, C. E., Susumu, K., Stewart, M. H., Field, L. D., **Sangtani, A.**, Medintz, I. L., & Delehanty, J. B., (2017). Cellular applications of semiconductor quantum dots at the US Naval Research Laboratory: 2006–2016. In *Reviews in Fluorescence* 2016, p. 203-242. Springer International Publishing.

Nag, O. K., Field, L. D., Chen, Y., **Sangtani, A.**, Breger, J. C., & Delehanty, J. B., (2016). Controlled actuation of therapeutic nanoparticles: an update on recent progress. *Therapeutic Delivery*, 7(4), 335-352.

Presentations

Sangtani, A., Petryayeva, E., Susumu, K., Oh, E., Huston, A.L., Lasarte-Aragonés, G., Medintz, I.L., Algar, W.R., Delehanty, J.B., Intracellularly-actuated nanoparticle-drug

bioconjugates for overcoming multidrug resistance in cancer cells. Nanoworld Conference, Boston, Massachusetts, April 22-24, 2019. (Accepted)

Sangtani, A., Petryayeva, E., Susumu, K., Oh, E., Huston, A.L., Lasarte-Aragonés, G., Medintz, I.L., Algar, W.R., Delehanty, J.B., Unassisted defeat of multidrug resistance using intracellularly-actuated nanoparticle bioconjugates in a model cancer cell line. NSF PROMISE AGEP Research Symposium, University of Maryland, College Park, February 15, 2019.

Sangtani, A., Petryayeva, E., Wu, M., Susumu, K., Oh, E., Huston, A.L., Lasarte-Aragonés, G., Medintz, I.L., Algar, W.R., Delehanty, J.B., Nanoparticle bioconjugate for controlled cellular delivery of doxorubicin. SPIE BiOS, San Francisco, California, January 27-February 1, 2018.

Sangtani, A., Petryayeva, E., Wu, M., Susumu, K., Oh, E., Huston, A.L., Lasarte-Aragonés, G., Medintz, I.L., Algar, W.R., Delehanty, J.B., Spatiotemporal modulation of doxorubicin toxicity via delivery as a nanoparticle-bioconjugate complex. ACS National Meeting, Washington, D.C., August 20-24, 2017.

Sangtani, A., Petryayeva, E., Wu, M., Susumu, K., Oh, E., Huston, A.L., Lasarte-Aragonés, G., Medintz, I.L., Algar, W.R., Delehanty, J.B., Modulation of doxorubicin toxicity through nanoparticle-assisted cellular delivery. 2017 TechConnect World Innovation Conference, Washington, D.C., May 15-17, 2017.

References

(1) Ding, Y., Zhou, Y. Y., Chen, H., Geng, D. D., Wu, D. Y., Hong, J., Shen, W. B., Hang, T. J., and Zhang, C. (2013) The performance of thiol-terminated PEG-paclitaxel-conjugated gold nanoparticles. *Biomaterials 34*, 10217-27.

(2) Jeon, H., Kim, J., Lee, Y. M., Kim, J., Choi, H. W., Lee, J., Park, H., Kang, Y., Kim, I. S., Lee, B. H., *et al.* (2016) Poly-paclitaxel/cyclodextrin-SPION nano-assembly for magnetically guided drug delivery system. *J Control Release 231*, 68-76.

(3) Ruan, S., Yuan, M., Zhang, L., Hu, G., Chen, J., Cun, X., Zhang, Q., Yang, Y., He, Q., and Gao, H. (2015) Tumor microenvironment sensitive doxorubicin delivery and release to glioma using angiopep-2 decorated gold nanoparticles. *Biomaterials 37*, 425-35.

(4) Li, J., Liu, F., Shao, Q., Min, Y., Costa, M., Yeow, E. K., and Xing, B. (2014) Enzyme-responsive cell-penetrating peptide conjugated mesoporous silica quantum dot nanocarriers for controlled release of nucleus-targeted drug molecules and real-time intracellular fluorescence imaging of tumor cells. *Adv Healthc Mater 3*, 1230-9.

(5) Poudel, B. K., Gupta, B., Ramasamy, T., Thapa, R. K., Pathak, S., Oh, K. T., Jeong, J. H., Choi, H. G., Yong, C. S., and Kim, J. O. (2017) PEGylated thermosensitive lipid-coated hollow gold nanoshells for effective combinational chemo-photothermal therapy of pancreatic cancer. *Colloid Surface B 160*, 73-83.

(6) Zhang, Z., Liu, C., Bai, J., Wu, C., Xiao, Y., Li, Y., Zheng, J., Yang, R., and Tan, W. (2015) Silver nanoparticle gated, mesoporous silica coated gold nanorods (AuNR@MS@AgNPs): low premature release and multifunctional cancer theranostic platform. *ACS Appl Mater Inter 7*, 6211-9.

(7) Wei, J., Shuai, X., Wang, R., He, X., Li, Y., Ding, M., Li, J., Tan, H., and Fu, Q. (2017) Clickable and imageable multiblock polymer micelles with magnetically guided and PEG-switched targeting and release property for precise tumor theranosis. *Biomaterials 145*, 138-153.

(8) Zhang, H., Wang, C., Chen, B., and Wang, X. (2012) Daunorubicin-TiO2 nanocomposites as a "smart" pH-responsive drug delivery system. *Int J Nanomedicine 7*, 235-42.

(9) Liu, Y., Yang, M., Zhang, J., Zhi, X., Li, C., Zhang, C., Pan, F., Wang, K., Yang, Y., Martinez De La Fuentea, J., *et al.* (2016) Human induced pluripotent stem cells for tumor targeted delivery of gold nanorods and enhanced photothermal therapy. *ACS Nano 10*, 2375-2385.

(10) Croissant, J. G., Zhang, D., Alsaiari, S., Lu, J., Deng, L., Tamanoi, F., Almalik, A. M., Zink, J. I., and Khashab, N. M. (2016) Protein-gold clusters-capped mesoporous silica nanoparticles for high drug loading, autonomous gemcitabine/doxorubicin co-delivery, and in-vivo tumor imaging. *J Control Release 229*, 183-91.

(11) Paris, J. L., Cabañas, M. V., Manzano, M., and Vallet-Regí, M. (2015) Polymer-grafted mesoporous silica nanoparticles as ultrasound-responsive drug carriers. *ACS Nano 9*, 11023-11033.

(12) Yu, C., Ding, B., Zhang, X., Deng, X., Deng, K., Cheng, Z., Xing, B., Jin, D., Ma, P., and Lin, J. (2018) Targeted iron nanoparticles with platinum-(IV) prodrugs and anti-EZH2 siRNA show great synergy in combating drug resistance in vitro and in vivo. *Biomaterials 155*, 112-123.

(13) Ma, M., Huang, Y., Chen, H., Jia, X., Wang, S., Wang, Z., and Shi, J. (2015) Bi2S3-embedded mesoporous silica nanoparticles for efficient drug delivery and interstitial radiotherapy sensitization. *Biomaterials 37*, 447-455.

(14) Oh, Y., Moorthy, M. S., Manivasagan, P., Bharathiraja, S., and Oh, J. (2017) Magnetic hyperthermia and pH-responsive effective drug delivery to the sub-cellular level of human breast cancer cells by modified CoFe2O4 nanoparticles. *Biochimie 133*, 7-19.

(15) Boeneman, K., Delehanty, J. B., Blanco-Canosa, J. B., Susumu, K., Stewart, M. H., Oh, E., Huston, A. L., Dawson, G., Ingale, S., Walters, R., *et al.* (2013) Selecting improved peptidyl motifs for cytosolic delivery of disparate protein and nanoparticle materials. *ACS Nano 7*, 3778.

(16) Zhao, N., Wu, B., Hu, X., and Xing, D. (2017) NIR-triggered high-efficient photodynamic and chemo-cascade therapy using caspase-3 responsive functionalized upconversion nanoparticles. *Biomaterials 141*, 40-49.

(17) Kamboj, V. P. (2000) Herbal Medicine. *Curr Sci India 78*, 35-39.

(18) Jones, A. W. (2011) Early drug discovery and the rise of pharmaceutical chemistry. *Drug Test Anal 3*, 337-44.

(19) Whayne, T. F. (2018) Clinical use of digitalis: A state of the art review. *Am J Cardiovasc Drug 18*, 427-440.

(20) Kwakye, G. F., Jiménez, J., Jiménez, J. A., and Aschner, M. (2018) Atropa belladonna neurotoxicity: implications to neurological disorders. *Food Chem Toxicol 16*, 346-353.

(21) Bosch, F., and Rosich, L. (2008) The contributions of Paul Ehrlich to pharmacology: a tribute on the occasion of the centenary of his Nobel Prize. *Pharmacology 82*, 171-9.

(22) Povl Krogsgaard-Larsen, T. L., Ulf Madsen (2002) *Textbook of drug design and discovery*, Taylor and Francis Inc. , New York, NY.

(23) Sangtani, A., Nag, O. K., Field, L. D., Breger, J. C., and Delehanty, J. B. (2017) Multifunctional nanoparticle composites: progress in the use of soft and hard nanoparticles for drug delivery and imaging. *WIRES Nanomed Nanobi 9*, e1466.

(24) Cho, K., Wang, X., Nie, S., Chen, Z. G., and Shin, D. M. (2008) Therapeutic nanoparticles for drug delivery in cancer. *Clin Cancer Res 14*, 1310-6.

(25) Tiwari, G., Tiwari, R., Sriwastawa, B., Bhati, L., Pandey, S., Pandey, P. And Bannerjee, S.K. (2012) Drug delivery systems: An updated review. *Int J Pharm Investig 2*, 2.

(26) Jin, S. a. Y., K. (2007) Nanoparticle-mediated drug delivery and gene therapy. *Biotechnol Progr 23*, 32-41.

(27) Singh, R., and Lillard, J. W., Jr. (2009) Nanoparticle-based targeted drug delivery. *Exp Mol Pathol 86*, 215-23.

(28) Choi, H. S., Liu, W., Misra, P., Tanaka, E., Zimmer, J. P., Ipe, B. I., Bawendi, M. G., and Frangioni, F. V. (2007) Renal clearance of nanoparticles. *Nat Biotechnol 25*, 1165-1170.

(29) Jabr-Milane, L. S., Van Vlerken, L. E., Yadav, S., and Amiji, M. M. (2008) Multi-functional nanocarriers to overcome tumor drug resistance. *Cancer Treat Rev 34*, 592-602.

(30) Nakamura, Y., Mochida, A., Choyke, P. L., and Kobayashi, H. (2016) Nanodrug delivery: Is the enhanced permeability and retention effect sufficient for curing cancer? *Bioconjugate Chem 27*, 2225-2238.

(31) Bobo, D., Robinson, K. J., Islam, J., Thurecht, K. J., and Corrie, S. R. (2016) Nanoparticle-based medicines: A review of FDA-approved materials and clinical trials to date. *Pharm Res 33*, 2373-2387.

(32) Etheridge, M. L., Campbell, S. A., Erdman, A. G., Haynes, C. L., Wolf, S. M., and Mccullough, J. (2013) The big picture on nanomedicine: the state of investigational and approved nanomedicine products. *Nanomedicine-UK 9*, 1-14.

(33) Acharya, S., and Sahoo, S. K. (2011) PLGA nanoparticles containing various anticancer agents and tumor delivery by EPR effect. *Adv Drug Deliver Rev 63*, 170-183.

(34) Torchilin, V. (2011) Tumor delivery of macromolecular drugs based on the EPR effect. *Adv Drug Deliver Rev 63*, 131-135.

(35) Gong, J., Chen, M., Zheng, Y., Wang, S., and Wang, Y. (2012) Polymeric micelles drug delivery system in oncology. *J Control Release 153*, 312-323.

(36) Brus, L. E. (1984) Electron–electron and electron-hole interactions in small semiconductor crystallites: The size dependence of the lowest excited electronic state. *J Chem Phys 80*, 4403-4409.

(37) Bera, D., Qian, L., Tseng, T.-K., and Holloway, P. H. (2010) Quantum dots and their multimodal applications: A review. *Materials 3*, 2260-2345.

(38) Larson, D. R., Zipfel, W. R., Williams, R. M., Clark, S. W., Bruchez, M. P., Wise, F. W., and Webb, W. W. (2003) Water-soluble quantum dots for multiphoton fluorescence imaging in vivo. *Science 300*, 1434-1436.

(39) Andrásfalvy, B. K., Galiñanes, G. L., Huber, D., Barbic, M., Macklin, J. J., Susumu, K., Delehanty, J. B., Huston, A. L., Makara, J. K., and Medintz, I. L.

(2014) Quantum dot–based multiphoton fluorescent pipettes for targeted neuronal electrophysiology. *Nat Methods 11*, 1237.

(40) Efros, A. L., and Efors, A. L. (1982) Interband absorption of light in a semiconductor sphere. *Sov Phys Semicond 16*, 772-775.

(41) Ekimov, A. I., Onushchenko, A.A. (1981) Quantum size effect in 3-dimensional microscopic semiconductor crystals. *JETP Lett 34*, 345-349.

(42) Hild, W. A., Breunig, M., and Goepferich, A. (2008) Quantum dots - nano-sized probes for the exploration of cellular and intracellular targeting. *Eur J Pharm Biopharm 68*, 153-68.

(43) Probst, C. E., Zrazhevskiy, P., Bagalkot, V., and Gao, X. (2013) Quantum dots as a platform for nanoparticle drug delivery vehicle design. *Adv Drug Deliv Rev 65*, 703-18.

(44) Xing, Y., So, M.-K., Koh, A. L., Sinclair, R., and Rao, J. (2008) Improved QD-BRET conjugates for detection and imaging. *Biochem Bioph Res Co 372*, 388-394.

(45) Tiwari, D., Tanaka, S.-I., Inouye, Y., Yoshizawa, K., Watanabe, T., and Jin, T. (2009) Synthesis and characterization of anti-HER2 antibody conjugated CdSe/CdZnS quantum dots for fluorescence imaging of breast cancer cells. *Sensors 9*, 9332-9354.

(46) Aldeek, F., Safi, M., Zhan, N., Palui, G. And Mattoussi, H. (2013) Understanding the self-assembly of proteins onto gold nanoparticles and quantum dots driven by metal-histidine coordination. *ACS Nano 7*, 10197-10210.

(47) Delehanty, J. B., Medintz, I. L., Pons, T., Brunel, F. M., Dawson, P. E., and Mattoussi, H. (2006) Self-assembled quantum dot−peptide bioconjugates for selective intracellular delivery. *Bioconjugate Chem 17*, 920-927.

(48) Medintz, I. L., Pons, T., Delehanty, J.B., Susumu, K., Brunel, F.M., Dawson, P.E., and Mattoussi, H. (2008) Intracellular delivery of quantum dot− protein cargos mediated by cell penetrating peptides. *Bioconjugate Chem 19*, 1785-1795.

(49) Medintz, I. L., Uyeda, H. T., Goldman, E. R., and Mattoussi, H. (2005) Quantum dot bioconjugates for imaging, labelling and sensing. *Nat Mater 4*, 435.

(50) Herman, B. (1989) Resonance energy transfer microscopy. *Method Cell Biol 30*, 219-243.

(51) Hussain, S. A. (2009) An introduction to fluorescence resonance energy transfer (FRET). *arXiv*.

(52) Wouters, F. S., Verveer, P. J., and Bastiaens, P. I. (2001) Imaging biochemistry inside cells. *Trends Cell Biol 11*, 203-211.

(53) Oh, E., Liu, R., Nel, A., Gemill, K.B., Bilal, M., Cohen, Y. And Medintz, I.L. (2016) Meta-analysis of cellular toxicity for cadmium-containing quantum dots. *Nat Nanotechnol 11*, 479.

(54) Hardman, R. (2006) A toxicologic review of quantum dots: toxicity depends on physicochemical and environmental factors. *Environ Health Perspect 114*, 165-72.

(55) Liu, J., Hu, R., Liu, J., Zhang, B., Wang, Y., Liu, X., Law, W. C., Liu, L., Ye, L., and Yong, K. T. (2015) Cytotoxicity assessment of functionalized CdSe, CdTe and InP quantum dots in two human cancer cell models. *Mater Sci Eng C Mater Biol Appl 57*, 222-31.

(56) Sun, H., Zhang, F., Wei, H., and Yang, B. (2013) The effects of composition and surface chemistry on the toxicity of quantum dots. *J Mater Chem B 1*, 6485.

(57) Brunetti, V., Chibli, H., Fiammengo, R., Galeone, A., Malvindi, M. A., Vecchio, G., Cingolani, R., Nadeau, J. L., and Pompa, P. P. (2013) InP/ZnS as a safer alternative to CdSe/ZnS core/shell quantum dots: In vitro and in vivo toxicity assessment. *Nanoscale 5*, 307-17.

(58) Lin, G., Ouyang, Q., Hu, R., Ding, Z., Tian, J., Yin, F., Xu, G., Chen, Q., Wang, X., and Yong, K. T. (2015) In vivo toxicity assessment of non-cadmium quantum dots in BALB/c mice. *Nanomedicine-UK 11*, 341-50.

(59) Sangtani, A., Muroski, M. E., and Delehanty, J. B. (2019) Mechanisms of actively triggered drug delivery from hard nanoparticle carriers, in *Targeted Nanosystems*

for Therapeutic Applications: New Concepts, Dynamic Properties, Efficiency, and Toxicity (Sakurai, K., and Ilies, M. A., Eds.) pp 157-185, American Chemical Society.

(60) Hsu, P. P., and Sabatini, D. M. (2008) Cancer cell metabolism: Warburg and beyond. *Cell 134*, 703-7.

(61) Lee, K. Y. J., Wang, Y., and Nie, S. (2015) In vitro study of a pH-sensitive multifunctional doxorubicin–gold nanoparticle system: Therapeutic effect and surface enhanced Raman scattering. *RSC Adv 5*, 65651-65659.

(62) Savla, R., Taratula, O., Garbuzenko, O., and Minko, T. (2011) Tumor targeted quantum dot-mucin 1 aptamer-doxorubicin conjugate for imaging and treatment of cancer. *J Control Release 153*, 16-22.

(63) Xiao, Y., Hong, H., Matson, V. Z., Javadi, A., Xu, W., Yang, Y., Zhang, Y., Engle, J. W., Nickles, R. J., Cai, W., *et al.* (2012) Gold nanorods conjugated with doxorubicin and cRGD for combined anticancer drug delivery and PET imaging. *Theranostics 2*, 757-68.

(64) Yang, D., Kang, X., Ma, P., Dai, Y., Hou, Z., Cheng, Z., Li, C., and Lin, J. (2013) Hollow structured upconversion luminescent NaYF(4):Yb(3)(+), Er(3)(+) nanospheres for cell imaging and targeted anti-cancer drug delivery. *Biomaterials 34*, 1601-12.

(65) Zheng, F. F., Zhang, P. H., Xi, Y., Chen, J. J., Li, L. L., and Zhu, J. J. (2015) Aptamer/graphene quantum dots nanocomposite capped fluorescent mesoporous silica nanoparticles for intracellular drug delivery and real-time monitoring of drug release. *Anal Chem 87*, 11739-45.

(66) Demeule, M., Regina, A., Che, C., Poirier, J., Nguyen, T., Gabathuler, R., Castaigne, J. P., and Beliveau, R. (2008) Identification and design of peptides as a new drug delivery system for the brain. *J Pharmacol Exp Ther 343*, 1064-1072.

(67) Huang, S., Li, J., Han, L., Liu, S., Ma, H., Huang, R., and Jiang, C. (2011) Dual targeting effect of Angiopep-2-modified, DNA-loaded nanoparticles for glioma. *Biomaterials 32*, 6832-6838.

(68) Deb, A., and Vimala, R. (2018) Camptothecin loaded graphene oxide nanoparticle functionalized with polyethylene glycol and folic acid for anticancer drug delivery. *J Drug Deliv Sci Tec 43*, 333-342.

(69) Huang, C.-L., Huang, C.-C., Mai, F.-D., Yen, C.-L., Tzing, S.-H., Hsieh, H.-T., Ling, Y.-C., and Chang, J.-Y. (2015) Application of paramagnetic graphene quantum dots as a platform for simultaneous dual-modality bioimaging and tumor-targeted drug delivery. *J Mater Chem B 3*, 651-664.

(70) Low, P. S., Henne, W. A., and Doorneweerd, D. D. (2007) Discovery and development of folic-acid-based receptor targeting for imaging and therapy of cancer and inflammatory diseases. *Accounts Chem Res 40*, 120-129.

(71) Stella, B., Arpicco, S., Peracchia, M. T., Desmaële, D., Hoebeke, J., Renoir, M., D'angelo, J., Cattel, L., and Couvreur, P. (2000) Design of folic acid-conjugated nanoparticles for drug targeting. *J Pharm Sci 89*, 1452-1464.

(72) Carr, D. H., Brown, J., Bydder, G. M., Steiner, R. E., Weinmann, H. J., Speck, U., Hall, A. S., and Young, I. R. (1984) Gadolinium-DTPA as a contrast agent in MRI: initial clinical experience in 20 patients. *Am J Roentgenol 143*, 215-224.

(73) Cai, X., Luo, Y., Zhang, W., Du, D., and Lin, Y. (2016) pH-Sensitive ZnO Quantum Dots-Doxorubicin Nanoparticles for Lung Cancer Targeted Drug Delivery. *ACS Appl Mater Inter 8*, 22442-22450.

(74) Liu, J., Ma, X., Jin, S., Xue, X., Zhang, C., Wei, T., Guo, W., and Liang, X. J. (2016) Zinc oxide nanoparticles as adjuvant to facilitate doxorubicin intracellular accumulation and visualize pH-responsive release for overcoming drug resistance. *Mol Pharm 13*, 1723-30.

(75) Ma, P., Xiao, H., Li, X., Li, C., Dai, Y., Cheng, Z., Jing, X., and Lin, J. (2013) Rational design of multifunctional upconversion nanocrystals/polymer nanocomposites for cisplatin (IV) delivery and biomedical imaging. *Adv Mater 25*, 4898-905.

(76) Chen, T., Yu, H., Yang, N., Wang, M., Ding, C., and Fu, J. (2014) Graphene quantum dot-capped mesoporous silica nanoparticles through an acid-cleavable acetal bond for intracellular drug delivery and imaging. *J Mater Chem B 2*, 4979-4982.

(77) Yang, B., Li, Y., Sun, X., Meng, X., Chen, P., and Liu, N. (2013) A pH-responsive drug release system based on doxorubicin conjugated amphiphilic polymer coated quantum dots for tumor cell targeting and tracking. *J Chem Technol Biot 88*, 2169-2175.

(78) Wen, H. Y., Dong, H. Q., Xie, W. J., Li, Y. Y., Wang, K., Pauletti, G. M., and Shi, D. L. (2011) Rapidly disassembling nanomicelles with disulfide-linked PEG shells for glutathione-mediated intracellular drug delivery. *Chem Commun 47*, 3550-3552.

(79) Kurtoglu, Y. E., Navath, R. S., Wang, B., Kannan, S., Romero, R., and Kannan, R. M. (2009) Poly(amidoamine) dendrimer-drug conjugates with disulfide linkages for intracellular drug delivery. *Biomaterials 30*, 2112-2121.

(80) Cerritelli, S., Velluto, D., and Hubbell, J. A. (2007) PEG-SS-PPS: Reduction-sensitive disulfide block copolymer vesicles for intracellular drug delivery. *Biomacromolecules 8*, 1996-1972.

(81) Townsend, D. M., Tew, K. D., and Tapiero, H. (2003) The importance of glutathione in human disease. *Biomed Pharmacother 57*, 145-155.

(82) Balendrian, G. K., Dabur, R., and Fraser, D. (2004) The role of glutathione in cancer. *Cell Biochem Funct 22*, 343-352.

(83) Ortega, A. L., Mena, S., and Estrela, J. M. (2011) Glutathione in cancer cell death. *Cancers (Basel) 3*, 1285-310.

(84) Parida, S., Maiti, C., Rajesh, Y., Dey, K. K., Pal, I., Parekh, A., Patra, R., Dhara, D., Dutta, P. K., and Mandal, M. (2017) Gold nanorod embedded reduction responsive block copolymer micelle-triggered drug delivery combined with photothermal ablation for targeted cancer therapy. *Biochim Biophys Acta 1861*, 3039-3052.

(85) Dai, Y., Kang, X., Yang, D., Li, X., Zhang, X., Li, C., Hou, Z., Cheng, Z., Ma, P., and Lin, J. (2013) Platinum (IV) pro-drug conjugated NaYF4 :Yb(3+) /Er(3+) nanoparticles for targeted drug delivery and up-conversion cell imaging. *Adv Healthc Mater 2*, 562-567.

(86) Feng, T., Ai, X., Ong, H., and Zhao, Y. (2016) Dual-responsive carbon dots for tumor extracellular microenvironment triggered targeting and enhanced anticancer drug delivery. *ACS Appl Mater Inter 8*, 18732-18740.

(87) Van Rijt, S. H., BöLüKbas, D. A., Argyo, C., Datz, S., Lindner, M., Eickelberg, O., KöNigshoff, M., Bein, T., and Meiners, S. (2015) Protease-mediated release of chemotherapeutics from mesoporous silica nanoparticles to ex vivo human and mouse lung tumors. *ACS Nano 9*, 2377-2389.

(88) Lee, S. J., Jeong, Y. I., Park, H. K., Kang, D. H., Oh, J. S., Lee, S. G., and Lee, H. C. (2015) Enzyme-responsive doxorubicin release from dendrimer nanoparticles for anticancer drug delivery. *Int J Nanomedicine 10*, 5489-503.

(89) Yang, Y., Aw, J., Chen, K., Liu, F., Padmanabhan, P., Hou, Y., Cheng, Z., and Xing, B. (2011) Enzyme-responsive multifunctional magnetic nanoparticles for tumor intracellular drug delivery and imaging. *Chem Asian J 6*, 1381-9.

(90) De La Torre, C., Mondragon, L., Coll, C., Sancenon, F., Marcos, M. D., Martinez-Manez, R., Amoros, P., Perez-Paya, E., and Orzaez, M. (2014) Cathepsin-B induced controlled release from peptide-capped mesoporous silica nanoparticles. *Chemistry 20*, 15309-14.

(91) Tian, J., Ding, L., Wang, Q., Hu, Y., Jia, L., Yu, J. S., and Ju, H. (2015) Folate receptor-targeted and cathepsin B-activatable nanoprobe for in situ therapeutic monitoring of photosensitive cell death. *Anal Chem 87*, 3841-8.

(92) Maji, S. K., Mandal, A. K., Nguyen, K. T., Borah, P., and Zhao, Y. (2015) Cancer cell detection and therapeutics using peroxidase-active nanohybrid of gold nanoparticle-loaded mesoporous silica-coated graphene. *ACS Appl Mater Inter 7*, 9807-9816.

(93) Thomas, G. (2002) Furin at the cutting edge: from protein traffic to embryogenesis and disease. *Nat Rev Mol Cell Biol 3*, 753-66.

(94) Jiang, T., Sun, W., Zhu, Q., Burns, N. A., Khan, S. A., Mo, R., and Gu, Z. (2015) Furin-mediated sequential delivery of anticancer cytokine and small-molecule drug shuttled by graphene. *Adv Mater 27*, 1021-8.

(95) Sangtani, A., Petryayeva, E., Wu, M., Susumu, K., Oh, E., Huston, A. L., Lasarte-Aragones, G., Medintz, I. L., Algar, W. R., and Delehanty, J. B. (2018)

Intracellularly actuated quantum dot-peptide-doxorubicin nanobioconjugates for controlled drug delivery via the endocytic pathway. *Bioconjugate Chem 29*, 136-148.

(96) Fernando, I. R., Ferris, D. P., Frasconi, M., Malin, D., Strekalova, E., Yilmaz, M. D., Ambrogio, M. W., Algaradah, M. M., Hong, M. P., Chen, X., *et al.* (2015) Esterase- and pH-responsive poly(beta-amino ester)-capped mesoporous silica nanoparticles for drug delivery. *Nanoscale 7*, 7178-83.

(97) Hoop, M., Mushtaq, F., Hurter, C., Chen, X. Z., Nelson, B. J., and Pane, S. (2016) A smart multifunctional drug delivery nanoplatform for targeting cancer cells. *Nanoscale 8*, 12723-8.

(98) Jishkariani, D., Lee, J. D., Yun, H., Paik, T., Kikkawa, J. M., Kagan, C. R., Donnio, B., and Murray, C. B. (2017) The dendritic effect and magnetic permeability in dendron coated nickel and manganese zinc ferrite nanoparticles. *Nanoscale 9*, 13922-13928.

(99) Ye, F., Barrefelt, A., Asem, H., Abedi-Valugerdi, M., El-Serafi, I., Saghafian, M., Abu-Salah, K., Alrokayan, S., Muhammed, M., and Hassan, M. (2014) Biodegradable polymeric vesicles containing magnetic nanoparticles, quantum dots and anticancer drugs for drug delivery and imaging. *Biomaterials 35*, 3885-94.

(100) Mejias, R., Perez-Yague, S., Gutierrez, L., Cabrera, L. I., Spada, R., Acedo, P., Serna, C. J., Lazaro, F. J., Villanueva, A., Morales Mdel, P., *et al.* (2011) Dimercaptosuccinic acid-coated magnetite nanoparticles for magnetically guided in vivo delivery of interferon gamma for cancer immunotherapy. *Biomaterials 32*, 2938-52.

(101) Lee, K., David, A. E., Zhang, J., Shin, M. C., and Yang, V. C. (2017) Enhanced accumulation of theranostic nanoparticles in brain tumor by external magnetic field mediated in situ clustering of magnetic nanoparticles. *J Ind Eng Chem 54*, 389-397.

(102) Zheng, F., Zhang, P., Xi, Y., Chen, X., He, Z., Meng, T., Chen, J., Li, L., and Zhu, J. J. (2017) Hierarchical nanocarriers for precisely regulating the therapeutic process via dual-mode controlled drug release in target tumor cells. *ACS Appl Mater Inter 9*, 36655-36664.

(103) Griffete, N., Fresnais, J., Espinosa, A., Wilhelm, C., Bee, A., and Menager, C. (2015) Design of magnetic molecularly imprinted polymer nanoparticles for controlled release of doxorubicin under an alternative magnetic field in athermal conditions. *Nanoscale 7*, 18891-18896.

(104) Hua, X., Yang, Q., Dong, Z., Zhang, J., Zhang, W., Wang, Q., Tan, S., and Smyth, H. D. (2017) Magnetically triggered drug release from nanoparticles and its applications in anti-tumor treatment. *Drug Deliv 24*, 511-518.

(105) Hervault, A., Dunn, A. E., Lim, M., Boyer, C., Mott, D., Maenosono, S., and Thanh, N. T. (2016) Doxorubicin loaded dual pH- and thermo-responsive magnetic nanocarrier for combined magnetic hyperthermia and targeted controlled drug delivery applications. *Nanoscale 8*, 12152-61.

(106) Yang, K. N., Zhang, C. Q., Wang, W., Wang, P. C., Zhou, J. P., and Liang, X. J. (2014) pH-responsive mesoporous silica nanoparticles employed in controlled drug delivery systems for cancer treatment. *Cancer Biol Med 11*, 34-43.

(107) Alphandery, E., Idbaih, A., Adam, C., Delattre, J. Y., Schmitt, C., Guyot, F., and Chebbi, I. (2017) Chains of magnetosomes with controlled endotoxin release and partial tumor occupation induce full destruction of intracranial U87-Luc glioma in mice under the application of an alternating magnetic field. *J Control Release 262*, 259-272.

(108) Kaushik, A., Jayant, R. D., Nikkhah-Moshaie, R., Bhardwaj, V., Roy, U., Huang, Z., Ruiz, A., Yndart, A., Atluri, V., El-Hage, N., *et al.* (2016) Magnetically guided central nervous system delivery and toxicity evaluation of magneto-electric nanocarriers. *Sci Rep-UK 6*, 25309.

(109) Wang, F., Shen, Y., Zhang, W., Li, M., Wang, Y., Zhou, D., and Guo, S. (2014) Efficient, dual-stimuli responsive cytosolic gene delivery using a RGD modified disulfide-linked polyethylenimine functionalized gold nanorod. *J Control Release 196*, 37-51.

(110) Rengan, A. K., Jagtap, M., De, A., Banerjee, R., and Srivastava, R. (2014) Multifunctional gold coated thermo-sensitive liposomes for multimodal imaging and photo-thermal therapy of breast cancer cells. *Nanoscale 6*, 916-23.

(111) Li, Z., Huang, H., Tang, S., Li, Y., Yu, X. F., Wang, H., Li, P., Sun, Z., Zhang, H., Liu, C., *et al.* (2016) Small gold nanorods laden macrophages for enhanced tumor coverage in photothermal therapy. *Biomaterials 74*, 144-54.

(112) Dykman, L. A., and Khlebtsov, N. G. (2016) Multifunctional gold-based nanocomposites for theranostics. *Biomaterials 108*, 13-34.

(113) Zhang, Z., Wang, J., Nie, X., Wen, T., Ji, Y., Wu, X., Zhao, Y., and Chen, C. (2014) Near infrared laser-induced targeted cancer therapy using thermoresponsive polymer encapsulated gold nanorods. *J Am Chem Soc 136*, 7317-7326.

(114) Luo, L., Bian, Y., Liu, Y., Zhang, X., Wang, M., Xing, S., Li, L., and Gao, D. (2016) Combined near infrared photothermal therapy and chemotherapy using gold nanoshells coated liposomes to enhance antitumor effect. *Small 12*, 4103-12.

(115) Ali, M. R., Rahman, M. A., Wu, Y., Han, T., Peng, X., Mackey, M. A., Wang, D., Shin, H. J., Chen, Z. G., Xiao, H., *et al.* (2017) Efficacy, long-term toxicity, and mechanistic studies of gold nanorods photothermal therapy of cancer in xenograft mice. *P Natl Acad Sci U S A 114*, E3110-E3118.

(116) Hesley, G. K., Gorny, K. R., Henrichsen, T. L., Woodrum, D. A., and Brown, D. L. (2008) A clinical review of focused ultrasound ablation with magnetic resonance guidance: an option for treating uterine fibroids. *Ultrasound Q 24*, 131-9.

(117) O'neill, B. E., Vo, H., Angstadt, M., Li, K. P., Quinn, T., and Frenkel, V. (2009) Pulsed high intensity focused ultrasound mediated nanoparticle delivery: mechanisms and efficacy in murine muscle. *Ultrasound Med Biol 35*, 416-24.

(118) Ziadloo, A., Xie, J., and Frenkel, V. (2013) Pulsed focused ultrasound exposures enhance locally administered gene therapy in a murine solid tumor model. *J Acoust Soc Am 133*, 1827-34.

(119) Yuan, P., and Song, D. (2018) MRI tracing non-invasive TiO2-based nanoparticles activated by ultrasound for multi-mechanism therapy of prostatic cancer. *Nanotechnology 29*, 125101.

(120) Chertok, B., and Langer, R. (2018) Circulating magnetic microbubbles for localized real-time control of drug delivery by ultrasonography-guided magnetic targeting and ultrasound. *Theranostics 8*, 341-357.

(121) Sailor, M. J., and Park, J. H. (2012) Hybrid nanoparticles for detection and treatment of cancer. *Adv Mater 24*, 3779-3802.

(122) Ting, C. Y., Fan, C. H., Liu, H. L., Huang, C. Y., Hsieh, H. Y., Yen, T. C., Wei, K. C., and Yeh, C. K. (2012) Concurrent blood-brain barrier opening and local drug delivery using drug-carrying microbubbles and focused ultrasound for brain glioma treatment. *Biomaterials 33*, 704-12.

(123) Treat, L. H., Mcdannold, N., Zhang, Y., Vykhodtseva, N., and Hynynen, K. (2012) Improved anti-tumor effect of liposomal doxorubicin after targeted blood-brain barrier disruption by MRI-guided focused ultrasound in rat glioma. *Ultrasound Med Biol 38*, 1716-25.

(124) Fan, C. H., Ting, C. Y., Lin, H. J., Wang, C. H., Liu, H. L., Yen, T. C., and Yeh, C. K. (2013) SPIO-conjugated, doxorubicin-loaded microbubbles for concurrent MRI and focused-ultrasound enhanced brain-tumor drug delivery. *Biomaterials 34*, 3706-15.

(125) Timbie, K. F., Afzal, U., Date, A., Zhang, C., Song, J., Miller, G. W., Suk, J. S., Hanes, J., and Price, R. J. (2017) MR image-guided delivery of cisplatin-loaded brain-penetrating nanoparticles to invasive glioma with focused ultrasound. *J Control Release 263*, 120-131.

(126) Kim, K., Oh, K. S., Park, D. Y., Lee, J. Y., Lee, B. S., Kim, I. S., Kim, K., Kwon, I. C., Sang, Y. K., and Yuk, S. H. (2016) Doxorubicin/gold-loaded core/shell nanoparticles for combination therapy to treat cancer through the enhanced tumor targeting. *J Control Release 228*, 141-149.

(127) Su, N., Dang, Y., Liang, G., and Liu, G. (2015) Iodine-125-labeled cRGD-gold nanoparticles as tumor-targeted radiosensitizer and imaging agent. *Nanoscale Res Lett 10*, 160.

(128) Song, G., Chao, Y., Chen, Y., Liang, C., Yi, X., Yang, G., Yang, K., Cheng, L., Zhang, Q., and Liu, Z. (2016) All-in-one theranostic nanoplatform based on hollow TaOx for chelator-free labeling imaging, drug delivery, and synergistically enhanced radiotherapy. *Adv Funct Mater 26*, 8243-8254.

(129) Tacar, O., Sriamornsak, P., and Dass, C. R. (2013) Doxorubicin: an update on anticancer molecular action, toxicity and novel drug delivery systems. *J Pharm Pharmacol 65*, 157-170.

(130) Thorn, C. F., Oshiro, C., Marsh, S., Hernandez-Boussard, T., Mcleod, H., Klein, T. E., and Altman, R. B. (2011) Doxorubicin pathways: pharmacodynamics and adverse effects. *Pharmacogenet Genom 21*, 440.

(131) Patel, A. G., and Kaufmann, S. H. (2012) Cancer: How does doxorubicin work? *Elife 1*, e00387.

(132) Olson, R. D., and Mushlin, P. S. (1990) Doxorubicin cardiotoxicity: analysis of prevailing hypotheses. *FASEB J 4*, 3076-3086.

(133) Singal, P. K., and Iliskovic, N. (1998) Doxorubicin-induced cardiomyopathy. *New Engl J Med 339*, 900-905.

(134) Chatterjee, K., Zhang, J., Honbo, N., and Karliner, J. S. (2010) Doxorubicin cardiomyopathy. *Cardiology 115*, 155-162.

(135) Steinberg, T. H. (1994) Cellular transport of drugs. *Clin Infect Dis 19*, 916-921.

(136) Reischl, D., and Zimmer, A. (2009) Drug delivery of siRNA therapeutics: potentials and limits of nanosystems. *Nanomed-Nanotechnol 5*, 8-20.

(137) Bareford, L. M., and Swaan, P. W. (2007) Endocytic mechanisms for targeted drug delivery. *Adv Drug Deliv Rev 59*, 748-758.

(138) Dawidczyk, C. M., Kim, C., Park, J. H., Russell, L. M., Lee, K. H., Pomper, M. G., and Searson, P. C. (2014) State-of-the-art in design rules for drug delivery platforms: lessons learned from FDA-approved nanomedicines. *J Control Release 187*, 133-144.

(139) Canton, I., and Battaglia, G. (2012) Endocytosis at the nanoscale. *Chem Soc Rev 41*, 2718-2739.

(140) Jazayeri, M. H., Amani, H., Pourfatollah, A. A., Pazoki-Toroudi, H., and Sedighimoghaddam, B. (2016) Various methods of gold nanoparticles (GNPs) conjugation to antibodies. *Sens Biosensing Res 9*, 17-22.

(141) Colombo, M., Fiandra, L., Alessio, G., Mazzucchelli, S., Nebuloni, M., De Palma, C., Kantner, K., Pelaz, B., Rotem, R., and Corsi, F. (2016) Tumour homing and therapeutic effect of colloidal nanoparticles depend on the number of attached antibodies. *Nat Commun 7*, 13818.

(142) García-Fernández, L., Garcia-Pardo, J., Tort, O., Prior, I., Brust, M., Casals, E., Lorenzo, J., and Puntes, V. F. (2017) Conserved effects and altered trafficking of Cetuximab antibodies conjugated to gold nanoparticles with precise control of their number and orientation. *Nanoscale 9*, 6111-6121.

(143) Gollavelli, G., and Ling, Y. C. (2014) Magnetic and fluorescent graphene for dual modal imaging and single light induced photothermal and photodynamic therapy of cancer cells. *Biomaterials 35*, 4499-4507.

(144) Niu, N., He, F., Ma, P. A., Gai, S., Yang, G., Qu, F., Wang, Y., Xu, J., and Yang, P. (2014) Up-conversion nanoparticle assembled mesoporous silica composites: synthesis, plasmon-enhanced luminescence, and near-infrared light triggered drug release. *ACS Appl Mater Inter 6*, 3250-3262.

(145) Frangioni, J. V. (2003) In vivo near-infrared fluorescence imaging. *Curr Opin Chem Biol 7*, 626-634.

(146) Blanco-Canosa, J. B., Wu, M., Susumu, K., Petryayeva, E., Jennings, T. L., Dawson, P. E., Algar, W. R., and Medintz, I. L. (2014) Recent progress in the bioconjugation of quantum dots. *Coordin Chem Rev 263*, 101-137.

(147) Susumu, K., Oh, E., Delehanty, J. B., Pinaud, F., Gemmill, K. B., Walper, S., Breger, J., Schroeder, M. J., Stewart, M. H., Jain, V., *et al.* (2014) A new family of pyridine-appended multidentate polymers as hydrophilic surface ligands for preparing stable biocompatible quantum dots. *Chem Mater 26*, 5327-5344.

(148) Susumu, K., Oh, E., Delehanty, J. B., Blanco-Canosa, J. B., Johnson, B. J., Jain, V., Hervey Iv, W. J., Algar, W. R., Boeneman, K., Dawson, P. E., *et al.* (2011) Multifunctional compact zwitterionic ligands for preparing robust biocompatible semiconductor quantum dots and gold nanoparticles. *J Am Chem Soc 133*, 9480-9496.

(149) Sapsford, K. E., Farrell, D., Sun, S., Rasooly, A., Mattoussi, H., and Medintz, I. L. (2009) Monitoring of enzymatic proteolysis on a electroluminescent-CCD microchip platform using quantum dot-peptide substrates. *Sensor Actuat B-Chem 139*, 13-21.

(150) Gemmill, K. B., DíAz, S. A., Blanco-Canosa, J. B., Deschamps, J. R., Pons, T., Liu, H. W., Deniz, A., Melinger, J., Oh, E., Susumu, K., *et al.* (2015) Examining the Polyproline Nanoscopic Ruler in the Context of Quantum Dots. *Chem Mater 27*, 6222-6237.

(151) Willner, D., Trail, P. A., Hofstead, S. J., King, H. D., Lasch, S. J., Braslawsky, G. R., Greenfield, R. S., Kaneko, T., and Firestone, R. A. (1993) (6-Maleimidocaproyl)hydrazone of doxorubicin. A new derivative for the preparation of immunoconjugates of doxorubicin. *Bioconjugate Chem 4*, 521-527.

(152) Delehanty, J. B., Bradburne, C. E., Boeneman, K., Susumu, K., Farrell, D., Mei, B. C., Blanco-Canosa, J. B., Dawson, G., Dawson, P. E., Mattoussi, H., *et al.* (2010) Delivering quantum dot-peptide bioconjugates to the cellular cytosol: escaping from the endolysosomal system. *Integr Biol- UK 2*, 265-77.

(153) Schnolzer, M., and Kent, S. B. (1992) Constructing proteins by dovetailing unprotected synthetic peptides: Backbone-engineered HIV protease. *Science 256*, 221.

(154) Oh, E., Fatemi, F. K., Currie, M., Delehanty, J. B., Pons, T., Fragola, A., Lévêque-Fort, S., Goswami, R., Susumu, K., Huston, A. L., *et al.* (2013) PEGylated luminescent gold nanoclusters: synthesis, characterization, bioconjugation, and application to one-and two-photon cellular imaging. *Part Part Syst Char 30*, 453-466.

(155) Delehanty, J. B., Blanco-Canosa, J. B., Bradburne, C. E., Susumu, K., Stewart, M. H., Prasuhn, D. E., Dawson, P. E., and Medintz, I. L. (2013) Site-specific cellular delivery of quantum dots with chemoselectively assembled modular peptides. *Chem Commun 49*, 7878-7880.

(156) Bradburne, C. E., Delehanty, J. B., Boeneman Gemmill, K., Mei, B. C., Mattoussi, H., Susumu, K., Blanco-Canosa, J. B., Dawson, P. E., and Medintz, I. L. (2013) Cytotoxicity of quantum dots used for in vitro cellular labeling: Role of QD surface ligand, delivery modality, cell type, and direct comparison to organic fluorophores. *Bioconjugate Chem 24*, 1570.

(157) Nag, O. K., Stewart, M. H., Deschamps, J. R., Susumu, K., Oh, E., Tsytsarev, V., Tang, Q., Efros, A. L., Vaxenburg, R., Black, B. J., *et al.* (2017) Quantum dot–peptide–fullerene bioconjugates for visualization of in vitro and in vivo cellular membrane potential. *ACS Nano 11*, 5598-5613.

(158) Lawrence, I., and Lin, K. (1989) A concordance correlation coefficient to evaluate reproducibility. *Biometrics*, 255-268.

(159) Oh, E., Delehanty, J. B., Sapsford, K. E., Susumu, K., Goswami, R., Blanco-Canosa, J. B., Dawson, P. E., Granek, J., Shoff, M., Zhang, Q., *et al.* (2011)

Cellular uptake and fate of PEGylated gold nanoparticles is dependent on both cell-penetration peptides and particle size. *ACS Nano 5*, 6434-48.

(160) Delehanty, J. B., Bradburne, C. E., Susumu, K., Boeneman, K., Mei, B. C., Farrell, D., Blanco-Canosa, J. B., Dawson, P. E., Mattousi, H., and Medintz, I. L. (2011) Spatiotemporal multicolor labeling of individual cells using peptide-functionalized quantum dots and mixed delivery techniques. *J Am Chem Soc 133*, 10482-10489.

(161) Breger, J. C., Muttenthaler, M., Delehanty, J. B., Thompson, D. A., Oh, E., Susumu, K., Deschamps, J. R., Anderson, G. P., Field, L. D., Walper, S. A., *et al.* (2017) Nanoparticle cellular uptake by dendritic wedge peptides: achieving single peptide facilitated delivery. *Nanoscale 9*, 10447-10464.

(162) Field, L. D., Walper, S. A., Susumu, K., Oh, E., Medintz, I. L., and Delehanty, J. B. (2015) Modulation of intracellular quantum dot to fluorescent protein Förster resonance energy transfer via customized ligands and spatial control of donor–acceptor assembly. *Sensors 15*, 30457-30468.

(163) Prasuhn, D. E., Blanco-Canosa, J. B., Vora, G. J., Delehanty, J. B., Susumu, K., Mei, B. C., Dawson, P. E., and Medintz, I. L. (2010) Combining chemoselective ligation with polyhistidine-driven self-assembly for the modular display of biomolecules on quantum dots. *ACS Nano 4*, 267-278.

(164) Prasuhn, D. E., Deschamps, J. R., Susumu, K., Stewart, M. H., Boeneman, K., Blanco-Canosa, J. B., Dawson, P. E., and Medintz, I. L. (2010) Polyvalent display and packing of peptides and proteins on semiconductor quantum dots: predicted versus experimental results. *Small 6*, 555-64.

(165) Algar, W. R., Prasuhn, D. E., Stewart, M. H., Jennings, T. L., Blanco-Canosa, J. B., Dawson, P. E., and Medintz, I. L. (2011) The controlled display of biomolecules on nanoparticles: a challenge suited to bioorthogonal chemistry. *Bioconjugate Chem 22*, 825-858.

(166) Banerjee, S., Kar, S., Manuel Perez, J., and Santra, S. (2009) Quantum dot-based on/off probe for detection of gluathione. *J Phys Chem C 22*, 9659-9663.

(167) Koo, A. N., Lee, H. J., Kim, S. E., Chang, J. H., Park, C., Kim, C., Park, J. H., and Lee, S. C. (2008) Disulfide-cross-linked PEG-poly(amino acid)s copolymer micelles for glutathione-mediated intracellular drug delivery. *Chem Commun*, 6570-2.

(168) Zhou, Z., Murdoch, W. J., and Shen, Y. (2016) Synthesis of an esterase-sensitive degradable polyester as facile drug carrier for cancer therapy. *J Polym Sci Part A 54*, 507-515.

(169) Hruby, M., Konak, C., and Ulbrich, K. (2005) Polymeric micellar pH-sensitive drug delivery system for doxorubicin. *J Control Release 103*, 137-48.

(170) Patil, R., Portilla-Arias, J., Ding, H., Konda, B., Rekechenetskiy, A., Inoue, S., Black, K. L., Holler, E., and Ljubimova, J. Y. (2012) Cellular delivery of doxorubicin via pH-controlled hydrazone linkage using multifunctional nano vehicle based on poly(beta-l-malic acid). *Int J Mol Sci 13*, 11681-93.

(171) Prabaharan, M., Grailer, J. J., Pilla, S., Steeber, D. A., and Gong, S. (2009) Amphiphilic multi-arm-block copolymer conjugated with doxorubicin via pH-sensitive hydrazone bond for tumor-targeted drug delivery. *Biomaterials 30*, 5757-5766.

(172) Medintz, I. L., Pons, T., Delehanty, J. B., Susumu, K., Brunel, F. M., Dawson, P. E., and Mattoussi, H. (2008) Intracellular delivery of quantum dot− protein cargos mediated by cell penetrating peptides. *Bioconjugate Chem. 19*, 1785-1795.

(173) Li, D., Li, G., Guo, W., Li, P., Wang, E., and Wang, J. (2008) Glutathione-mediated release of functional plasmid DNA from positively charged quantum dots. *Biomaterials 29*, 2776-2782.

(174) Verma, A., and Stellacci, F. (2010) Effect of surface properties on nanoparticle–cell interactions. *Small 6*, 12-21.

(175) Tan, S. J., Jana, N. R., Gao, S., Patra, P. K., and Ying, J. Y. (2010) Surface-ligand-dependent cellular interaction, subcellular localization, and cytotoxicity of polymer-coated quantum dots. *Chem Mater 22*, 2239-2247.

(176) Zhang, Q., Xiang, G., Zhang, Y., Yang, K., Fan, W., Lin, J., Zeng, F., and Wu, J. (2006) Increase of doxorubicin sensitivity for folate receptor positive cells when given as the prodrug N-(phenylacetyl) doxorubicin in combination with folate-conjugated PGA. *J Pharm Sci 95*, 2266-2275.

(177) Zahedifard, M., Faraj, F. L., Paydar, M., Looi, C. Y., Hajrezaei, M., Hasanpourghadi, M., Kamalidehghan, B., Majid, N. A., Ali, H. M., and Abdulla, M. A. (2015) Synthesis, characterization and apoptotic activity of quinazolinone

Schiff base derivatives toward MCF-7 cells via intrinsic and extrinsic apoptosis pathways. *Sci Rep-UK 5*, 11544.

(178) Lee, R. J., and Low, P. S. (1995) Folate-mediated tumor cell targeting of liposome-entrapped doxorubicin in vitro. *BBA-Rev Biomembranes 1233*, 134-144.

(179) Austin, C. D., Wen, X., Gazzard, L., Nelson, C., Scheller, R. H., and Scales, S. J. (2005) Oxidizing potential of endosomes and lysosomes limits intracellular cleavage of disulfide-based antibody–drug conjugates. *P Natl Acad Sci USA 102*, 17987-17992.

(180) Bae, Y., Nishiyama, N., Fukushima, S., Koyama, H., Yasuhiro, M., and Kataoka, K. (2005) Preparation and biological characterization of polymeric micelle drug carriers with intracellular pH-triggered drug release property: Tumor permeability, controlled subcellular drug distribution, and enhanced in vivo antitumor efficacy. *Bioconjugate Chem 16*, 122-130.

(181) Bae, Y., Fukushima, S., Harada, A., and Kataoka, K. (2003) Design of environment-sensitive supramolecular assemblies for intracellular drug delivery: Polymeric micelles that are responsive to intracellular pH change. *Angew Chem Int Edit 115*, 4788-4791.

(182) Sawant, R. M., Hurley, J. P., Salmaso, S., Kale, A., Tolcheva, E., Levchenko, T. S., and Torchilin, V. P. (2006) "SMART" drug delivery systems: Double-targeted pH-responsive pharmaceutical nanocarriers. *Bioconjugate Chem 17*, 943-949.

(183) Du, J. Z., Du, X. J., Mao, C. Q., and Wang, J. (2011) Tailor-made dual pH-sensitive polymer-doxorubicin nanoparticles for efficient anticancer drug delivery. *J Am Chem Soc 133*, 17560-3.

(184) Runquist, E. A., and Havel, R. J. (1991) Acid hydrolases in early and late endosome fractions from rat liver. *J Biol Chem 266*, 22557-22563.

(185) Wong, P. T., and Choi, S. K. (2015) Mechanisms of drug release in nanotherapeutic delivery systems. *Chem Rev 115*, 3388-432.

(186) Eom, Y. W., Kim, M. A., Park, S. S., Goo, M. J., Kwon, H. J., Sohn, S., Kim, W. H., Yoon, G., and Choi, K. S. (2005) Two distinct modes of cell death induced by doxorubicin: apoptosis and cell death through mitotic catastrophe accompanied by senescence-like phenotype. *Oncogene 24*, 4765-4777.

(187) Danz, E. D. B., Skramsted, J., Henry, N., Bennett, J. A., and Keller, R. S. (2009) Resveratrol prevents doxorubicin cardiotoxicity through mitochondrial stabilization and the Sirt1 pathway. *Free Radical Biology and Medicine 46*, 1589-1597.

(188) Dong, X., and Mumper, R. J. (2010) Nanomedicinal strategies to treat multidrug-resistant tumors: current progress. *Nanomedicine-UK 5*, 597-615.

(189) Xue, X., and Liang, X. J. (2012) Overcoming drug efflux-based multidrug resistance in cancer with nanotechnology. *Chin J Cancer 31*, 100.

(190) Blanco, E., Shen, H., and Ferrari, M. (2015) Principles of nanoparticle design for overcoming biological barriers to drug delivery. *Nat Biotechnol 33*, 941-951.

(191) Nazarenus, M., Zhang, Q., Soliman, M. G., Del Pino, P., Pelaz, B., Carregal-Romero, S., Rejman, J., Rothen-Rutishauser, B., Clift, M. J., and Zellner, R. (2014) In vitro interaction of colloidal nanoparticles with mammalian cells: What have we learned thus far? *Beilstein J Nanotec 5*, 1477-1490.

(192) Afrimzon, E., Deutsch, A., Shafran, Y., Zurgil, N., Sandbank, J., Pappo, I., and Deutsch, M. (2008) Intracellular esterase activity in living cells may distinguish between metastatic and tumor-free lymph nodes. *Clin Exp Metastasis 25*, 213-224.

(193) Fukami, T., and Yokoi, T. (2012) The emerging role of human esterases. *Drug Metab Pharmacok*, DMPK-12-RV-042.

(194) Yamazaki, Y., Furukawa, F., Nishikawa, A., Takahashi, M., and Oka, S. (1998) Histochemical determination of stereoselectivity of esterases in normal pancreas and pancreatic tubular adenocarcinoma of hamsters. *Biotech Histochem 73*, 23-31.

(195) Sangtani, A., Petryayeva, E., Susumu, K., Oh, E., Huston, A. L., Lasarte-Aragones, G., Medintz, I. L., Algar, W. R., and Delehanty, J. B. (2019) Nanoparticle-peptide-drug Bioconjugates for Unassisted Defeat of Multidrug Resistance in a Model Cancer Cell Line. *Bioconjugate Chem*.

(196) Gottesman, M. M., Fojo, T., and Bates, S. E. (2002) Multidrug resistance in cancer: role of ATP-dependent transporters. *Nat Rev Cancer 2*, 48-58.

(197) Housman, G., Byler, S., Heerboth, S., Lapinska, K., Longacre, M., Snyder, N., and Sarkar, S. (2014) Drug resistance in cancer: an overview. *Cancers (Basel) 6*, 1769-92.

(198) Persidis, A. (1999) Cancer multidrug resistance. *Nat Biotechnol 17*, 94.

(199) Mansoori, B., Mohammadi, A., Davudian, S., Shirjang, S., and Baradaran, B. (2017) The different mechanisms of cancer drug resistance: A brief review. *Adv Pharm Bull 7*, 339-348.

(200) Dong, X., Mattingly, C. A., Tseng, M. T., Cho, M. J., Liu, Y., Adams, V. R., and Mumper, R. J. (2009) Doxorubicin and paclitaxel-loaded lipid-based nanoparticles overcome multidrug resistance by inhibiting P-glycoprotein and depleting ATP. *Cancer Res 69*, 3918-26.

(201) Kievit, F. M., Wang, F. Y., Fang, C., Mok, H., Wang, K., Silber, J. R., Ellenbogen, R. G., and Zhang, M. (2011) Doxorubicin loaded iron oxide nanoparticles overcome multidrug resistance in cancer in vitro. *J Control Release 152*, 76-83.

(202) Chen, A. M., Zhang, M., Wei, D., Stueber, D., Taratula, O., Minko, T., and He, H. (2009) Co-delivery of doxorubicin and Bcl-2 siRNA by mesoporous silica nanoparticles enhances the efficacy of chemotherapy in multidrug-resistant cancer cells. *Small 5*, 2673-7.

(203) Soma, C. E., Dubernet, C., Bentolila, D., Benita, S., and Couvreur, P. (2000) Reversion of multidrug resistance by co-encapsulation of doxorubicin and cyclosporin A in polyalkylcyanoacrylate nanoparticles. *Biomaterials 21*, 1-7.

(204) Song, X. R., Cai, Z., Zheng, Y., He, G., Cui, F. Y., Gong, D. Q., Hou, S. X., Xiong, S. J., Lei, X. J., and Wei, Y. Q. (2009) Reversion of multidrug resistance by co-encapsulation of vincristine and verapamil in PLGA nanoparticles. *Eur J Pharm Sci 37*, 300-5.

(205) Zhu, H., Chen, H., Zeng, X., Wang, Z., Zhang, X., Wu, Y., Gao, Y., Zhang, J., Liu, K., Liu, R., *et al.* (2014) Co-delivery of chemotherapeutic drugs with vitamin E TPGS by porous PLGA nanoparticles for enhanced chemotherapy against multi-drug resistance. *Biomaterials 35*, 2391-400.

(206) Sonali, M., Viswanadh, K., Singh, R. P., Agrawal, P., Mehata, A. K., Pawde, D. M., Narendra, Sonkar, R., and Muthu, M. S. (2018) Nanotheranostics: Emerging Strategies for Early Diagnosis and Therapy of Brain Cancer. *Nanotheranostics 2*, 70-86.

(207) Kapse-Mistry, S., Govender, T., Srivastava, R. And Yergeri, M. (2014) Nanodrug delivery in reversing multidrug resistance in cancer cells. *Front Pharmacol 5*, 159.

(208) Tian, G., Zheng, X., Zhang, X., Yin, W., Yu, J., Wang, D., Zhang, Z., Yang, X., Gu, Z., and Zhao, Y. (2015) TPGS-stabilized NaYbF4:Er upconversion nanoparticles for dual-modal fluorescent/CT imaging and anticancer drug delivery to overcome multi-drug resistance. *Biomaterials 40*, 107-16.

(209) Yi, X., Zhao, D., Zhang, Q., Xu, J., Yuan, G., Zhuo, R., and Li, F. (2017) Preparation of multilocation reduction-sensitive core crosslinked folate-PEG-coated micelles for rapid release of doxorubicin and tariquidar to overcome drug resistance. *Nanotechnology 28*, 085603.

(210) Xue, H., Yu, Z., Liu, Y., Yuan, W., Yang, T., You, J., He, X., Lee, R. J., Li, L., and Xu, C. (2017) Delivery of miR-375 and doxorubicin hydrochloride by lipid-coated hollow mesoporous silica nanoparticles to overcome multiple drug resistance in hepatocellular carcinoma. *Int J Nanomedicine 12*, 5271-5287.

(211) Mirski, S. E., Gerlach, J. H., and Cole, S. P. (1987) Multidrug resistance in a human small cell lung cancer cell line selected in adriamycin. *Cancer Res 47*, 2594-2598.

(212) Wang, F., Wang, Y.-C., Dou, S., Xiong, M.-H., Sun, T.-M., and Wang, J. (2011) Doxorubicin-tethered responsive gold nanoparticles facilitate intracellular drug delivery for overcoming multidrug resistance in cancer cells. *ACS Nano 5*, 3679-3692.

(213) Li, J. M., Zhang, W., Su, H., Wang, Y. Y., Tan, C. P., Ji, L. N., and Mao, Z. W. (2015) Reversal of multidrug resistance in MCF-7/Adr cells by codelivery of doxorubicin and BCL2 siRNA using a folic acid-conjugated polyethylenimine hydroxypropyl-beta-cyclodextrin nanocarrier. *Int J Nanomedicine 10*, 3147-62.

(214) Oliveira, M. S., Aryasomayajula, B., Pattni, B., Mussi, S. V., Ferreira, L. a. M., and Torchilin, V. P. (2016) Solid lipid nanoparticles co-loaded with doxorubicin

and alpha-tocopherol succinate are effective against drug-resistant cancer cells in monolayer and 3-D spheroid cancer cell models. *Int J Pharm 512*, 292-300.

(215) Zeng, X., Morgenstern, R., and Nystrom, A. M. (2014) Nanoparticle-directed sub-cellular localization of doxorubicin and the sensitization breast cancer cells by circumventing GST-mediated drug resistance. *Biomaterials 35*, 1227-39.

(216) Gliga, A. R., Skoglund, S., Wallinder, I. O., Fadeel, B., and Karlsson, H. L. (2014) Size-dependent cytotoxicity of silver nanoparticles in human lung cells: the role of cellular uptake, agglomeration and Ag release. *Part Fibre Toxicol 11*, 11.

(217) Agostinis, P., Berg, K., Cengel, K. A., Foster, T. H., Girotti, A. W., Gollnick, S. O., Hahn, S. M., Hamblin, M. R., Juzeniene, A., and Kessel, D. (2011) Photodynamic therapy of cancer: an update. *CA-Cancer J Clin 61*, 250-281.

(218) Huang, Z. (2005) A review of progress in clinical photodynamic therapy. *Technol Cancer Res T 4*, 283-293.

(219) Drobizhev, M., Stepanenko, Y., Dzenis, Y., Karotki, A., Rebane, A., Taylor, P. N., and Anderson, H. L. (2004) Understanding strong two-photon absorption in π-conjugated porphyrin dimers via double-resonance enhancement in a three-level model. *J Am Chem Soc 126*, 15352-15353.

(220) Shaikh, A. J., Rabbani, F., Sherazi, T. A., Iqbal, Z., Mir, S., and Shahzad, S. A. (2015) Binding strength of porphyrin− gold nanoparticle hybrids based on number and type of linker moieties and a simple method to calculate inner filter effects of gold nanoparticles using fluorescence spectroscopy. *J Phys Chem A 119*, 1108-1116.

(221) Gong, H., Dong, Z., Liu, Y., Yin, S., Cheng, L., Xi, W., Xiang, J., Liu, K., Li, Y., and Liu, Z. (2014) Engineering of multifunctional nano-micelles for combined photothermal and photodynamic therapy under the guidance of multimodal imaging. *Adv Funct Mater 24*, 6492-6502.

(222) Mitsunaga, M., Ogawa, M., Kosaka, N., Rosenblum, L. T., Choyke, P. L., and Kobayashi, H. (2011) Cancer cell–selective in vivo near infrared photoimmunotherapy targeting specific membrane molecules. *Nature Med 17*, 1685.

(223) Kim, J., Santos, O. A., and Park, J.-H. (2014) Selective photosensitizer delivery into plasma membrane for effective photodynamic therapy. *J Control Release 191*, 98-104.

(224) Akhlynina, T. V., Jans, D. A., Rosenkranz, A. A., Statsyuk, N. V., Balashova, I. Y., Toth, G., Pavo, I., Rubin, A. B., and Sobolev, A. S. (1997) Nuclear targeting of chlorin e6 enhances its photosensitizing activity. *J Biol Chem 272*, 20328-20331.

(225) Jimenez, C. M., Rubio, Y. G., Saunier, V., Warther, D., Stojanovic, V., Raehm, L., Frochot, C., Arnoux, P., Garcia, M., and Morère, A. (2016) 20-nm-sized mesoporous silica nanoparticles with porphyrin photosensitizers for in vitro photodynamic therapy. *J Sol-Gel Sci Techn 79*, 447-456.

(226) Rangasamy, S., Ju, H., Um, S., Oh, D.-C., and Song, J. M. (2015) Mitochondria and DNA targeting of 5, 10, 15, 20-tetrakis (7-sulfonatobenzo [b] thiophene) porphyrin-induced photodynamic therapy via intrinsic and extrinsic apoptotic cell death. *J Med Chem 58*, 6864-6874.

(227) Lee, C.-S., Park, W., Park, S.-J., and Na, K. (2013) Endolysosomal environment-responsive photodynamic nanocarrier to enhance cytosolic drug delivery via photosensitizer-mediated membrane disruption. *Biomaterials 34*, 9227-9236.

(228) Maziere, J., Santus, R., Morliere, P., Reyftmann, J.-P., Candide, C., Mora, L., Salmon, S., Maziere, C., Gatt, S., and Dubertret, L. (1990) Cellular uptake and photosensitizing properties of anticancer porphyrins in cell membranes and low and high density lipoproteins. *J Photochem Photobio B 6*, 61-68.

(229) Li, Z., Wang, C., Cheng, L., Gong, H., Yin, S., Gong, Q., Li, Y., and Liu, Z. (2013) PEG-functionalized iron oxide nanoclusters loaded with chlorin e6 for targeted, NIR light induced, photodynamic therapy. *Biomaterials 34*, 9160-9170.

(230) Zhang, Y., Huang, F., Ren, C., Yang, L., Liu, J., Cheng, Z., Chu, L., and Liu, J. (2017) Targeted chemo-photodynamic combination platform based on the DOX prodrug nanoparticles for enhanced cancer therapy. *ACS Appl Mater Inter 9*, 13016-13028.

(231) Zhang, W., Li, S., Liu, X., Yang, C., Hu, N., Dou, L., Zhao, B., Zhang, Q., Suo, Y., and Wang, J. (2018) Oxygen-generating MnO2 nanodots-anchored versatile nanoplatform for combined chemo-photodynamic therapy in hypoxic cancer. *Adv Funct Mater 28*, 1706375.

(232) Hou, W., Zhao, X., Qian, X., Pan, F., Zhang, C., Yang, Y., De La Fuente, J. M., and Cui, D. (2016) pH-sensitive self-assembling nanoparticles for tumor near-infrared fluorescence imaging and chemo–photodynamic combination therapy. *Nanoscale 8*, 104-116.

(233) Dou, Q. Q., Teng, C. P., Ye, E., and Loh, X. J. (2015) Effective near-infrared photodynamic therapy assisted by upconversion nanoparticles conjugated with photosensitizers. *Int J Nanomedicine 10*, 419.

(234) Hu, D., Chen, L., Qu, Y., Peng, J., Chu, B., Shi, K., Hao, Y., Zhong, L., Wang, M., and Qian, Z. (2018) Oxygen-generating hybrid polymeric nanoparticles with encapsulated doxorubicin and chlorin e6 for trimodal imaging-guided combined chemo-photodynamic therapy. *Theranostics 8*, 1558.

(235) Nag, O. K., Naciri, J., Oh, E., Spillmann, C. M., and Delehanty, J. B. (2016) Lipid raft-mediated membrane tethering and delivery of hydrophobic cargos from liquid crystal-based nanocarriers. *Bioconjugate Chem 27*, 982-993.

(236) Martynenko, I., Kuznetsova, V., Orlova, A. O., Kanaev, P., Maslov, V., Loudon, A., Zaharov, V., Parfenov, P., Gun'ko, Y. K., and Baranov, A. (2015) Chlorin e6–ZnSe/ZnS quantum dots based system as reagent for photodynamic therapy. *Nanotechnology 26*, 055102.

(237) Valanciunaite, J., Klymchenko, A. S., Skripka, A., Richert, L., Steponkiene, S., Streckyte, G., Mely, Y., and Rotomskis, R. (2014) A non-covalent complex of quantum dots and chlorin e 6: efficient energy transfer and remarkable stability in living cells revealed by FLIM. *RSC Adv 4*, 52270-52278.

(238) Visheratina, A., Alisova, I., Kundelev, E., Orlova, A., Maslov, V., Fedorov, A., and Baranov, A. (2015) Complexes of CdSe/ZnS quantum dots with chlorin e6 in nonaqueous media. *Opt Spectrosc 119*, 733-737.

(239) Visheratina, A., Martynenko, I., Orlova, A., Maslov, V., Fedorov, A., Baranov, A., and Gun'ko, Y. K. (2014) Investigation of biocompatible complexes of Mn 2+-doped ZnS quantum dots with chlorin e6. *J Opt Technol 81*, 444-448.

(240) Susumu, K., Mei, B. C., and Mattoussi, H. (2009) Multifunctional ligands based on dihydrolipoic acid and polyethylene glycol to promote biocompatibility of quantum dots. *Nat Protoc 4*, 424.

(241) Susumu, K., Uyeda, H. T., Medintz, I. L., Pons, T., Delehanty, J. B., and Mattoussi, H. (2007) Enhancing the stability and biological functionalities of quantum dots via compact multifunctional ligands. *J Am Chem Soc 129*, 13987-13996.

(242) Susumu, K., Field, L. D., Oh, E., Hunt, M., Delehanty, J. B., Palomo, V., Dawson, P. E., Huston, A. L., and Medintz, I. L. (2017) Purple-, blue-, and green-emitting multishell alloyed quantum dots: synthesis, characterization, and application for ratiometric extracellular pH sensing. *Chem Mater 29*, 7330-7344.

(243) Valanciunaite, J., Skripka, A., Streckyte, G., and Rotomskis, R. (2010) in *P Soc Photo-Opt Ins* pp 737607, International Society for Optics and Photonics.

(244) Steponkiene, S., Valanciunaite, J., Skripka, A., and Rotomskis, R. (2014) Cellular uptake and photosensitizing properties of quantum dot-chlorin e6 complex: in vitro study. *J Biomed Nanotechnol 10*, 679-686.

(245) Berney, C., and Danuser, G. (2003) FRET or no FRET: a quantitative comparison. *Biophy J 84*, 3992-4010.

(246) Wallace, B., and Atzberger, P. J. (2017) Förster resonance energy transfer: Role of diffusion of fluorophore orientation and separation in observed shifts of FRET efficiency. *PloS one 12*, e0177122.

(247) Mccann, J. J., Choi, U. B., Zheng, L., Weninger, K., and Bowen, M. E. (2010) Optimizing methods to recover absolute FRET efficiency from immobilized single molecules. *Biophy J 99*, 961-970.

(248) Charras, G. (2008) A short history of blebbing. *J Microsc- Oxford 231*, 466-478.

(249) Jia, H.-R., Jiang, Y.-W., Zhu, Y.-X., Li, Y.-H., Wang, H.-Y., Han, X., Yu, Z.-W., Gu, N., Liu, P., and Chen, Z. (2017) Plasma membrane activatable polymeric nanotheranostics with self-enhanced light-triggered photosensitizer cellular influx for photodynamic cancer therapy. *J Control Release 255*, 231-241.

(250) Jia, H.-R., Zhu, Y.-X., Xu, K.-F., Liu, X., and Wu, F.-G. (2018) Plasma membrane-anchorable photosensitizing nanomicelles for lipid raft-responsive and light-controllable intracellular drug delivery. *J Control Release 286*, 103-113.

(251) Nag, O. K., Naciri, J., Erickson, J. S., Oh, E., and Delehanty, J. B. (2018) Hybrid liquid crystal nanocarriers for enhanced zinc phthalocyanine-mediated photodynamic therapy. *Bioconjugate Chem 29*, 2701-2714.

(252) Lovell, J. F., Liu, T. W., Chen, J., and Zheng, G. (2010) Activatable photosensitizers for imaging and therapy. *Chem Rev 110*, 2839-2857.

(253) Charron, G., Stuchinskaya, T., Edwards, D. R., Russell, D. A., and Nann, T. (2012) Insights into the mechanism of quantum dot-sensitized singlet oxygen production for photodynamic therapy. *J Phys Chem C 116*, 9334-9342.

(254) Song, X., Liang, C., Gong, H., Chen, Q., Wang, C., and Liu, Z. (2015) Photosensitizer-conjugated albumin−polypyrrole nanoparticles for imaging-guided in vivo photodynamic/photothermal therapy. *Small 11*, 3932-3941.

(255) Zhu, W., Dong, Z., Fu, T., Liu, J., Chen, Q., Li, Y., Zhu, R., Xu, L., and Liu, Z. (2016) Modulation of hypoxia in solid tumor microenvironment with MnO2 nanoparticles to enhance photodynamic therapy. *Adv Funct Mater 26*, 5490-5498.

(256) Delehanty, J., Das, S., Goldberg, E., Sangtani, A., and Knight, D. (2018) Synthesis of a reactive oxygen species-responsive doxorubicin derivative. *Molecules 23*, 1809.

(257) Pawlicki, M., Collins, H. A., Denning, R. G., and Anderson, H. L. (2009) Two-photon absorption and the design of two-photon dyes. *Angew Chem Int Edit 48*, 3244-3266.

(258) Qi, Z.-D., Li, D.-W., Jiang, P., Jiang, F.-L., Li, Y.-S., Liu, Y., Wong, W.-K., and Cheah, K.-W. (2011) Biocompatible CdSe quantum dot-based photosensitizer under two-photon excitation for photodynamic therapy. *J Mater Chem 21*, 2455-2458.

(259) Fowley, C., Nomikou, N., Mchale, A. P., Mccarron, P. A., Mccaughan, B., and Callan, J. F. (2012) Water soluble quantum dots as hydrophilic carriers and two-photon excited energy donors in photodynamic therapy. *J Mater Chem 22*, 6456-6462.

(260) Huang, Y., Qiu, F., Shen, L., Chen, D., Su, Y., Yang, C., Li, B., Yan, D., and Zhu, X. (2016) Combining two-photon-activated fluorescence resonance energy

transfer and near-infrared photothermal effect of unimolecular micelles for enhanced photodynamic therapy. *ACS nano 10*, 10489-10499.

(261) Oh, N., and Park, J.-H. (2014) Endocytosis and exocytosis of nanoparticles in mammalian cells. *Int J Nanomedicine 9*, 51.

(262) Sakhtianchi, R., Minchin, R. F., Lee, K.-B., Alkilany, A. M., Serpooshan, V., and Mahmoudi, M. (2013) Exocytosis of nanoparticles from cells: role in cellular retention and toxicity. *Adv Colloid Interfac 201*, 18-29.

(263) Jiang, X., RöCker, C., Hafner, M., Brandholt, S., DöRlich, R. M., and Nienhaus, G. U. (2010) Endo-and exocytosis of zwitterionic quantum dot nanoparticles by live HeLa cells. *ACS nano 4*, 6787-6797.

(264) Ivanov, A. I. (2014) Pharmacological inhibitors of exocytosis and endocytosis: novel bullets for old targets, in *Exocytosis and Endocytosis* pp 3-18, Springer.

(265) Rowland, C. E., Susumu, K., Stewart, M. H., Field, L. D., Sangtani, A., Medintz, I. L., and Delehanty, J. B. (2017) Cellular Applications of Semiconductor Quantum Dots at the US Naval Research Laboratory: 2006–2016, in *Reviews in Fluorescence 2016* pp 203-242, Springer.